Department of Physics and Astronomy
University of Heidelberg

Bachelor Thesis in Physics
submitted by

Jonas Buchholz

born in Göttingen (Germany)

2019

Analysis of the spatial distribution of membrane proteins Claudin2, Claudin5 and Occludin in Human Peritoneal Mesothelial Cells treated with peritoneal dialysis fluids using Single Molecule Localization Microscopy

This Bachelor Thesis has been carried out by Jonas Buchholz at the
Kirchhoff Institute in Heidelberg
under the supervision of
Prof. Dr. Michael Hausmann

Zusammenfassung

Die räumliche Verteilung der Membranproteine Claudin2, Claudin5 und Occludin in menschlichen peritonealen mesothelialen Zellen (HPMC) wurde nach Behandlung mit unterschiedlichen peritonealen Dialyseflüssigkeiten (PD-Flüssigkeiten) mit Hilfe hochauflösender Lokalisationsmikroskopie untersucht, um Erkenntnisse über Veränderungen parazellulärer Membraneigenschaften auf molekularer Ebene zu gewinnen. Mittelwert und Standardabweichung der Signalzahlen pro Lokalisationsaufnahme wurden für alle Testserien berechnet und die absolute und relative Verteilung der Abstände zwischen Signalen wurde im Bereich von 0 bis 200 nm untersucht. Signalanzahlen waren erheblich höher für Claudin2 als für Claudin5 und Occludin, und eine Verminderung der Signalanzahlen nach Behandlung sowohl mit konventioneller als auch biokompatibler peritonealer Dialyseflüssigkeit konnte beobachtet werden. Behandlung mit PD-Flüssigkeiten mit der Zugabe von 8mMol Alanyl-glutamin resultierte in einer weiteren Reduktion der Signalzahlen für konventionelle PD-Flüssigkeiten, aber einer Erhöhung der Signalzahlen für biokompatible PD-Flüssigkeiten. Ergebnisse der Signalzahluntersuchungen waren inkonsistent für Claudin5 und Occludin, da Testserien mit gleicher Behandlung aber verschiedener Fluoreszenzfärbung unterschiedliche Eigenschaften zeigten.
Analyse der Distanzverteilungen zeigte eine Erhöhung der relativen Häufigkeit von Abständen von ca. 25 nm zwischen Claudin2-Signalen nach Behandlung mit biokompatibler PD-Flüssigkeit. Dieser Effekt konnte nicht beobachtet werden nach Behandlung mit konventioneller PD-Flüssigkeit. Behandlungen sowohl mit konventioneller als auch biokompatibler PD-Flüssigkeit mit der Zugabe von Alanyl-glutamin resultierten in Claudin2-Distanzverteilungen, die vergleichbar mit der Kontrollgruppe waren. Eine ähnliche Entwicklung der Distanzverteilungen für Abstände von ca. 40 nm konnte für Teile der Claudin5 und Occludin Testserien beobachtet werden. Sowohl für Claudin5 als auch für Occludin hingen charakteristische Distanzen und relative Häufigkeit der Abstände zusätzlich von der Fluoreszenzfärbung ab.

Abstract

Super-resolution single molecule localization microscopy (SMLM) was used to analyze the spatial distribution of membrane proteins Claudin2, Claudin5 and Occludin in human peritoneal mesothelial cells (HPMC) after exposure to peritoneal dialysis fluids (PD-fluids) in order to examine changes of paracellular membrane properties on a molecular level. The mean and standard deviation of signal numbers per recording were calculated for all test series, and absolute and relative frequency of occurrence of distances between signals were analyzed in the range of 0 to 200 nm. Signal numbers were found to be substantially higher for Claudin2 than for Claudin5 and Occludin, and a decrease in signal numbers after treatment with conventional peritoneal dialysis fluid (CPDF) as well as biocompatible peritoneal dialysis fluid (BPDF) could be observed. Treatment of cells with PD-fluids and the addition of 8mMol alanyl-glutamine (AlaGln) led to a further reduction of Claudin2 signal numbers for CPDF, but to an increase of signal numbers for BPDF. Results were inconsistent for Claudin5 and Occludin as test series with the same treatment solution but different fluorescent staining expressed different properties.
Distance analysis revealed an increase in frequency of occurrence of distances between signals of about 25 nm for Claudin2 after treatment with BPDF. The same trend could not be seen after CPDF treatment. Exposure to CPDF+AlaGln as well as BPDF+AlaGln yielded a distribution of Claudin2 signals comparable to the control group. Similar changes in distance distribution for distances of about 40 nm could be observed for Claudin5 and Occludin, but characteristic distances depended on the fluorescent staining.

Contents

I Introduction

For centuries, medical imaging and microscopy have been essential for our understanding of biological processes and their underlying principles. Over time, new technologies and advances in science allowed for better and more precise measurement techniques. However, as a direct consequence of the wave nature of light, it seemed that light microscopy was limited to resolutions of about 200 nm [1].

Novel high-resolution fluorescence microscope techniques allow resolutions below the diffraction limit of conventional light microscopy, revealing structures that could not be registered before. For this work, Single Molecule Localization Microscopy (SMLM) was used to analyze the spatial distribution of tight-junction associated membrane proteins Claudin2, Claudin5 and Occludin in Human Peritoneal Mesothelial Cells (HPMC) treated with dialysis fluids.

In peritoneal dialysis (PD), dialysis fluids are introduced into the peritoneum via a catheter. This serves as a therapy for patients with acute kidney failure, as PD-fluids help to remove toxins and excess fluids from the blood as well as correct electrolyte problems [2]. However, as a result of continuous peritoneal dialysis, morphological changes to the peritoneum can be observed, some of the most common being peritoneal fibrosis [3] and loss of ultrafiltration [4]. Studies suggest mesothelial-to-mesenchymal transitions of peritoneal cells to play an important role in the process leading to tissue fibrosis, yet many details of this mechanism still remain unclear [5].

SMLM is a microscopy technique that centers around the fluorescent labeling of targets and the use of mathematical tools to calculate the center maximum of individual signals, thus improving the resolution of an optical setup. To achieve this, a spatial separation of signals on the detector is necessary in order to accurately fit the signal positions. In the optical setup used for this work, high laser intensities were applied to the samples in order to induce reversible bleaching of the fluorescent labels. As a result, only a fraction of signals were active at any given time. This allowed mathematical fitting of individual signal positions and ultimately a reconstruction of a super-resolved localization image from a stack of recordings.

As SMLM promises resolutions that are by far exceeding the range of conventional light microscopy, a structural analysis of membrane proteins associated with tight junctions in HPMC may lead to new insights regarding the morphological changes in peritoneal tissue.

II Background

II.1 Optical Imaging

All optical imaging systems are limited in their achievable resolution by diffraction and other disruptive factors. While some physical effects such as spherical and chromatic aberrations can be corrected by the use of sophisticated lens systems, the diffraction limit of light microscopy is a direct consequence of the wave nature of light. Equation 1 gives a mathematical description of this fundamental resolution limit as described by Rayleigh [6], where λ is the wavelength of the light, NA is the numerical aperture (NA = n $\cdot$ sin α with n: refractive index of the medium and α the opening angle between marginal rays and optical axis) and d gives the minimal distance between points that can be registered as independent signals.

$$d = \frac{1.22 \cdot \lambda}{NA} \tag{1}$$

An idealized point-like object in the object plane corresponds to a Fraunhofer diffraction patter in the focal plane of an imaging system. As all lenses are only able to capture a certain fraction of this pattern, high orders of diffraction are cut off, resulting in information loss and thus limiting the resolution.
To mathematically describe the response of an optical system to a point-like input, the point spread function (PSF) is introduced. The PSF gives a relationship between an object O($\vec{x}$) and the final image A($\vec{x}$) after being processed by the optical system, assuming homogeneous illumination:

$$A(\vec{x}) = (O \otimes PSF)(\vec{x}) \tag{2}$$

As intensities of adjacent point-emitters in the object plane add linearly, knowledge of the PSF would theoretically allow for a complete reconstruction of the original object from a microscopy image. In practice, background noise and the cut-off of high orders of diffraction make this a challenging task. The PSF of a circular aperture can be described by an Airy function, thus the center maximum (Airy disc) can be approximated by a 3D Gaussian. The full width half maximum (FWHM) of the fitted function then gives a reasonable resolution limit of the optical system in conventional light microscopy.

II.2 Fluorescence Microscopy & SMLM

II.2.1 Fluorescence Microscopy Techniques

Fluorescence describes the process of excitation of a substance by light absorption followed by emission of light by the same substance. Usually, the time difference between absorption and emission is in the order of nanoseconds [7] and the emitted light will be of longer wavelength than the absorbed light (Stokes shift). Functional groups capable of fluorescence are called fluorophores. In fluorescence microscopy, fluorophores are attached to target biomolecules in order to map structures or analyze the spatial distribution of the targets. Because of the Stokes shift, the emission signal can be separated from the much stronger excitation signal by using dichromatic filters. Additionally, the fact that fluorophores each have characteristic absorption and emission spectra opens the possibility of staining multiple different targets at the same time. A common method of staining is by using fluorophores attached to antibodies which then specifically bind the target (immunostaining).

II.2.2 Singel Molecule Localization Microscopy

Single Molecule Localization Microscopy (SMLM) is an advanced microscopy technique that aims to achieve resolutions below the diffraction limit of conventional light microscopy. SMLM makes use of the fact that some fluorophores can be reversibly 'switched' into a non-fluorescent dark state (photo bleaching) [8]. One method of

inducing photo bleaching is by applying high laser intensities to the sample ($\approx$10kW/cm^2 in focal plane) [9]. As the fluorophores independently recover into the fluorescent bright state, ideally only one fluorophore at a time is active within a diffraction limited area. Thus, the PSF of different signals will be registered separately on the detector. This allows Gaussian fitting and calculation of the center of maximum intensity for each signal, resulting in a theoretically infinite resolution [10]. In practice, the resolution is limited by the signal intensity and background noise, and an improvement by a factor of about 10 in resolution has proven realistic [11].
For this work, SMLM was used to obtain super-resolution images of peritoneal cells. A stack of images was taken for every recording in order to obtain a sufficient amount of information. For each image in the stack, the signal positions were determined by Gaussian fitting, see Fig. 1. Each calculated signal position was saved into a matrix, which allowed a reconstruction of a super-resolved image or further quantitative analysis. The mathematical algorithms and software used to process the data are discussed in detail in chapter III.4

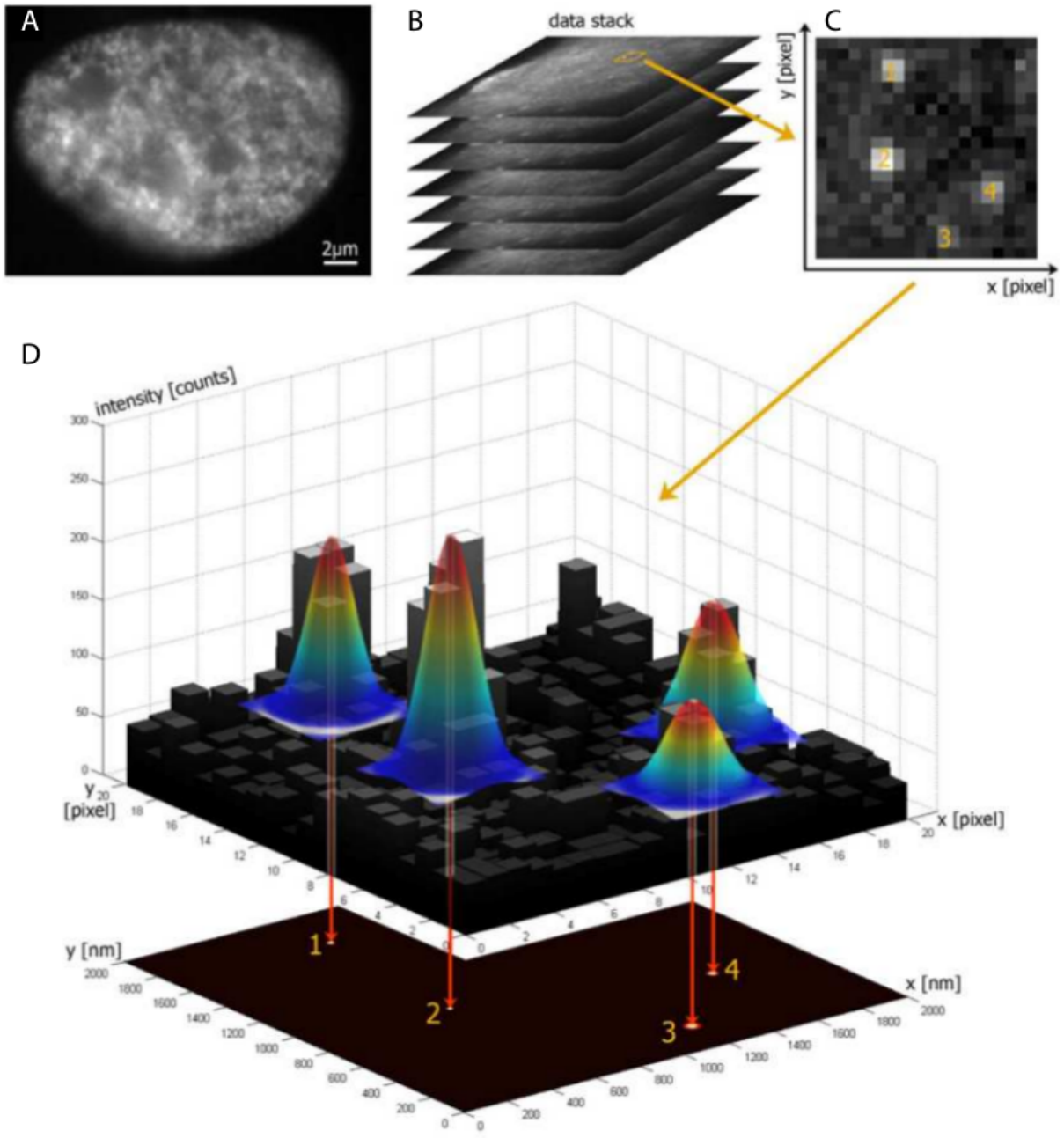

Figure 1: SMLM signal detection: A stack of images is recorded. For every individual image, ideally only one fluorophore is active within a diffraction limited area. This allows for Gaussian fitting a calculation of the center maximum of the signal, severely improving the resolution of the system. Knowledge of the individual signal positions is the basis for image reconstruction and quantitative analysis of the spatial distribution of the targets in the sample.

II.2.3 Localization Accuracy

The images were recorded with a CCD-camera, so every pixel of the camera relates to an area on the object (pixel size). The pixel size of the camera and set-up used for this work is 112 nm, thus all point-like signals on the object within a $112 \cdot 112\ nm^2$ area would be represented by the same pixel on the camera. With localization microscopy, a resolution below the diffraction limit of light and below the pixel size of the camera is possible. The resolution can be described by a single parameter: the localization accuracy Δx.
In a simple approach, the localization accuracy depends on the Gaussian fit and on the number of photons that have been captured:

$$\langle(\Delta x)^2\rangle = \frac{s^2}{N} \tag{3}$$

with s the standard deviation of the fitted PSF and N the number of registered photons.
Taking the pixel size a and background noise b into account, Equation 3 becomes:

$$\langle(\Delta x)^2\rangle = \frac{s^2 + \frac{a^2}{12}}{N} + \frac{4\sqrt{\pi}s^3b^2}{aN^2} \tag{4}$$

A more detailed description of the localization accuracy can be found in the PhD thesis of Matthias Krufczik [12], and a derivation of Equation 4 was made by Thompson et al [13].

II.3 Biomedical Background

II.3.1 Peritoneal Dialysis

Peritoneal dialysis is a treatment method for patients with kidney disease or renal failure. In general, dialysis refers to the selective movement of fluids and solutes through a semipermeable membrane, in this case from a patient's blood to a dialysate. In peritoneal dialysis, the patient's own peritoneum serves as this semipermeable membrane, partially substituting for the function of the kidneys. Other types of dialysis include hemodialysis and continuous arteriovenous hemofiltration [14].
To set up for peritoneal dialysis, first a catheter has to surgically be inserted into the abdomen, providing access for dialysis fluids to reach the peritoneum [15]. The process of peritoneal dialysis then involves the introduction of 2-3 liters of dialysis fluid into the abdomen, which remain there for several hours to allow for diffusion of toxins across the peritoneal membrane [16]. There are different methods of performing peritoneal dialysis, which must be decided on based on the patient's abilities and needs [14]:

- **Intermittent peritoneal dialysis (IPD)**: In intermittent peritoneal dialysis, a cycler is used to manually or mechanically introduce a predetermined amount of dialysate (about 2l) into the abdomen, where it is instilled for 20 to 30 minutes and allowed to drain by gravity [17]. Clients are dialyzed for three to ten hours at a time and three to five times a week.
- **Continuous ambulatory peritoneal dialysis (CAPD)**: In CAPD, a continuous presence of dialysis fluids in the peritoneum is achieved. The PD-fluid is removed and a fresh solution instilled about five times a day. In between drainage and instillation processes, the patient is disconnected from tubing and free to perform other activities. As drainage and instillation take about 30 to 45 minutes of time, the impact on the life of patients is minimized by this technique as compared to other dialysis methods that require long dialysis sessions on multiple days of the week. Patients can be trained to independently perform PD-fluid drainage and instillation [18].
- **Continuous cycling peritoneal dialysis**: This method provides a combination of the two previously discussed PD-techniques. A cycler performs multiple (three-four) dialysis exchanges at night, with the

Component	Concentration
Osmotic agent:	
Glucose monohydrate	16,5 g
Buffer:	
Sodium lactate	35-40 mmol/L
Electrolytes:	
Sodium	132-134 mEq/L
Potassium	None
Calcium	1,5-3,5 mEq/L
Chloride	95 - 102.5 mEq/L
Magnesium	0,5-1,5 mEq/L

Table 1: Components of exemplary PD-fluid (from [25])

PD-fluid of the last cycle being left in the abdomen throughout the day. The exchanges are performed every night and the patient is free to move during the day, but confined to bed at night [14].

Peritoneal dialysis offers a number of benefits over other dialysis techniques. The impact on a patient's life is minimized, resulting in higher patient autonomy and satisfaction. Additional benefits are lower costs of peritoneal dialysis (PD) as compared to Hemodialysis (HD), and an increased rate of survival in the first one to two years of End-Stage Renal Disease [19]. However, disadvantages of PD include higher rates of technical failure and risks for infectious complications such as peritonitis. Recurrent peritonitis can lead to peritoneal membrane and ultrafiltration failure [20], and around 18% of infection related mortality in PD-patients are due to peritonitis [21].
Additionally, continuous and permanent loss of ultrafiltration capacity of the peritoneum could be observed among long-term PD-patients. Analysis of the affected population suggested a progressive deterioration of the peritoneum and indicated that the risk for this condition increased exponentially with duration of the PD-treatment [4]. Further studies showed a connection between fibrosis and mesothelial-to-mesenchymal transitions in peritoneal cells resulting in changed properties of the extracellular matrix in peritoneal tissue. As many details of this mechanism still remain unclear, a link between frequent inflammation and mesothelial cell damage, ultimately leading to fibrosis, appears likely, with one condition inducing the other and vice versa. Furthermore, bioincompatible dialysis fluids (glucose, glucose degradation products and advanced glycation end products) seem to be responsible for altering mesothelial cell function and proliferation [22] [23].

II.3.2 Dialysis Fluids

In peritoneal dialysis, fluids (PD-fluids) are introduced into the peritoneal cavity via a catheter in order to help filter toxins and remove excess fluid from the blood. In most cases, PD-fluids contain electrolytes to not disturb blood composition, a pH buffer and an osmotic agent [24]. A typical ingredient composition of conventional PD-fluids is shown in Table 1. For this work, the commercial dialysis fluids bica*Vera* and CAPD from Fresenius Medical Care were used to study the effects of PD-fluids on Human Peritoneal Mesothelial Cells.

With the realization that bioincompatible dialysis fluids might be responsible for morphological changes to peritoneal tissue [26] [27], an effort was made to reduce glucose degradation products (GDP) and reach neutral pH in PD-fluids. Conventional glucose based PD-fluids have pH-values around 5,5 and are stored in single-chamber bags, resulting in high GDP. The dialysis solution CAPD by Fresenius is a single chamber glucose based PD-fluid [28].

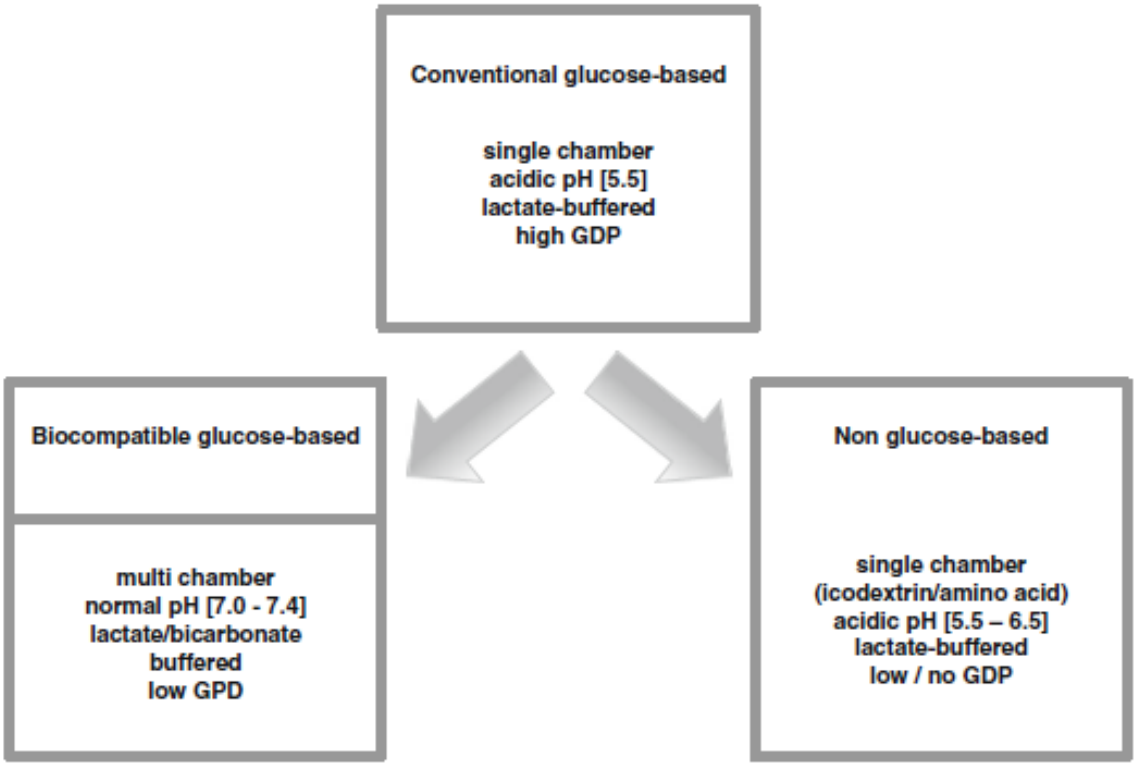

Figure 2: Overview over different PD-fluids: Conventional PD-fluids use glucose as osmotic agent and lactate buffers, resulting in acidic pH and high GDP. Novel biocompatible PD-fluids use alternative osmotic agents and buffers or multi-bag systems to reduce GDP concentration. From [28]

To reduce GDP occurrence, alternative osmotic agents such as icodextrin or amino acids are used in some novel PD-fluids available for clinical use. Another method of improving biocompatibility is by storing the buffer and osmotic agents in separate compartments. This allows the usage of bicarbonate buffers with neutral pH and reduction of GDP by keeping glucose in a separated acidic compartment (pH 2-3). Bica *Vera* by Fresenius is a multi-bag glucose-based PD-fluid. An overview over different kinds of PD-fluids is given in Fig. 2.

Although initial clinical trials suggested improvements in mesothelial cell viability by usage of biocompatible dialysis fluids in PD [29] [30], new studies challenge these views. A recent Cochrane analysis about impacts of PD-solution concluded that low GDP PD-fluids did not induce further harm to PD-patients, but could also not effectively prevent infectious complications and long-term peritoneal damage [31].
Other attempts to improve the biocompatibility of PD-solutions include the addition of non-toxic agents, such as carnitine or alanyl-glutamine. Several studies indicated beneficial effects of these substances, such as improved glucose metabolism for carnitine-enriched PD-fluids [32] or protection of the peritoneal membrane by addition of alanyl-glutamine [33] [34]. For this work, additional test series with alanyl-glutamine added to both dialysis solutions, bica *Vera* and CAPD, were performed.

II.3.3 Tight Junctions

Paracellular transport of water and solutes, such as ions, is limited by intercellular multi-protein complexes called tight junctions. At least 40 different proteins contribute to tight junctions [35], however, the three major transmembrane proteins are Occludin, Claudins and junction adhesion molecule (JAM) proteins. For this work, Claudin2, Claudin5 and Occludin have been marked for high-resolution microscopy using immunostaining.
Occludin is a transmembrane protein with both, N- and C-terminus, inside the cell. It forms two extracellular and one intracellular loop and weighs about 65kDa (522-amino acids in humans). Functions of Occludin include organization of cellular structure and regulation of paracellular transport properties [36] [37]. More

specifically, Occludin is believed to play an important role in tight junction stability and barrier function, with both extracellular loops being involved in permeability regulation. Additionally, the second extracellular loop is thought to be important for localization of Occludin in tight junctions (first extracellular domain: 46 aa, second extracellular domain: 48 aa) [38]. However, studies with embryonic stem cells were able to show functional tight-junction complexes without Occludin [39].

Claudins are a family of proteins involved in tight junction structure and function first described by Furuse et al. in 1998 [40]. Since then, twenty-four different members of the claudin family have been described in humans, all of which have two extracellular and one intracellular loop and intracellular N- and C-terminus [41]. Claudins weigh 20 to 27 kDa, the first extracellular loop consists of on average 53 aa and the second extracellular loop averages 24 aa. Claudins are believed to play an important role in paracellular permeability and membrane selectivity, and different claudins have been associated with different structural functions.

While Claudin5 among other things has been associated with the blood-brain barrier [42], Claudin2 is believed to play an important role in leaky tissue, such as the kidney proximal tubule. Studies were able to show an increase in paracellular water flow in MDCK C7 cells transfected with Claudin2, indicating that paracellular water channels might be mediated by Claudin2 expression [43]. Additionally, a higher paracellular conductivity could be associated with Claudin2 overexpression, suggesting the forming of cation-selective channels in the presence of Claudin2 [44]. Studies in isolated S2 segments of proximal tubules of knockout mice lacking Claudin2 showed a significant decrease in transepithelial reabsorption of electrolytes and water compared to wild types [45], underlining the importance of Claudin2 for leaky tissue.

Target	Conjugate	Class	Host	Clone	Supplier
Claudin2	Alexa Fluor568	Monoclonal	Mouse	12H12	Thermofisher
Claudin5	Alexa Flour568	Monoclonal	Mouse	4C3C2	Invitrogen
Claudin5	Alexa Flour488	Polyclonal	Rabbit	Z43.JK	Invitrogen
Occludin	Alexa Flour488	Polyclonal	Rabbit		Invitrogen (Ref. 71-1500)

Table 2: List of antibodies

III Methods

III.1 Cell Preparation

The Human Peritoneal Mesothelial Cells (HPMC) were seeded in a density of about 10^6 cells per well and grown on cover slips in six well plates until confluence. Cells were then incubated with the treatment solutions (PD-fluid, 1ml pure solution per well) for 5 hours at 37°C and 5% CO_2. The incubation conditions were selected to match resistance and transport experiments that were performed with HPMC in transwell systems.
For fixation, the treatment solution was removed and the cells were fixated with methanol/acetone mixture (1:1) for 10 minutes at room temperature. The fixative was then removed and the cells were washed 5 times for 3 minutes with 1xPBS (Biochrom, Germany).
Bovine Serum Albumin (0.3mM in PBS) was used for blocking. The cover slips were incubated with 1ml BSA per well for 60 minutes at room temperature. The primary antibody was prepared in the blocking buffer in a 1:1000 dilution and the cells were incubated over night (12h) at 4°C. The solution was removed and the cells were washed 5 times for 3 minutes with PBS on the next day.
The secondary antibody (containing a fluorescent label) was prepared in the blocking buffer and cells were incubated for 12 hours at 4°C and washed afterwards. All used antibodies are listed in Table 2.
A 4% paraformaldehyde in PBS solution was used for fixation (20 minute incubation at room temperature) before the second staining was performed. After fixation, the samples were washed 5 times with PBS for 3 minutes and the second staining was carried out, using different antibodies and fluorescent dyes.
For the nuclear staining, a 30nM DAPI-solution was used (15 minutes incubation at room temperature). Samples were washed with PBS 5 times for 3 minutes afterwards.
10 μl ProLong Gold were prepared on a glass slide using a pipette, and the cover slip was removed from the well and put on the glass slide. The sample was then shielded from light and left to harden for 24 hours at room temperature.
All preparations were performed by the Nephrology Laboratory of the Center for Pediatric and Adolescent Medicine, University Hospital Heidelberg.

III.2 Optical Setup

All measurements were performed with a custom built optical setup located in INF 325 room 111b, Heidelberg University. The setup was originally created to allow a combination of the two super-resolution microscopy techniques SMLM and structured illumination microscopy (SIM). For this work, only SMLM was used. A detailed description of the development of this setup can be found in the PhD thesis of Sabrina Roßberger [see 46].

Four lasers were available for this setup, as listed in Table 3. Dichromatic filters and emission filters are listed in Table 4 and Table 5, respectively. All data regarding the optical setup has been acquired from Roßberger [46].

A schematic of the setup is shown in Fig. 3. The beam expander in the SMLM light path served to focus

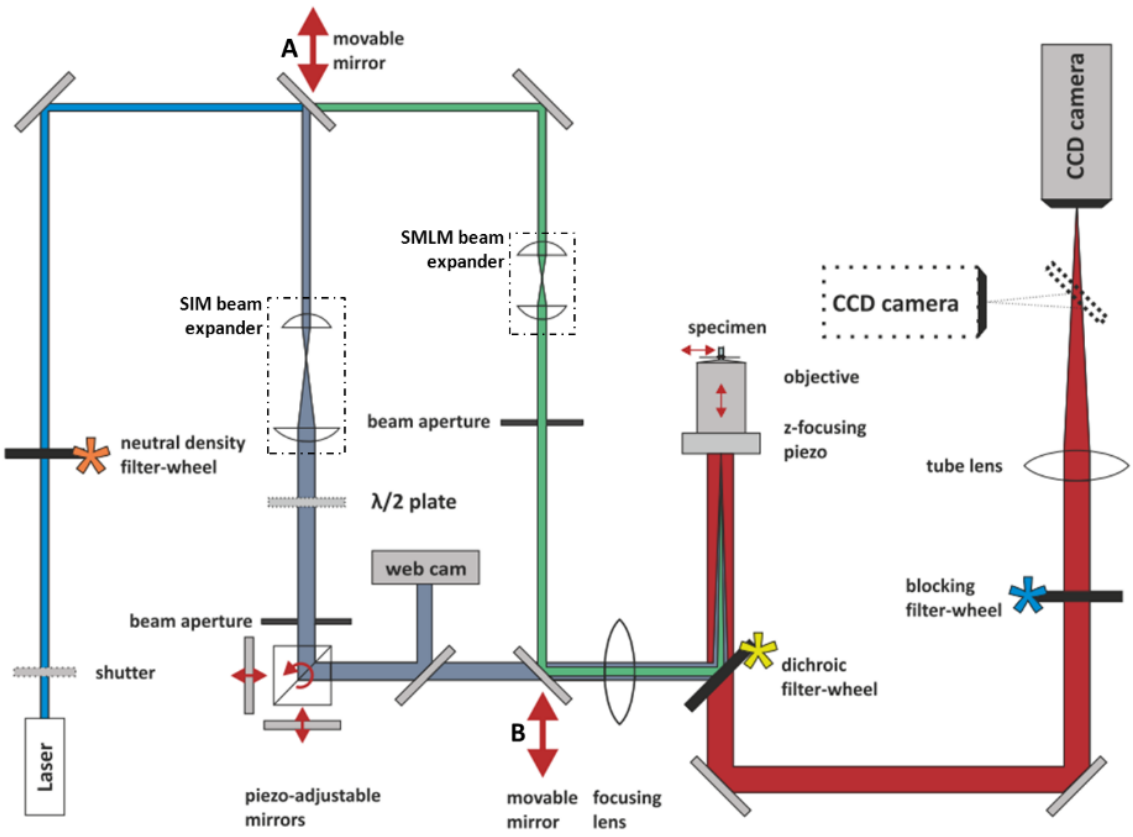

Figure 3: Optical Setup: Four different laser frequencies could be individually selected by custom built shutters, and their intensities were regulated by a neutral density filter-wheel (orange asterisk). The movable mirror A allowed to switch between a beam path used for Structured Illumination and a path for SMLM. A focusing lens served to focus the excitation light onto the specimen, and a tube lens projected the fluorescence light onto the CCD-camera. A dichromatic splitter filter-wheel (yellow asterisk) and blocking filter-wheel (blue asterisk) allowed wavelength specific separation of excitation and emitted light. From [47]

the beam on a smaller field of illumination, resulting in greater light intensities on the sample as compared to the SIM path. Even though no SIM measurements were taken for this work, the optical path was used to take wide-field overview images without bleaching the fluorophores before a measurement.
For easy adjustment, the focusing lens (VIS ARB2, d = 31.5, f = 300) was mounted on a x-z-translation system (QiOptiq Photonics, Goettingen, Germany). The light was focused on the objective (HCX PL APO 100x/1.4 oil, Leica, Wetzlar, Germany) from which it was refocused into the sample plane. For coarse adjustment of focus, the objective was mounted on an adjust micrometer (G061061000, Qioptiq Photonics, Goettingen, Germany). An additional focusing element (P-725.1CD, 100μm, pfoc, Physik Instrumente (PI), Karlsruhe, Germany) allowed for fine adjustment of focus.

The dichromatic edge-filters, see Table 4, served to split the excitation from the emission light. The excitation

Wavelength [nm]	Power [mW]	Type	Model	Manufacturer
405	150	DPSS	n/a	BFi Optilas, Dietzenbach, Germany
488	200	DPSS	Coherent Sapphire 568 HP	Coheren, Dieburg, Germany
568	200	DPSS	Coherent Sapphire 568 HP	Coheren, Dieburg, Germany
671	300	DPSS	VA-I-300-671	Beijing Viasho Technology Co. Ltd, Beijing, PRC

Table 3: List of available lasers

Wavelength [nm]	Model	Manufacturer
405	Di02-R405	Semrock, Rochester, NY
488	Di02-R488	Semrock, Rochester, NY
568	Di02-R568	Semrock, Rochester, NY
680	Q680LP	Semrock, Rocherster, NY

Table 4: Dichromatic Filters

Wavelength [nm]	Model	Manufacturer
405	BLP01-405	Semrock, Rochester, NY
488	BLP01-488	Semrock, Rochester, NY
568	BLP01-561	Semrock, Rochester, NY
690	LP XF 3104	Omega Optical, Olching, Germany

Table 5: Emission Filters

light was reflected into the objective and illuminated the sample, which was mounted on a microscope table (for Nikon Eclipse TI and TE 2000, 00-24-437-0000, Maerzhaeuser, Wetzlar, Germany) on top of a custom built invar (Fe65Ni35) stage (Fig. 4). The emitted fluorescence light was transmitted through the dichromatic filter after passing through the objective. Emission filters (see Tab. 5) were placed in front of the CCD-camera (Sensicam QE, PCO, Kelheim, Germany) to filter all remaining excitation light. To fully automate the setup, the dichromatic filters were mounted on a filter wheel (CDFW5/M, Thorlabs, Munich, Germany) operated by a stepper motor (P430 258 005 01, Portescap, La Chaux-de-Fonds, Switzerland). Similarly, the emission filters were mounted on a motor driven filter wheel (FW102C, Thorlabs, Munich, Germany). The microscope table was controlled by a commercial controller (mc2000, Maerzhaeuser, Wetzlar, Germany). All parts were operated by a custom developed software, see Roßberger [46].
The setup can be further extended by implementing a second CCD-camera and an additional dichromatic filter, similar to the setup described by Baddeley et al [8].

III.3 Image Acquisition

The custom made program PYME Acquire was used to operate the microscope and collect data [see 46]. A screenshot of the interface of the software is shown in Fig. 5. As described in Chapter II.2, SMLM requires a stack of images to calculate individual signal positions from spatially separated PSFs. Thus, a series of 2000 images was taken for every recording. Each image was recorded with an integration time of 50 ms and saved into a .h5 file for further processing.
Before starting a measurement, a region of interest (ROI) was defined. The size and position of the ROI was determined by the laser focus on the sample: the center of focus for both, the 488 nm and the 568 nm laser, was selected to assure homogeneous and high intensity illumination for both wavelengths. To find appropriate cells for recording, the DAPI staining and the 405nm laser was used in SIM-mode. In SIM-mode, the laser focuses on a larger area, thus the intensity on the sample is lower to prevent untimely bleaching of the fluorophores. After a location was selected, overview images for the three channels 405 nm, 488 nm and 568 nm were taken in wide-field to help with the interpretation of the localization data. The focus was selected in the 488 nm channel to assure that the structures of interest were in the focus plane, rather than the DAPI-stained cell nuclei.
Every recording was started in the 568 nm channel, because lower energy light does not induce photo bleaching for the 488 nm fluorophores. A wait time of 5 to 10 seconds between switching to SMLM-mode and the start of

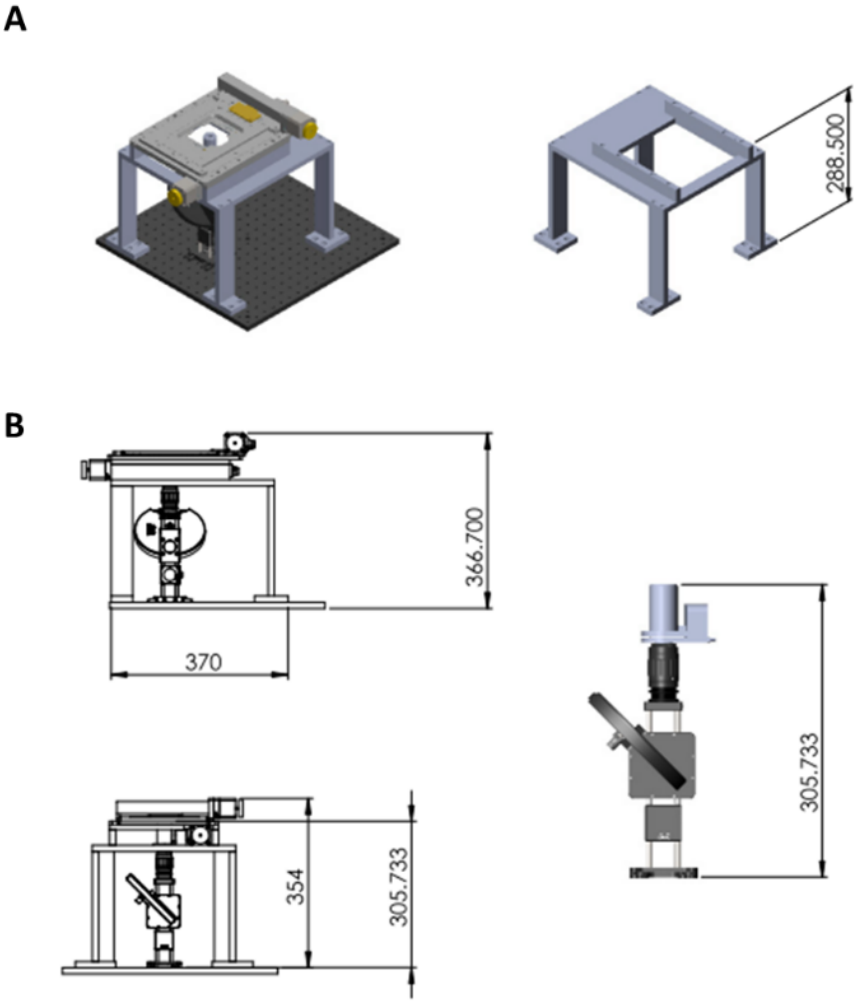

Figure 4: Microscope stage
A: 3D-schematic of custom built invar stage with microscope table (Maerzhaeuser) mounted on top. The stage was designed to implement a dichromatic filterwheel, a manual focus adjustment micrometer, a software-controlled fine adjustment unit and the objective into the setup.
B: Side view.
All length dimensions in mm.
From [46]

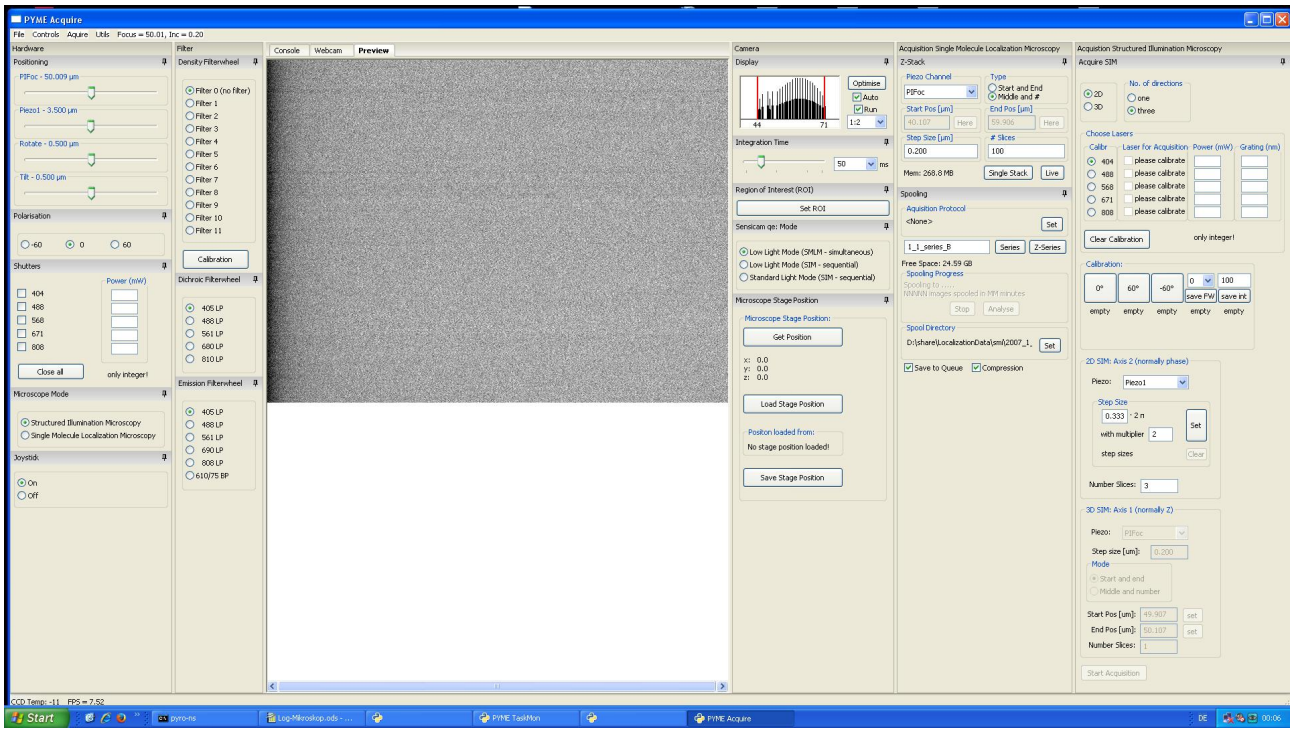

Figure 5: Pyme Acquire user interface: Picture acquisition was performed with a custom developed software called Pyme Acquire. Fine adjustment of focused could be done using the PIFoc option. Laser shutters could be individually opened and closed and different filter positions could be selected using the software. A switch between SIM and SMLM beam path was implemented in the interface and the spooling directory for recordings was selected before each measurement. Other options in the user interface were for the purpose of Structured Illumination Microscopy and therefore were not needed for recording of localization images.

the recording was implemented to allow for adequate photo bleaching before starting the measurement. After 2000 images had been taken in the 568 nm channel, the system was switched into the 488 nm channel and the same procedure was applied.

III.4 Data Analysis

III.4.1 Signal Position

In order to calculate the signal positions from the image stack, an algorithm called fastSPDM developed by Grüll et al. [48] was used. The algorithm is illustrated in Fig. 6, and the individual steps can be described as follows:

1) Firstly, the background for each image in the stack is calculated (see Fig. 6A). The background can be described by a Poisson distribution with the width $\sigma_{N_B} = \sqrt{N_B}$. A homogeneous background can be assumed because changes in background intensity are small relative to the intensities of the blinking fluorophores. N_B is described by:

$$N_{B,t} = N_{B,t-1} + \frac{1}{N}(min(Img_t - N_{B,t-1}, \sigma_{N_{B,t-1}})) \tag{5}$$

with $N_{B,t}$ the background intensity of an image on position t in the image stack; Img_t the intensity of image t; $\sigma_{N_{B,t-1}}$ the maximal allowed change in background intensities between adjacent images and $\frac{1}{N}$ the smoothing factor.

The intensities are smoothed with N greater than the average number of images with blinking events. The change in background intensity is limited by $\sigma_{N_{B,t-1}}$ such that blinking events don't influence the

Treatment Solution	Slice Number	No. of Recordings	Staining 488nm	Staining 568nm
BPDF (BicaVera)	1	25	Claudin5	Claudin2
	2	25	Occludin	Claudin2
	3	25	Occludin	Claudin5
BPDF + 8mM alanyl-glutamine	4	25	Claudin5	Claudin2
	5	25	Occludin	Claudin2
	6	25	Occludin	Claudin5
CAPD	7	25	Claudin5	Claudin2
	8	25	Occludin	Claudin2
	9	25	Occludin	Claudin5
CAPD + 8mM alanyl-glutamine	10	25	Claudin5	Claudin2
	11	25	Occludin	Claudin2
	12	25	Occludin	Claudin5
PBS	13	25	Claudin5	Claudin2
	14	25	Occludin	Claudin2
	15	25	Occludin	Claudin5
	16	5	Claudin2	Claudin5
	17	5	Claudin2	Occludin
PBS + 8mM alanyl-glutamine	18	25	Claudin2	Claudin5
	19	25	Claudin2	Occludin
	20	25	Claudin5	Occludin

Table 6: List of samples: Three different treatment solutions have been analyzed with different staining. For each staining, two of the three membrane proteins Claudin2, Claudin5 and Occludin were labeled. For every sample, additionally the cell nuclei were stained with DAPI solution to help with the interpretation of the data.

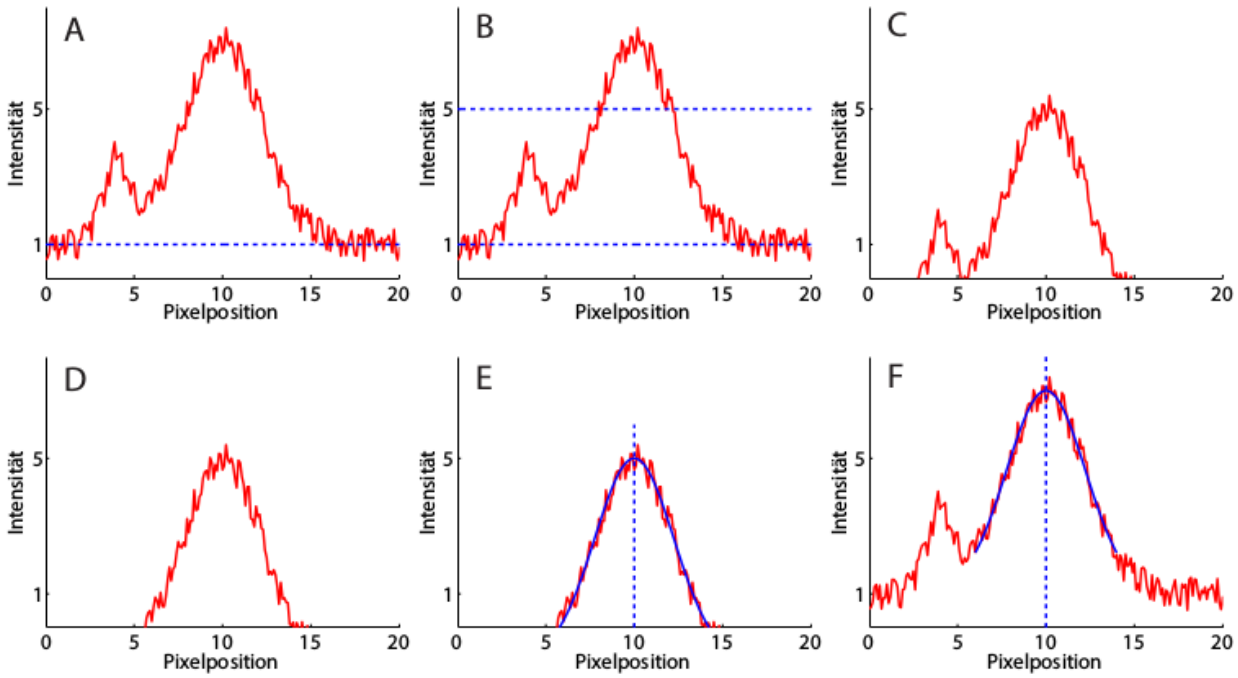

Figure 6: fastSPDM algorithm:
x-axis: Position in pixel; y-axis: Intensity. Shows intensity profile of a fictional 1D-image in an image stack.
The signal is processed by **A**: Determination of the background intensity σ_{N_B}; **B**: Signal detection with threshold factor; **C**: Subtraction of $2\sigma_{N_B}$; **D** Finding other local maxima and setting them to zero; **E**: Applying a Gaussian fit to the intensity; **F**: Shows the fitted center maximum in the initial intensity profile.
From Krufczik [12]

background intensity too much.

2) In order to be detected as a blinking event, the maximum intensity of a signal has to be above a threshold $k = n \cdot N_{B,t}$, as can be seen in Fig. 6B. Typical values for this threshold factor n are between 3 and 5.

3) The background is subtracted from the signal: Each image of the stack has a rectangular shape in x and y direction. Ideally, the PSF of the signal lies completely within this rectangle (region of interest, ROI). To minimize the impact of the size of the ROI on the localization accuracy, $2\sigma_{N_B}$ is subtracted from every intensity value and all negative intensities are set to zero.

4) It is possible that the PSF of two blinking events are overlapping. To prevent this from influencing the fit accuracy, the signal is scanned for local minima starting from the center maximum. All intensities behind a local minimum are set to zero. To prevent noise from being detected as a local minimum, a tolerance of σ_{N_B} is implemented.

5) A Gaussian (eq. 6) is fitted to the signal to calculate the center maximum $\vec{\mu}$ and the standard deviation $\vec{\sigma}$. Additionally, the localization accuracy $\Delta\mu_x$ can be calculated according to equation 10, with q_i the intensity of the pixel i:

$$f(\vec{x}) = \frac{Q}{2\pi\sigma_x\sigma_y} e^{-\frac{(\frac{x-\mu_x}{\sigma_x})^2+(\frac{y-\mu_y}{\sigma_y})^2}{2}} \tag{6}$$

$$Q = \sum q_i \tag{7}$$

$$\vec{\mu} = \sum \frac{q_i}{Q} x_i \tag{8}$$

Column	Contents of Signal Matrix
1	Signal amplitude (number of photo-electrons)
2	lateral y-coordinate [nm]
3	lateral x-coordinate [nm]
4	Uncertainty of y-coordinate [nm]
5	Uncertainty of x-coordinate [nm]
6	Standard deviation of Gauß-Fit in y-direction [nm]
7	Standard deviation of Gauß-Fit in x-direction [nm]
8	Number of photo-electrons in the signal
9	Position of images in the stack in which the signal has been detected

Table 7: Contents of signal matrix returned by the signal detection algorithm

$$\sigma_x^2 = \sum (x_i - \mu_x)^2 \frac{q_i}{Q} \tag{9}$$

$$\Delta\mu_x = \sqrt{\frac{1}{12Q} + \sum (\frac{x_i - \mu_x}{Q})^2 (q_i + N_B)} \tag{10}$$

A more detailed description of this algorithm can be found in the PhD thesis of Matthias Krufczik [12].

III.4.2 Image Reconstruction

The signal detection software (see chapter III.4.4) returns a matrix that contains information about the signal positions, uncertainties and additional information [12]. An overview over the contents of the matrix is given in Table 7.

Other than in conventional light microscopy, the information gathered with SMLM is not directly returned as a picture. However, for some applications it is useful to convert the information into images in order to interpret structural features. The two most important methods used in this work for constructing images from the coordinate-matrix are discussed below:

1) **Standard image** : A coordinate grid is generated and every signal is mapped according to its x and y coordinates. Every pixel in the grid then has a value that corresponds to the number of signals within the area of that pixel. Additionally, the image is blurred with the localization uncertainty. As the generated grid theoretically allows for an infinite resolution, a standard image can be used to display the maximum resolution of the SMLM-technique. However, this often results in images with many separated point like signals, making it hard to identify larger structures. Standard images are useful when zooming in to small structures because they can make use of the full resolution of SMLM.

2) **Density image** : The density can be calculated as follows: for every point P_i, the number of signals within a circle with the center P_i and radius r are counted, see Fig. 7. Similar to the Standard image, a grid of pixels is created for the density image. Each pixel with a density $\rho_i > 0$ then serves as the center of a Gaussian with standard deviation σ, as in equation 11.

$$h_i(x_i, y_i) = \rho_i \cdot \frac{1}{2\pi\sigma^2} e^{-\frac{x_i^2 + y_i^2}{2\sigma^2}} \tag{11}$$

with h the intensity of the pixel for color-coding. The final image is created by linearly adding all of the

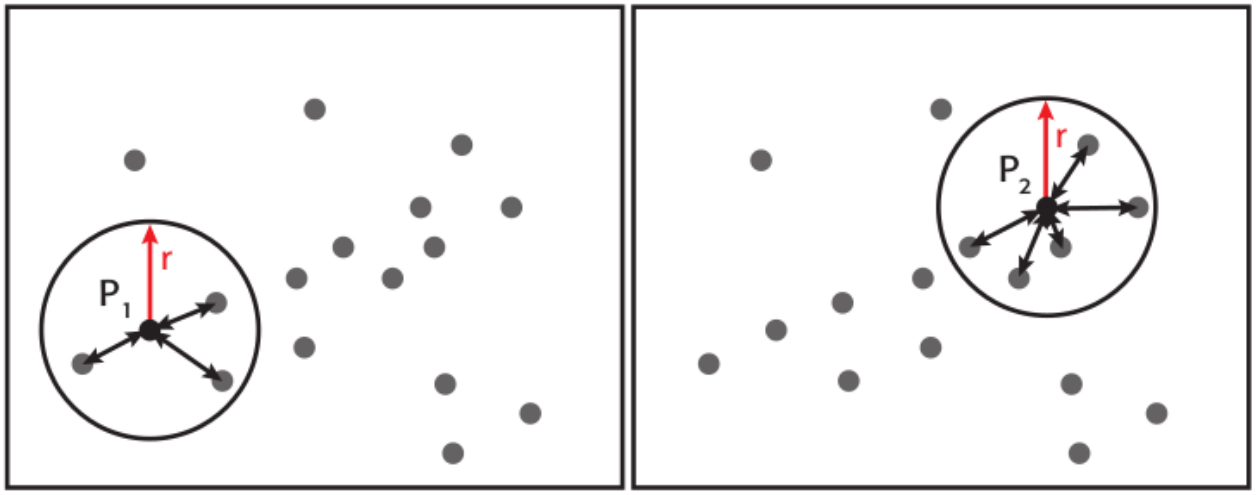

Figure 7: Calculation of density: Every point P_i is the center of a circle with radius r. The density of point P_i corresponds to the number of signals within that circle. In this example, the density is $\rho(P_1) = 3$ and $\rho(P_2) = 5$.

blurred densities.

Density images are useful to visualize larger structures and help with the interpretation of the acquired data. However, because of the Gaussian blurring and overlap of signals, information is lost and the resolution is lower than the maximal resolution of SMLM.

Additionally to standard and density images, wide field images of the target structures have been taken before every SMLM-measurement, as described in chapter III.3. These three types of images are sufficient to visualize larger and small structures and thus are crucial for the interpretation of the acquired data.

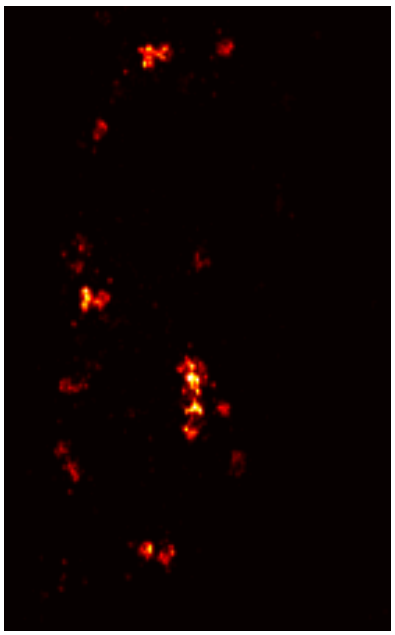

Figure 8: Density image

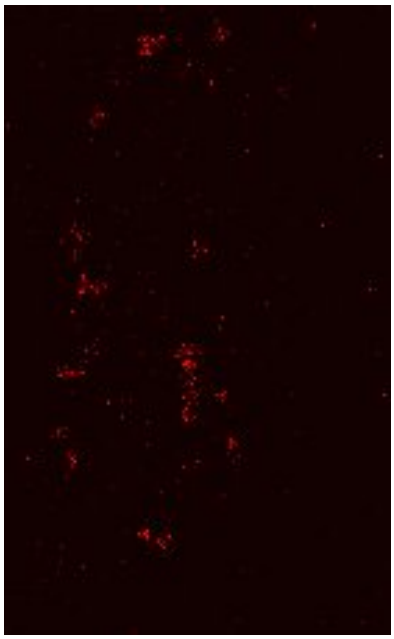

Figure 9: Standard image

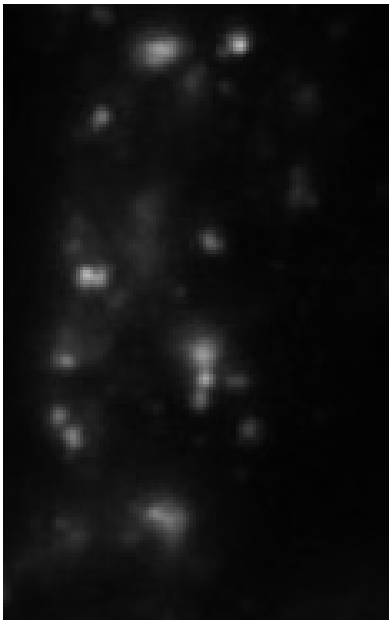

Figure 10: Widefield overview image

III.4.3 Distance Analysis

A useful and important tool to further analyze the spatial distribution of targets in a sample is by examining the distances between signals. In this regard, SMLM offers many advantages over conventional microscopy, the most prominent being that the signal coordinates are known on a nanometer scale to begin with. In distance analysis, all distances between signals are calculated. This allows to check the frequency of occurrence of specific

distances. Even small changes in spatial distribution can be detected and visualized using distance analysis tools, revealing additional information about the structure.

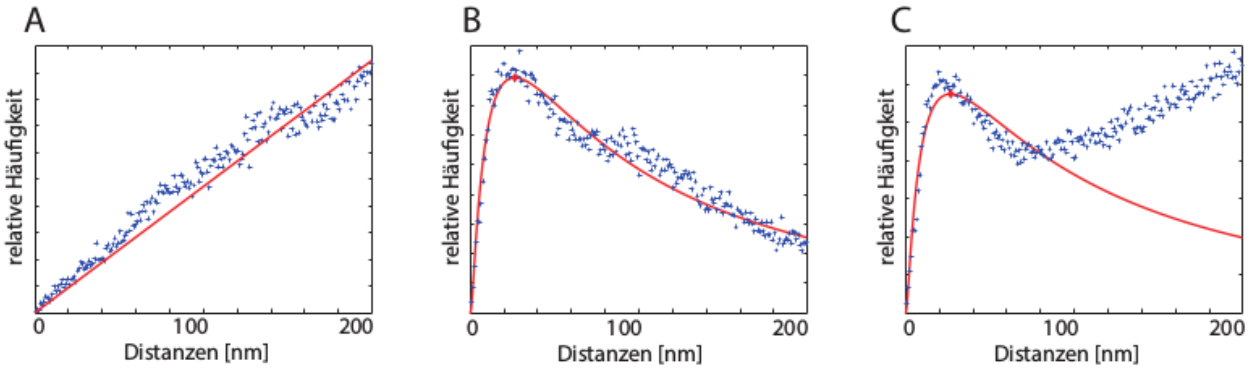

Figure 11: Distance Analysis: x-axis: relative frequency of occurrence; y-axis: distance in nm
Three common distributions in distance analysis are a linear dependency between frequency of occurrence and distance (***A***), a log-normal distribution (***B***) or a combination of linear and logarithmic dependencies (***C***)

Figure 11 gives an overview over typical distance distributions in a sample:

A) In case of a random distribution of the targets, a linear dependency between relative frequency of occurrence and distance is expected: $f(x) = mx$, see Fig. 11A. In the 2-D plane of an image, all signals with the same distance d to a point $\vec{p}$ are on a circle with radius r = d around $\vec{p}$. The circumference of a circle grows linearly with the radius, thus for a random target distribution, the same applies to the number of targets on the circle.

B) Most structures with a characteristic distance can be described by a log-normal distribution: $f(x) = A \cdot e^{\frac{(ln(x)-b)^2}{c^2}}$ with A the amplitude of the maximum, e^b the position of the maximum and c the width of the distribution, see Fig. 11B. Fitting this function to the data allows to compare characteristic distances of different samples on a nanometer scale.

C) In many cases, the distance distribution in a sample will be a combination of linear and logarithmic dependencies, as displayed in Fig. 11C. This is due to the fact that many characteristic distances are on a small scale (40nm - 100nm). When looking at the target distribution on a larger scale, the sample appears homogeneous. Thus, in order to accurately fit the characteristic distance, only data up to a specific distance D must be taken into account. The linear dependency for higher distances does not contain any additional information and therefore doesn't need further analysis.

III.4.4 Software

Two programs based on Matlab were used for most of data analysis:

1) **startSPDM**: startSPDM is a software that reads .h5 files and returns a matrix containing signal positions and additional information, as listed in Table 7. Furthermore, the program returns a histogram with localization accuracies on the x-axis and corresponding number of detected signals on the y-axis (Fig. 14. Two localization pictures are generated from the signal position matrix by startSPDM: a loc_scaled file where all signals are blurred with the corresponding localization accuracy and a loc_NN file, where the distance to the nearest neighbor is used as width for the normal distribution that represents the signal [49]. This ensures that structural features are easier to identify as signals will always intersect, thus brightening the image. As of now for this work, the term localization image will refer to the loc_NN files (example

in Fig. 15). The program is based on the algorithm described in Chapter III.4.1 and the localization accuracy is calculated according to Chapter II.2.3. Thus, the program requires the camera pixel size as an input. Other parameters that can be adjusted are the threshold factor for signal detection and the image pixel size for the generated images.
For this work, a threshold factor of 3 was used for every Claudin5 and Occludin staining, and a threshold factor of 5 was used for every Claudin2 staining. A screenshot of the startSPDM GUI can be seen in Fig. 12.

2) **Chromatinanalyse**: Chromatinanalyse is a custom developed software with the goal to automatize quantitative analysis of SMLM-data. The program takes a list of signal position matrices (as given by startSPDM) as input and returns a number of images and plots for both, individual recordings as well as the test series as a whole. The pixel size of generated images and the length of a test series can be adjusted in a GUI (Fig. 13). Additionally, the program allows customization of various tools for further analysis. The following operations have been performed for this work with Chromatinanalyse:

   - Density images: For every recording, a density image was created. For this work, the radius for the density calculation was set to 1000 nm, the standard deviation of the Gaussian blurring was set to 50 and a pixel size of 10 nm/pixel was chosen for image creation.
   - Standard image: A standard image was created for every recording.
   - Distance analysis: Distance analysis as described in Chapter III.4.3 was performed for single recordings and for the test series as a whole. The binning size, maximal distance considered for analysis and cut-off distance for the log-normal fit were adjusted according to the experiment. For most test series, the range of 0 to 200 nm was analyzed with 200 histogram bins. The maxima of all fitted log-normal distributions of a test series were plotted into boxplots for comparison.
     Four different methods were implemented for distance analysis of the test series as a whole:
     * As all distances have been calculated and summarized in histogram bins for every individual recording, one way of visualizing the distance distribution for the whole test series is by appending all results of single recordings into the same histogram. The disadvantage of this method is that measurements with high signal numbers will be weighed more than recordings with low signal detection. As of now, this method will be referred to as "Distance Analysis: All Distances" in this work.

     * To norm the y-scale, the number D_j of signals with distance x_j in histogram bin j can be divided by the overall number of calculated distances $D = \sum_j D_j$ of the series. This still leaves the individual recordings of the series weighed unevenly, but makes comparison of different series more convenient. This method will be referred to as "Distance Analysis: Norm".

     * Instead of adding all the numbers $d_{j,i}$ of recording i and histogram bin j, and average can be calculated:
       $d_{j,average} = \frac{1}{N} \sum_i d_{j,i}$, with N the number of individual recordings per test series. This method is particularly advantageous when characteristic distances are fluctuating but signal numbers of individual recordings are comparable, or if the number of recordings per series is different ("Distance Analysis: Norm 2").
     * Another way of calculating an average is by:
       $d_{j,average} = \frac{1}{N} \sum_i \frac{d_{j,i}}{D_i}$, with $D_i = \sum_j d_{j,i}$ the overall number of calculated distances for recording i. In this method, individual recordings are weighed independently of the number of signals, thus

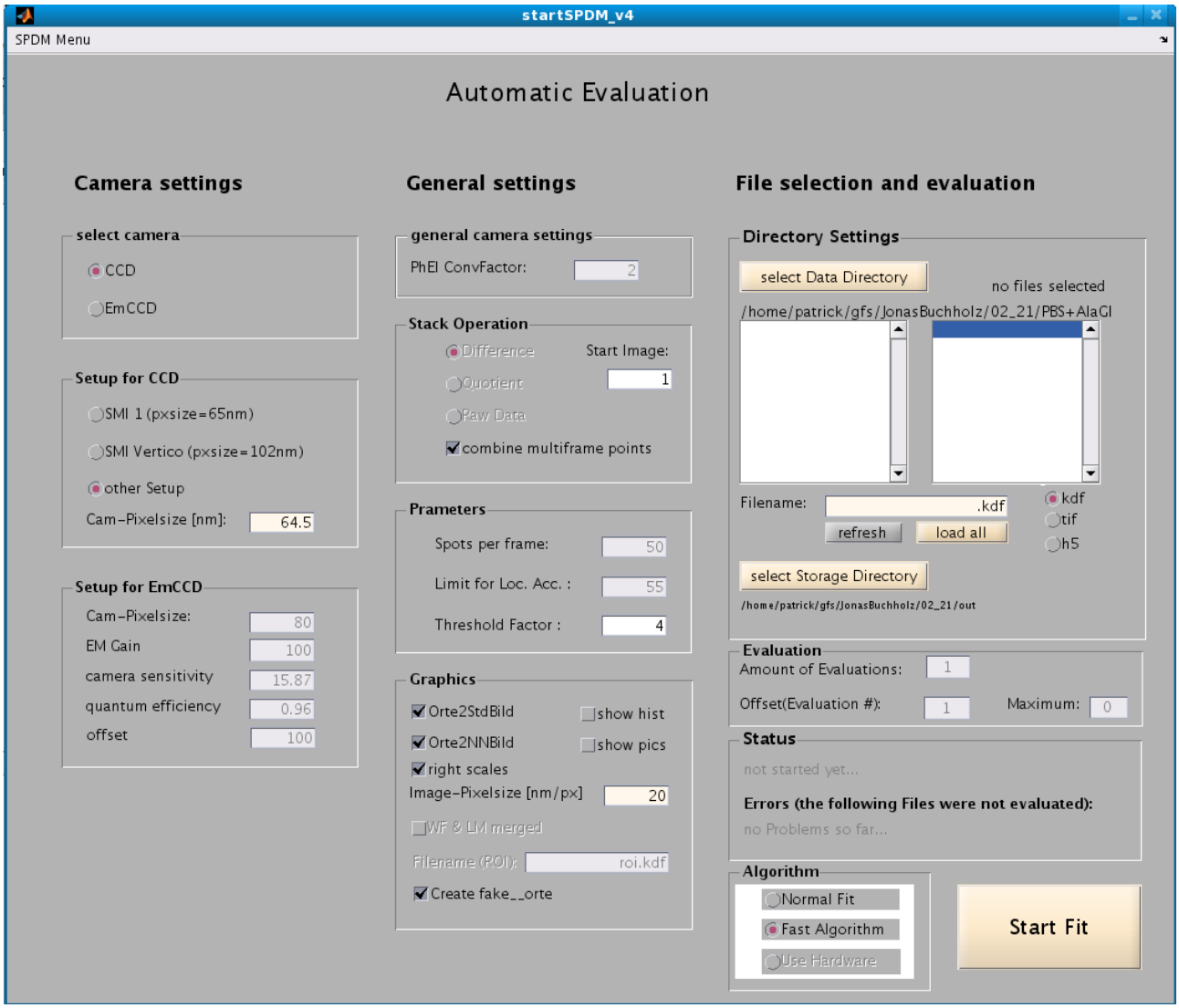

Figure 12: startSPDM GUI: The files for analysis can be selected with a GUI. Additional parameters include the camera pixel size (112 nm), the threshold factor, the image pixel size and a target directory for output files.

this method is useful for test series with a highly fluctuating signal number between individual recordings ("Distance Analysis: Norm 3").

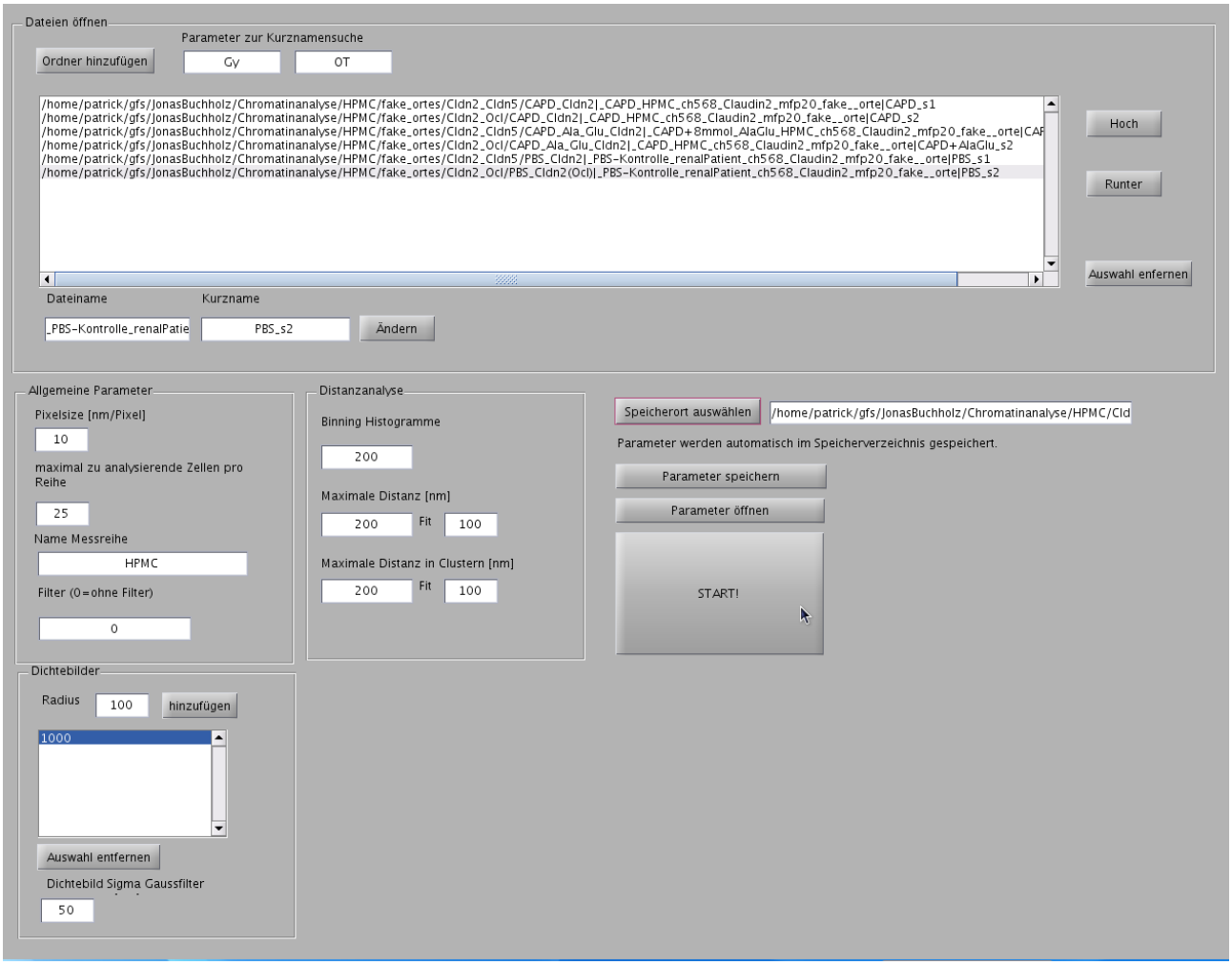

Figure 13: Chromatinanalyse GUI: GUI of the program Chromatinanalyse used for quantitative analysis of the localization data. Input parameters are the directories with .mat files of the analyzed test series, the radius for density calculations, the pixel size of generated images and the standard deviation for Gaussian blurring. Additional parameters are for distance analysis and include number of histogram bins and maximal distance for fits.

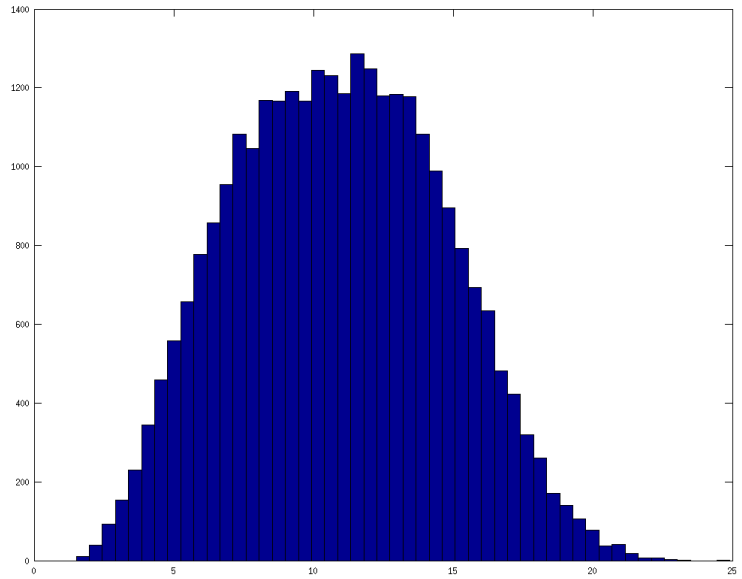

Figure 14: Localization Accuracy: x-axis: Localization Accuracy in nm; y-axis: Number of signals corresponding to the localization accuracy.
The histogram gives a good overview over the quality of the signal detection and fit.

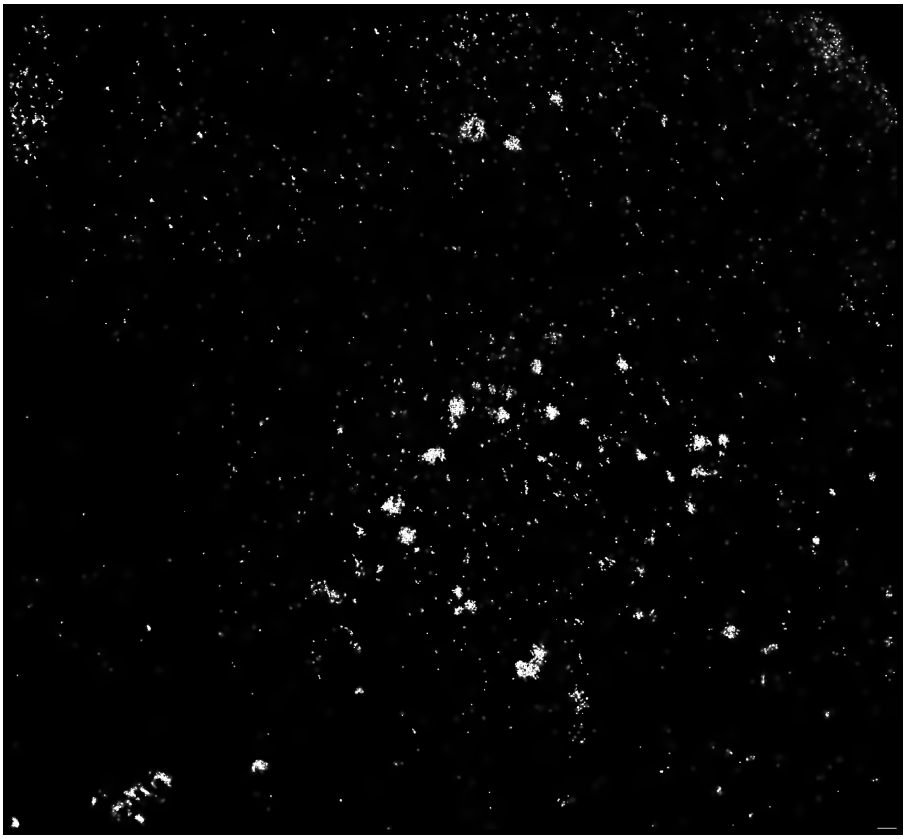

Figure 15: Generated loc_NN-image: Detected signal positions are mapped in a generated grid pattern. The image is useful for interpretation of the data and makes use of the full resolution of SMLM.

Treatment	Slice No.	Staining	Channel	Target	Signal Numbers	Loc. Accuracy [nm]
BicaVera	1	s1	568	Cldn2	43790 ± 5020	14 ± 5
BicaVera	1	s1	488	Cldn5	9330 ± 1110	31 ± 8
BicaVera	2	s2	568	Cldn2	23980 ± 2850	15 ± 5
BicaVera	2	s2	488	Ocl	12630 ± 660	33 ± 8
BicaVera	3	s3	568	Cldn5	12320 ± 830	30 ± 10
BicaVera	3	s3	488	Ocl	11790 ± 660	33 ± 8
BicaVera + AlaGln	4	s1	568	Cldn2	64210 ± 6420	14 ± 6
BicaVera + AlaGln	4	s1	488	Cldn5	18900 ± 713	31 ± 8
BicaVera + AlaGln	5	s2	568	Cldn2	48950 ± 4910	13 ± 5
BicaVera + AlaGln	5	s2	488	Ocl	9760 ± 700	33 ± 8
BicaVera + AlaGln	6	s3	568	Cldn5	10930 ± 734	30 ± 10
BicaVera + AlaGln	6	s3	488	Ocl	6460 ± 340	33 ± 8
PBS	13	s1	568	Cldn2	112370 ± 10190	14 ± 5
PBS	13	s1	488	Cldn5	21780 ± 1200	31 ± 8
PBS	14	s2	568	Cldn2	69240 ± 4380	13 ± 6
PBS	14	s2	488	Ocl	16450 ± 780	32 ± 8
PBS	15	s3	568	Cldn5	7550 ± 290	30 ± 11
PBS	15	s3	488	Ocl	7800 ± 220	32 ± 8

Table 8: Overview over signal numbers and localization accuracies of the analyzed samples: The slice numbers match the numbers in Table 6. The additional specification 'Staining' refers to which targets were stained together in a sample. As of now, s1 refers to Cldn2-Cldn5 targets, s2 refers to Cldn2-Ocl targets and s3 refers to Cldn5-Ocl targets. Total signal numbers were calculated by Chromatinanalyse, the mean and standard deviation were calculated using Python. The listed uncertainties were calculated by $\Delta = \frac{\sigma}{\sqrt{N}}$ with N the number of recordings in a test series. Similarly, a python script was used to calculate the mean and standard deviation of the localization accuracies of the test series as given by startSPDM.

IV Results

A complete list of the analyzed samples is given in Chapter III.3, Table 6.

IV.1 BPDF (BicaVera)

The effect of biocompatible peritoneal dialysis fluids (BPDF) on the spatial distribution of membrane proteins associated with tight junctions was analyzed. A set of 6 slices with BicaVera or BicaVera + alanyl-glutamine treatment were analyzed with SMLM. A control group of cells treated with PBS was used for comparison. For every treatment solution, 3 different stainings were performed, each of which marked two of the three transmembrane proteins Claudin2, Claudin5 or Occludin. An overview over the analyzed samples and their signal numbers and localization accuracies is given in Table 8.

IV.1.1 Claudin2

An overview over samples treated with different treatment solutions can be seen from Fig. 16 to Fig. 18. All images are localization images as returned by startSPDM. For interpretation, wide-field images of the cell nuclei are displayed above each image.

The difference in size and shape of the images is due to differences in the ROI while recording. For every

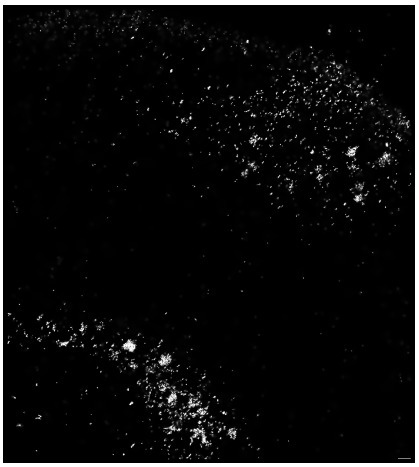

Figure 16: BicaVera (BPDF)

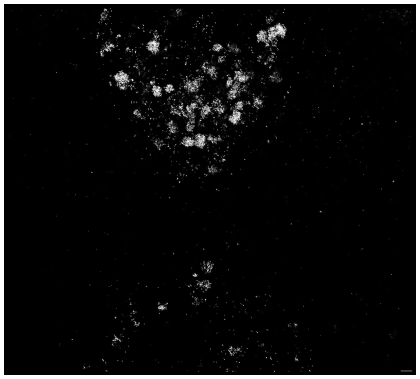

Figure 17: BPDF + AlaGln

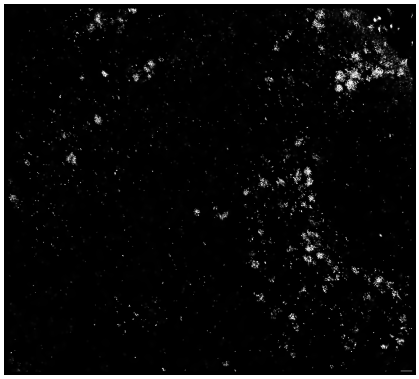

Figure 18: PBS-control

sample, a ROI was individually selected based on the laser focus on the sample. As a result, the recorded image frames show slight variations in size for samples from different measurements.

The density images of the above recordings are displayed from Fig. 19 to Fig. 21. For scale, a $1\mu m$ segment has been printed on the images. Comparing the density and localization images to the overview images, it appeared that the Claudin2 signals were primarily located outside of the cell nuclei.

For further analysis, Fig. 22 to Fig. 24 provide a zoomed-in view of high density areas in the localization images. Based on these exemplary images, a difference between the signal structure in the PD-fluid treated cells (Fig. 22) compared to the control group (Fig. 24) could be proposed:
The signals in the control group seemed to have appeared clustered with high signal numbers in individual clusters. In comparison, cluster size and signal number appear to have decreased in the cells treated with BicaVera. Treatment of cells with BicaVera and alanyl-glutamine solution led to a similar outcome as observed in the control group, as cluster size and number were comparable (Fig. 23 and Fig. 24).

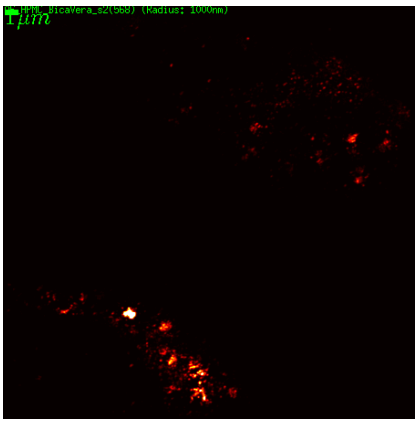

Figure 19: BicaVera (BPDF)

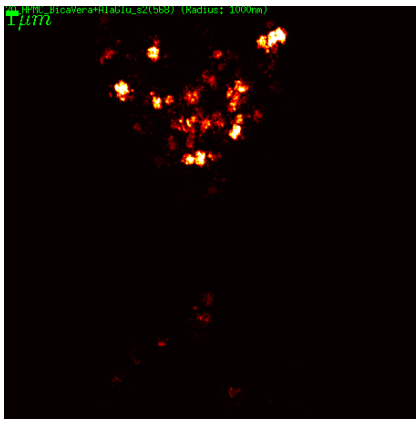

Figure 20: BicaVera + 8mmol AlaGlu

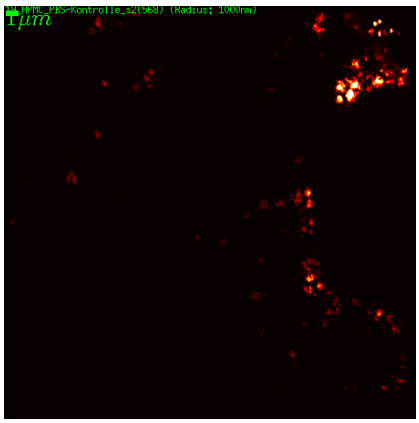

Figure 21: PBS-control

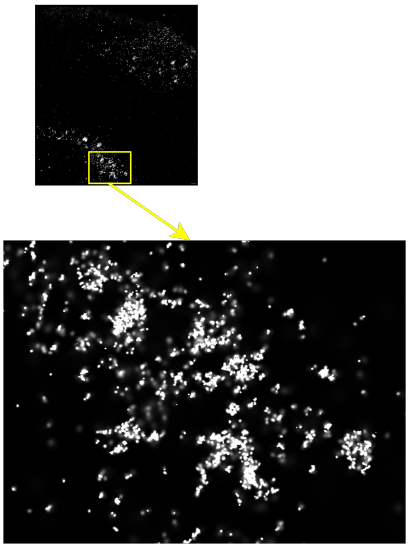

Figure 22: BicaVera (BPDF)

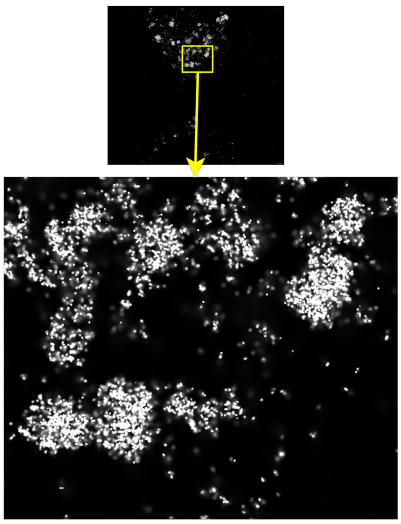

Figure 23: BicaVera + 8mmol AlaGlu

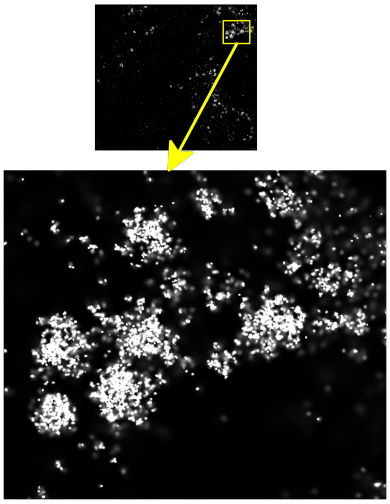

Figure 24: PBS-control

An overview over the signal numbers of different Cldn2 test series is given in Fig. 25. The names of the test series as displayed on the x-axis of Fig. 25 correspond to the treatment solutions, as described in Chapter III.1. For both, the s1 and the s2 staining, signal numbers decreased for the test series with cells treated with BicaVera as compared to the PBS-treated control group. The series treated with BicaVera with an addition of 8mMol AlaGln showed similar signal numbers to the control group. The results of the two stainings were comparable, however, signal numbers of the s2 test series were slightly lower than numbers of the s1 test series.

Distance analysis plots are shown from Fig. 26 and Fig. 27.
For Fig. 26, all distances between signals for all recordings of a test series have been plotted against the frequency of their occurrence. Naturally, the test series with the highest signal number showed the highest frequency of occurrence for close to all distances, as more signals could be taken into account for the calculation of distances.
The distances between signals corresponding to the same treatment but with different staining s1 or s2 showed similar characteristics (Fig. 26), but with a shift in frequency of occurrence of distances. This corresponded well to the signal numbers, as all test series with s1 staining expressed a slightly higher signal number compared to the s2 staining, with the two control groups having shown the most severe differences.

To get a better understanding of the changes in characteristic distances in the samples, the y-axis was scaled according to the signal numbers in a test series. Different methods of scaling have been discussed in Chapter III.4.4. As signal numbers were different for the individual test series, the "Norm 3" method provided a good overview and allowed for a comparison of characteristic distances in the differently treated samples. The Norm 3 distance analysis for all Claudin2 treatments is displayed in Fig. 27, with frequency of occurrence on the y-axis and distance between signals on the x-axis.
Test series treated with the same treatment solutions showed very similar characteristics. A smooth point of inflection in distance distribution at around 20 nm could be observed for both PBS control groups (Fig. 27). Another weak point of inflection could be observed at around 120 - 140 nm. The distance distribution of the test series with BicaVera treatment showed a much more pronounced point of inflection at around 20 - 30 nm before flattening and remaining straight. The BicaVera + alanyl-glutamine solution treatment showed characteristics that were very similar to the control group.
As discussed in Chapter III.4.3, a straight line in distance analysis plots corresponds to a random distribution

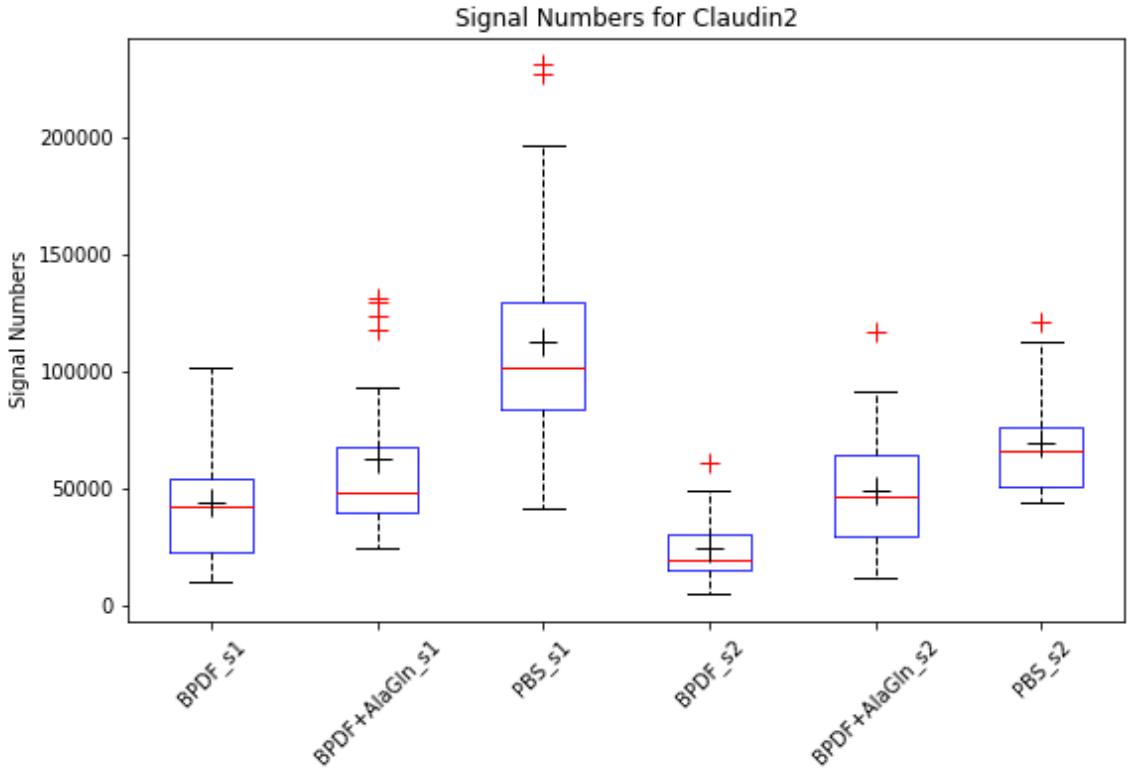

Figure 25: Number of Cldn2-signals:
Every box in the plot is representative of a test series. The y-axis corresponds to the number of signals detected by the registration algorithm in individual recordings. A box contains 50% of the recordings of the series and the dotted black line connects the maximal and minimal value of the series. The mean is represented by a black cross and the median is displayed as a red line. Values of individual recordings that are more than three times the length of the box away from the median are shown as red crosses. The names of the test series are displayed on the x-axis. All test series correspond to Cldn2 measurements, and the different treatment solutions are given by the name of the test series. The additional specifications s1 and s2 correspond to the staining, meaning that for s1, Cldn2 was stained together with Cldn5, and for s2, Cldn2 was stained with Ocl. A complete overview over the stainings is given in Table 6 in Chapter III.3.

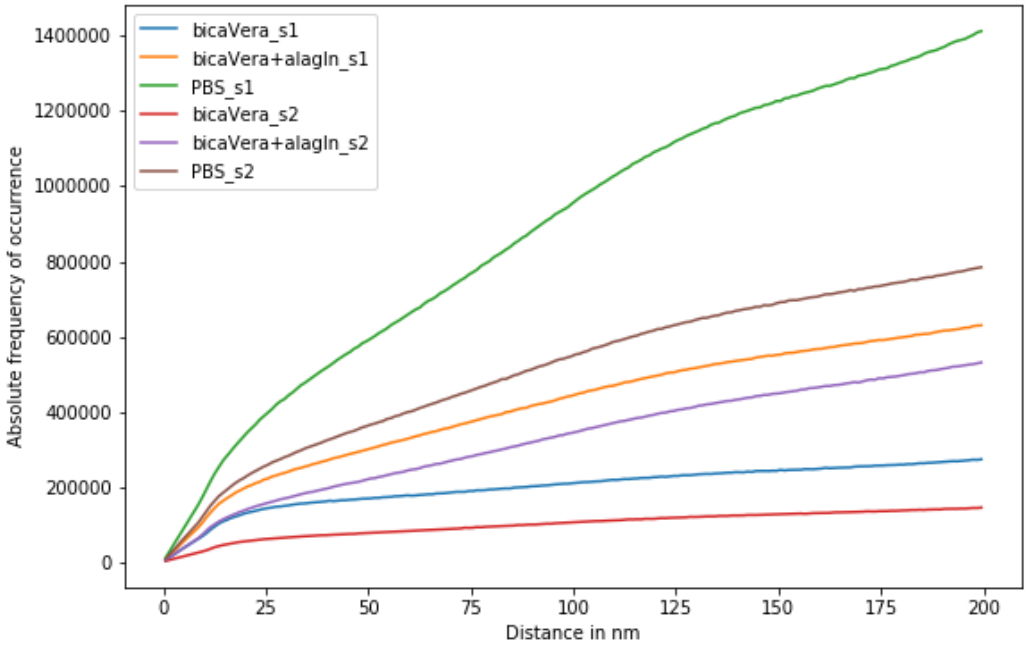

Figure 26: Distance analysis Cldn2: All distances.
For distance analysis, all distances between signals have been calculated and plotted against their frequency of occurrence, see Chapter III.4.4 for a detailed description. The y-axis gives how many times the corresponding distance occurred in a test series. On the x-axis are distances between 0 and 200 nm.

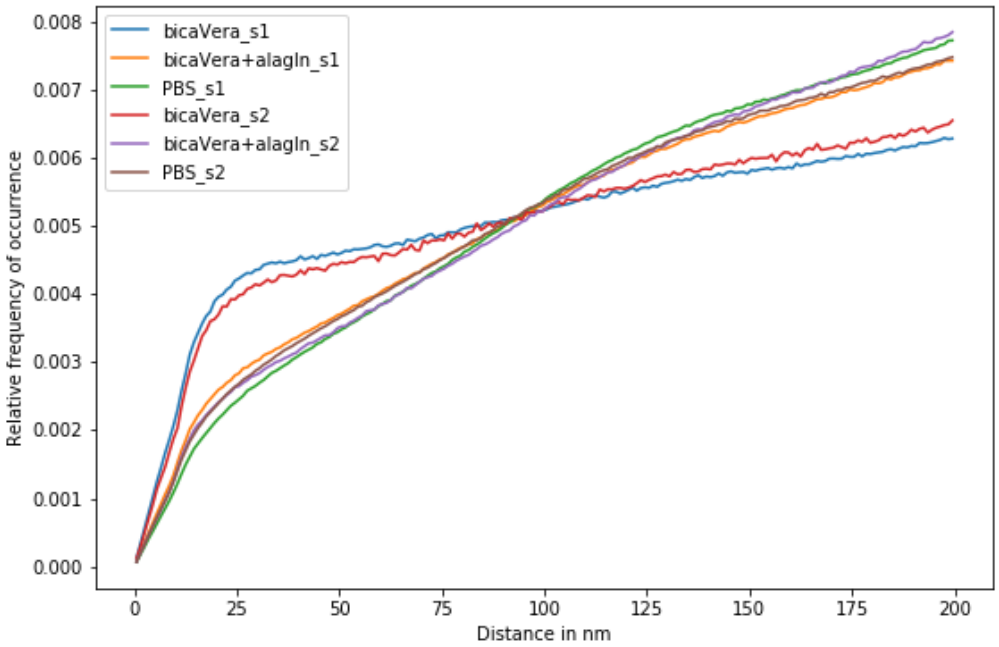

Figure 27: Distance analysis Cldn2: Norm 3
The relative frequency of occurrence of distances between 0 and 200 nm was calculated according to the Norm 3 method, see Chapter III.4.4. The y-axis gives the relative frequency of occurrence and the x-axis corresponds to the distances. This method is particularly useful when comparing test series with different signal numbers.

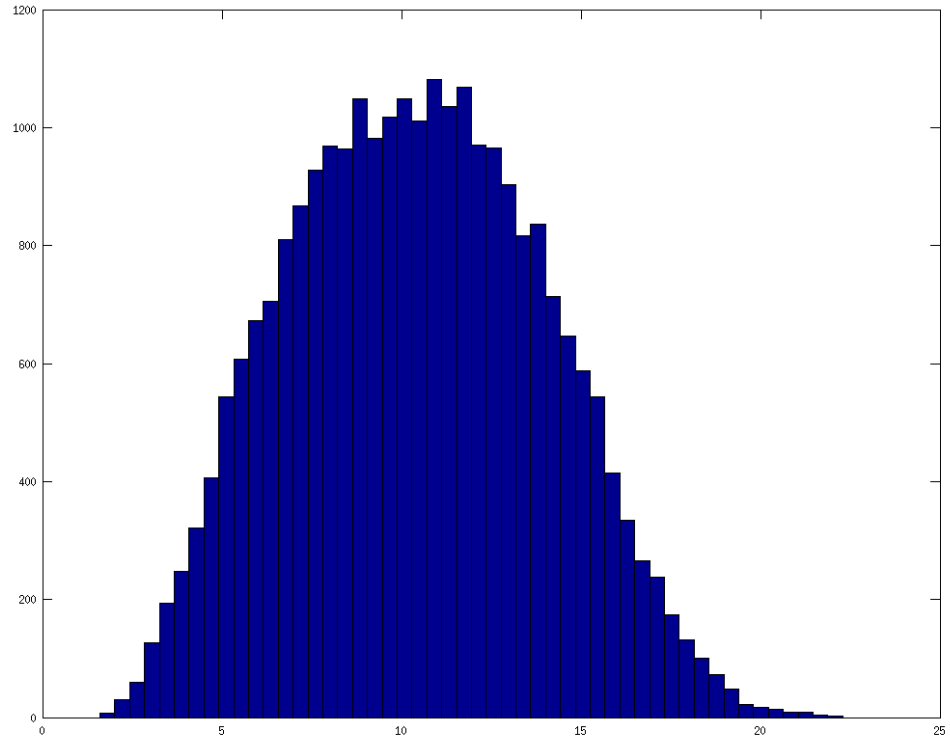

Figure 28: Localization Accuracy BicaVera (BPDF): Overview over the localization accuracies of a single exemplary recording. The x-axis gives the localization accuracy in nm and the y-axis shows the number of signals in the recording with the corresponding localization accuracy.

of signals, and most structures with characteristic distances can be approximated by a log-normal distribution. The very pronounced point of inflection for the BicaVera treated test series proposed a difference in spatial distribution of the Claudin2 proteins compared to the control group on a scale below the diffraction limit of conventional light microscopy. Since the characteristic distance for the BicaVera treatment seemed to be at around 20-30 nm, the target distribution appeared random when looking at larger distances. Thus, the distance analysis plot flattened to a straight line. The same applied to the other two treatments, but the much weaker points of inflection indicated a structural difference compared to the BicaVera treated samples. These differences could not fully be explained by the difference in cluster size and numbers as seen in Fig. 22 to 24, because the size of the clusters was much larger than 20 nm. From comparison of the localization images (Fig. 16 to Fig. 18) to the density images (Fig. 19 to Fig. 21), the diameter of clusters was determined to be in the range of about 1 μm.

Since the resolution of SMLM is bounded by a number of limiting factors, it was necessary to calculate the localization accuracy for the individual recordings. Every detected signal for every recording in every test series had a different localization accuracy, depending on different factors as discussed in Chapter II.2.3. The localization accuracy distribution for three exemplary recordings are shown in Fig. 28 to Fig. 30. Other recordings from the test series showed very similar localization accuracies. As the localization accuracy for most signals was below 20 nm, it is reasonable to assume that the resolution was sufficiently high to analyze the characteristic distances found in Fig. 27.

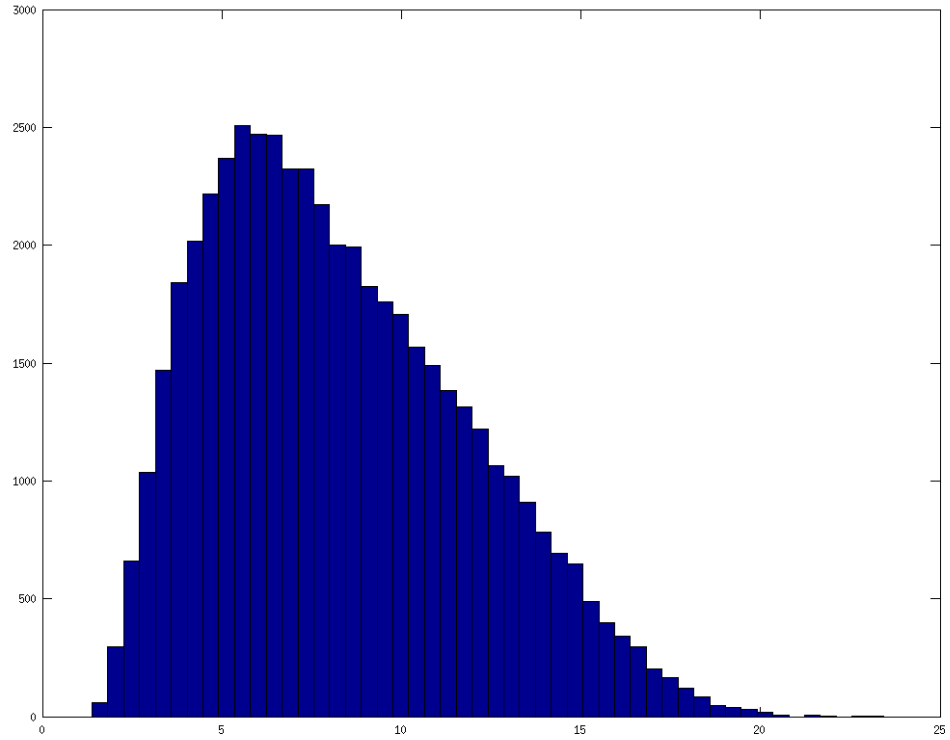

Figure 29: Localization Accuracy BicaVera + 8mmol AlaGln: The x-axis gives the localization accuracy in nm and the y-axis gives the number of signals with the corresponding localization accuracy for the exemplary recording.

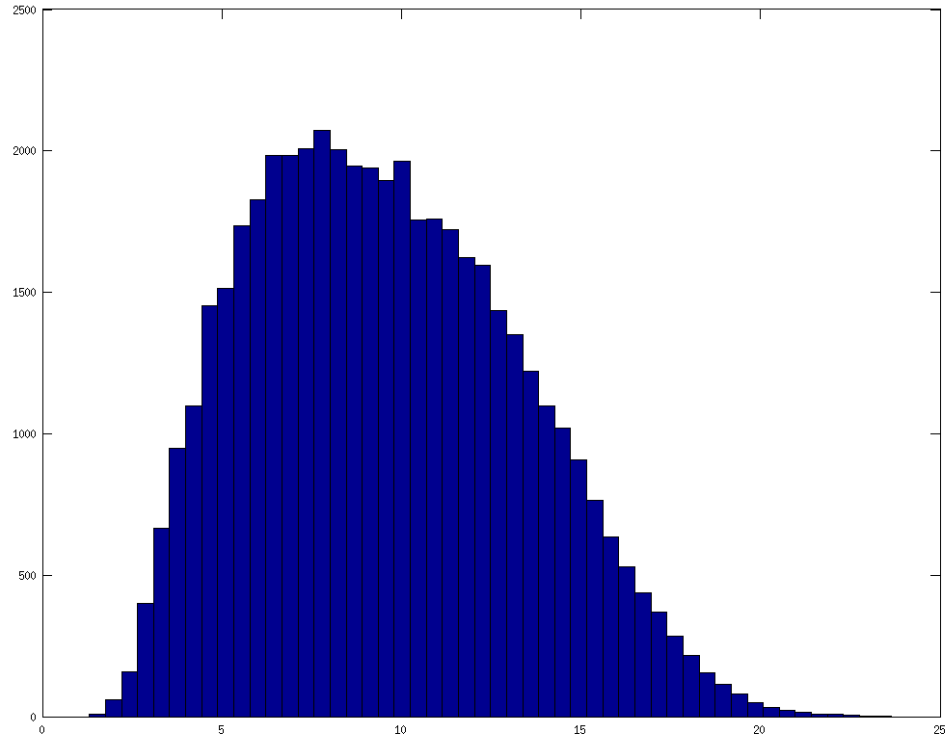

Figure 30: Localization Accuracy PBS-control: localization accuracy in nm on the x-axis and number of signals on the y-axis.

IV.1.2 Claudin5

Similarly to Claudin2, the Claudin5 protein was stained in human peritoneal mesothelial cells treated with different dialysis fluids. For Claudin5, two different stainings were performed: depending on the sample and the other stained protein, Alexa Flour488 or Alexa Flour568 was used. As of now, the type of staining will be related to as Ch. 488 or Ch. 568 in image descriptions.
To give an overview over the Claudin5 distribution in cells treated with BicaVera and BicaVera + alanyl-glutamine as compared to the control group, three exemplary recordings have been selected. The localization images and corresponding wide field overview images are shown in Fig. 31 to Fig. 33.

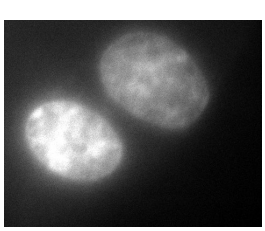

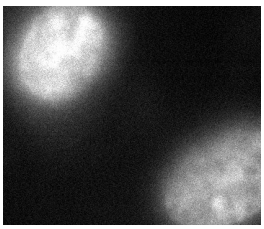

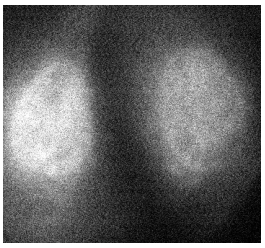

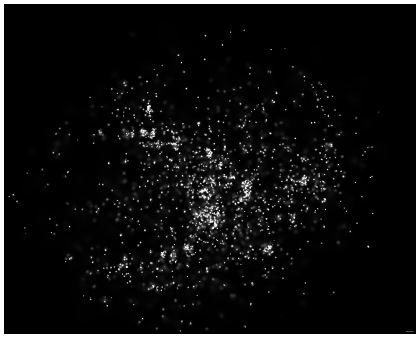

Figure 31: BicaVera (BPDF) Cldn5: Ch. 488; Localization Image

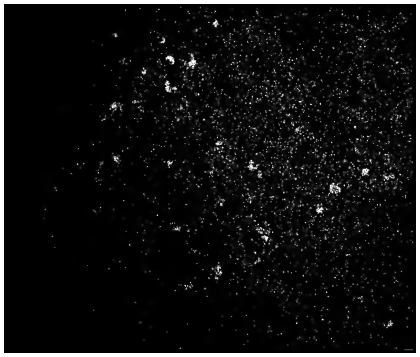

Figure 32: BicaVera + 8mmol AlaGln Cldn5: Ch. 488; Localization Image

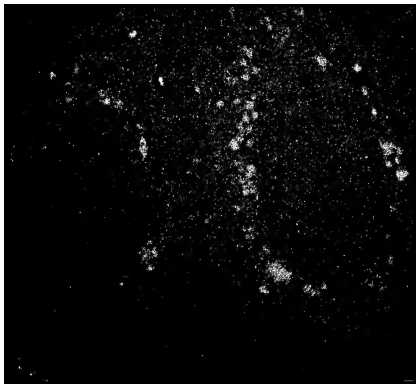

Figure 33: PBS-control Cldn5: Ch. 488; Localization Image

Similarly to the Claudin2 recordings, the signals occured in clusters around the cell nuclei and between cells. The cluster structures were less distinct in the example of a BicaVera treated cell, as well as in the cell treated with BicaVera + 8mMol alanyl-glutamine solution compared to the control group treated with PBS.

From the density images (Fig. 34 to Fig. 36), it appeared that the BicaVera treated cell showed less areas with high density than the control group. The cell treated with BicaVera + 8mMol alanyl-glutamine solution

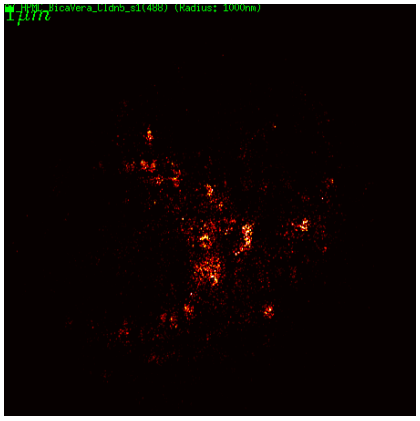

Figure 34: BicaVera (BPDF): Density Image

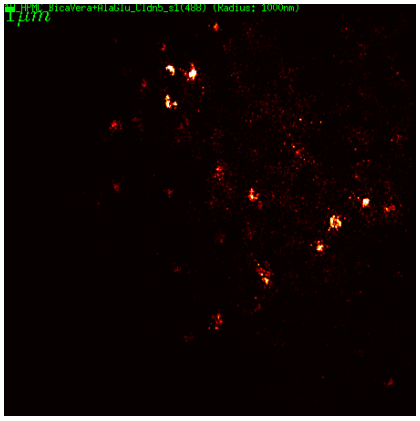

Figure 35: BicaVera + 8mmol AlaGln: Density Image

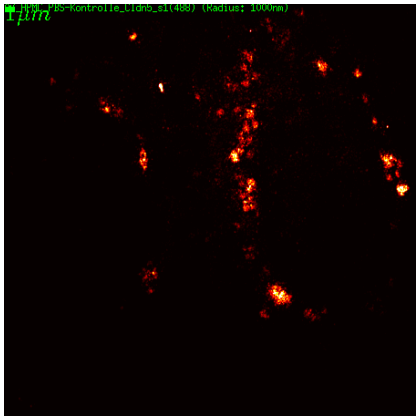

Figure 36: PBS-control: Density Image

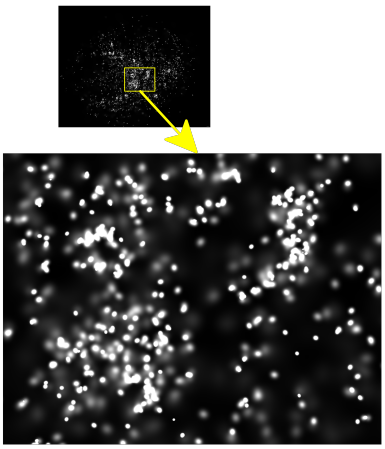

Figure 37: BicaVera

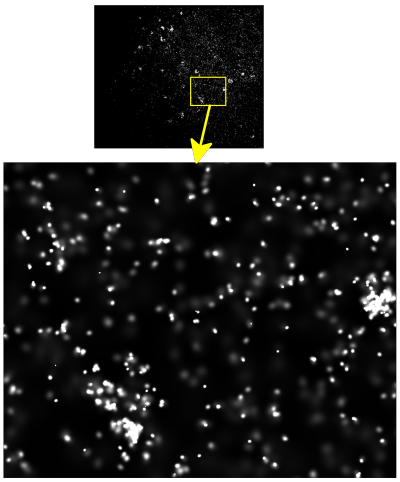

Figure 38: BicaVera + 8mmol AlaGln

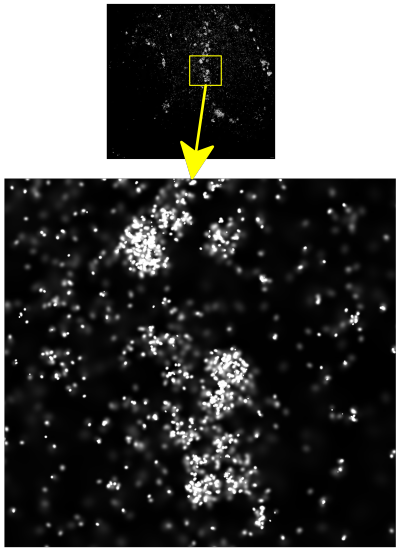

Figure 39: PBS-control

also had a lower number of signal clusters than the control group, but some spots of very high signal density could be seen (Fig. 35).

A zoomed in view of high-density areas in the localization images is shown in Fig. 37 to Fig. 39. A difference in signal distribution could be proposed based on the shown examples, as the signals in the control group seemed to be more clustered. Signal numbers counts and distance analysis tools were used to further evaluate the differences between test series.

The signal numbers for all Claudin5 test series are shown in Fig. 40. For the first staining (s1), a difference in signal numbers between cells treated with BicaVera and the control group could be observed: signal numbers in the test series treated with BicaVera were significantly lower than for the control group. Similarly as for the Claudin2 treatment, a regeneration of signal numbers in the test series with added alanyl-glutamine solution to the dialysis fluid could be observed.

The second staining (s3) refers to the samples 3, 6 and 9 in Table 6, with Claudin5 and Occludin being the target proteins. For this staining, an opposite trend could be observed: The control group showed the least number of signals. Signal numbers for the BicaVera + 8mMol AlaGln treatment were similar to the BicaVera treated test series, but with a larger variation.

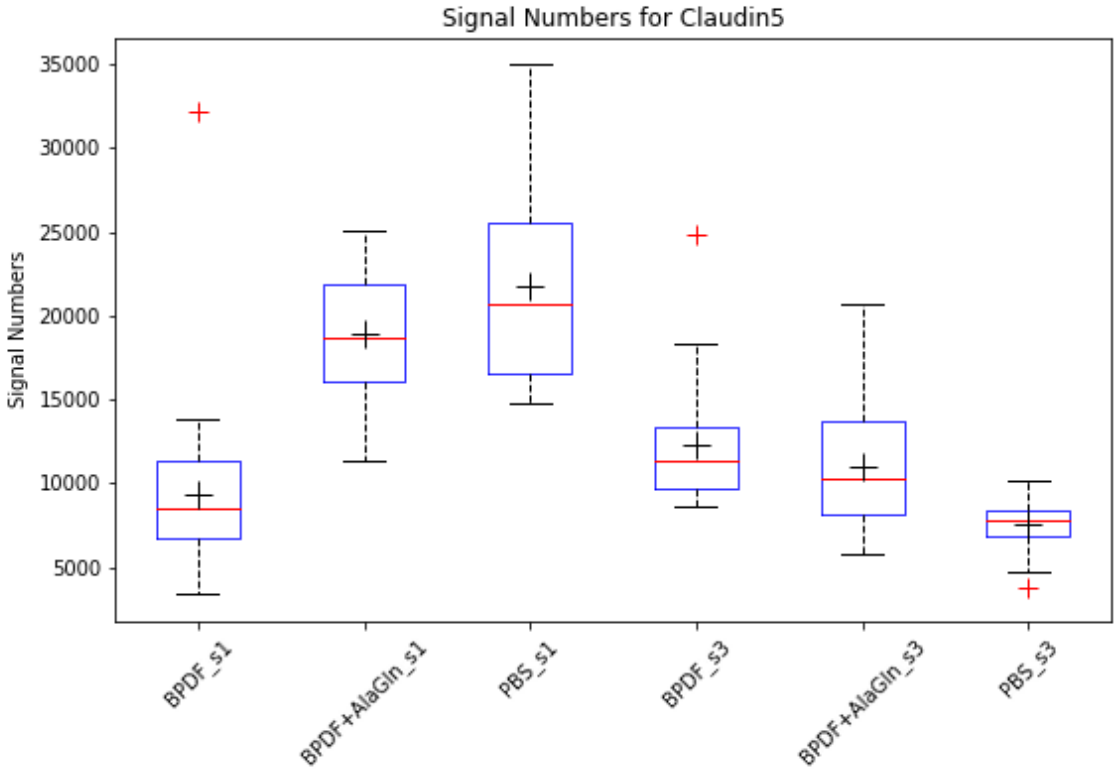

Figure 40: Signal numbers Cldn5: Boxes contain 50% of the measurements of a test series, the mean is given by a black cross and the median is represented by a red line. The highest and lowest values of a series are connected by a dotted black line and runaway values are shown as red crosses.

An exemplary localization image from the PBS-control group in the s3 staining is shown in Fig. 41.

The organization of signals for this staining and treatment appeared different from the Cldn5 control group in the s1 staining (Fig. 33). Signals were less clustered and more evenly distributed. Comparing the localization image to the overview image, it was harder to recognize the cellular features in the localization image as compared to the s1-staining (Fig. 33.)

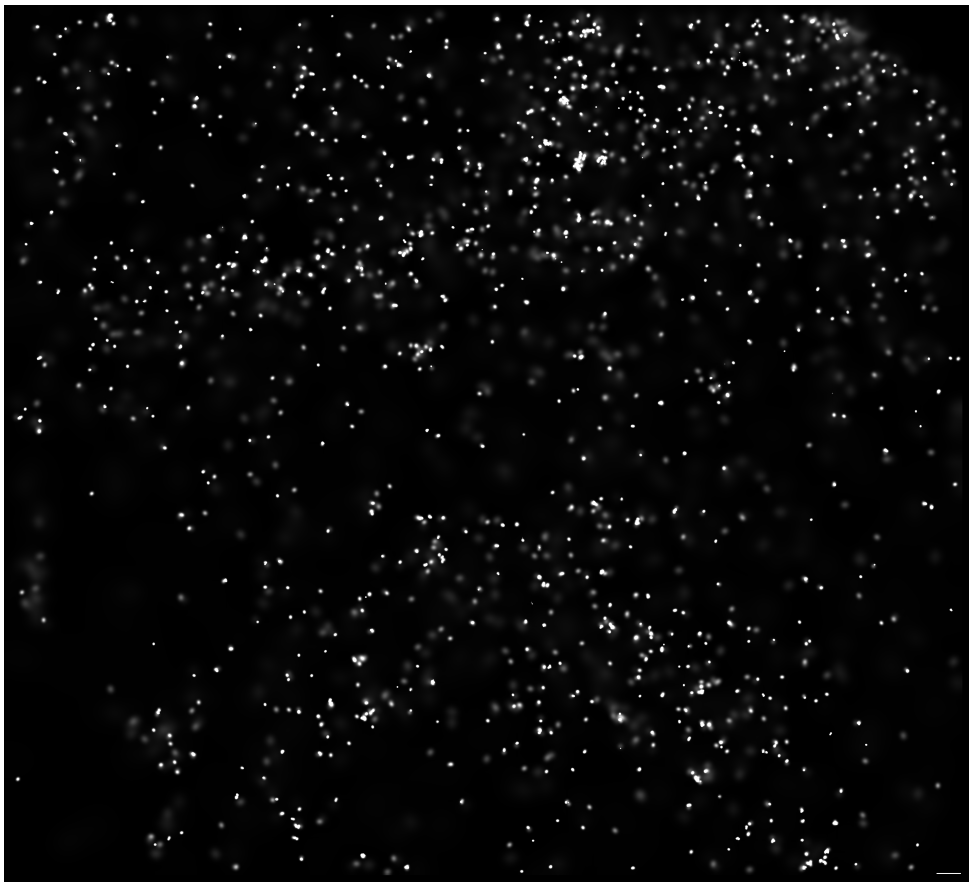

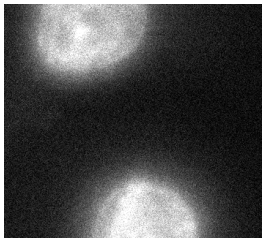

Figure 41: Localization image of Cldn5 (Ch. 568) in HPMC treated with PBS

To quantify the qualitative differences in signal structure observed in the exemplary localization images, distance analysis was used. All calculated distances between signals for all Claudin5 test series have been plotted against their frequency of occurrence in Fig. 42.

The Claudin5 test series in the s1 staining showed very similar characteristics to the corresponding Claudin2 test series. The s1 PBS-control test series distance distribution was similar to a random signal distribution with a slight cluster of distances in the 40 to 50 nm range. The deviation from a random distribution became more pronounced for the BicaVera + alanyl-glutamine treatment and was most pronounced for the BicaVera treatment, with the cluster of distances shifted to smaller distances.

The distance distribution for the s3-staining showed a different trend. A more pronounced clustering of distances at around 40 nm could be seen for all test series. As signal numbers were different for the different test series, the y-axis was scaled accordingly in order to discuss the characteristic distances.

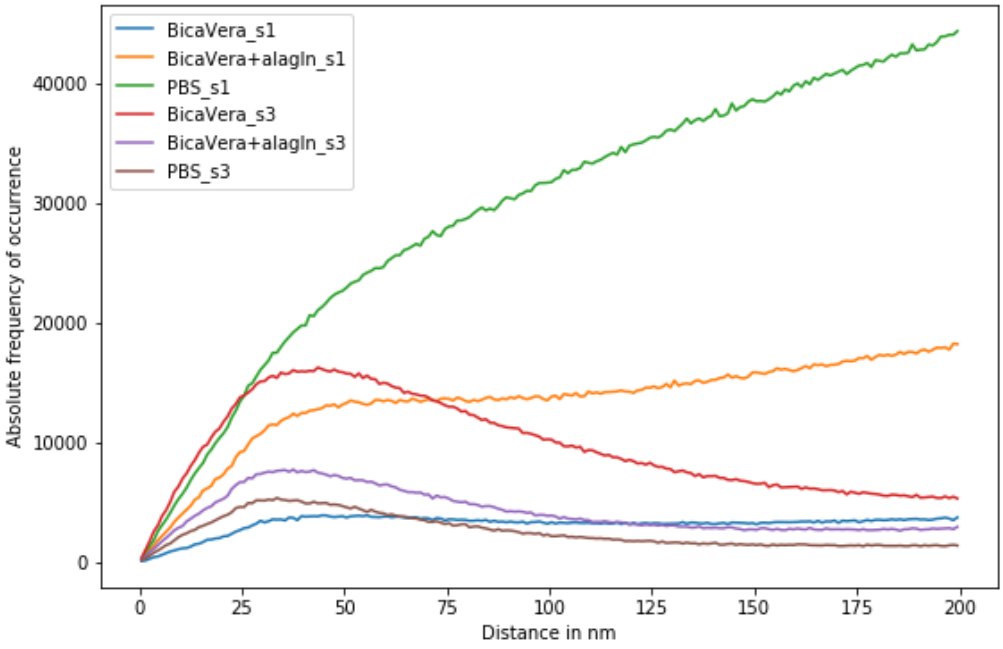

Figure 42: Distance analysis Cldn5: All distances
Distances between all signals of all recordings were calculated and appended into histogram bins for visualization. The x-axis gives the length of a distance in nm, and the y-axis gives the absolute frequency of occurrence.

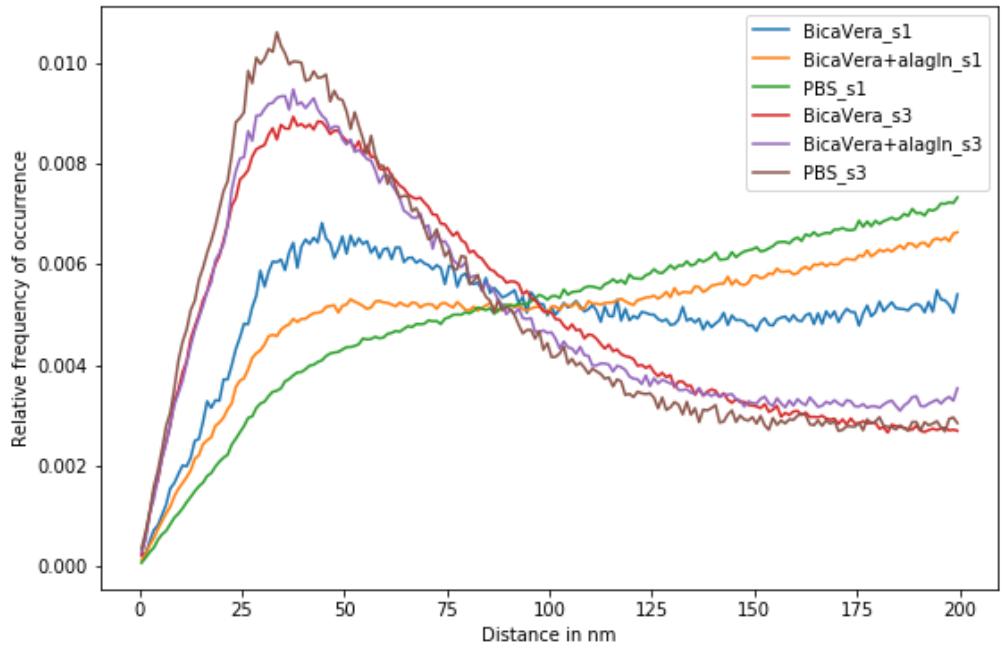

Figure 43: Distance analysis Cldn5: Norm 3
Length of distances between signals on the x-axis and relative frequency of occurrence on the y-axis. A detailed description of the scaling of the y-axis is given in Chapter III.4.4.

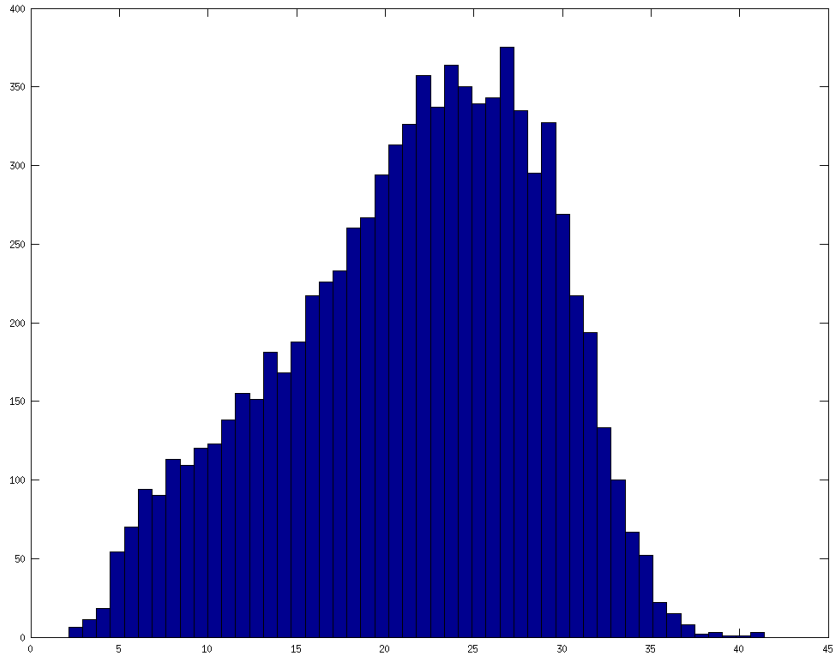

Figure 44: Exemplary localization accuracy for Claudin5 recordings (PBS-control, Ch. 568)

The "Norm3" distance analysis plot for all Claudin5 test series is shown in Fig. 43.
With the scaling of the y-axis, the differences between the two stainings became more obvious. While the test series with s1 staining again showed characteristics similar to the ones observed for the Claudin2 signals, all test series with s3 staining had a much more pronounced peak at around 30 to 40 nm.
For both Claudin2 stainings and the s1 staining for Claudin5, the PBS-control test series was the test series with a distance distribution closest to a straight line as compared to the other treatments. For the Claudin5 s3 staining, the opposite was the case: the PBS-control series showed the most pronounced peak.
The differences between the stainings were also reflected in the signal numbers, as discussed above. Since the treatment of cells during preparation was identical for both stainings, it is possible that the measured differences were due to disruptive factors during cell preparation that affected the signal numbers as well as the distribution of signals.

The localization accuracy distribution for an exemplary recording of a Claudin5 test series is shown in Fig. 44. Most signals had a localization accuracy of around 25 nm with a secondary peak at around 10 to 15 nm. This example was chosen as most localization accuracy distributions of Cldn5 recordings resembled this recording. However, the secondary peak in localization accuracy appeared to be more pronounced in the s3-staining, see Fig. 45 and Fig. 46.

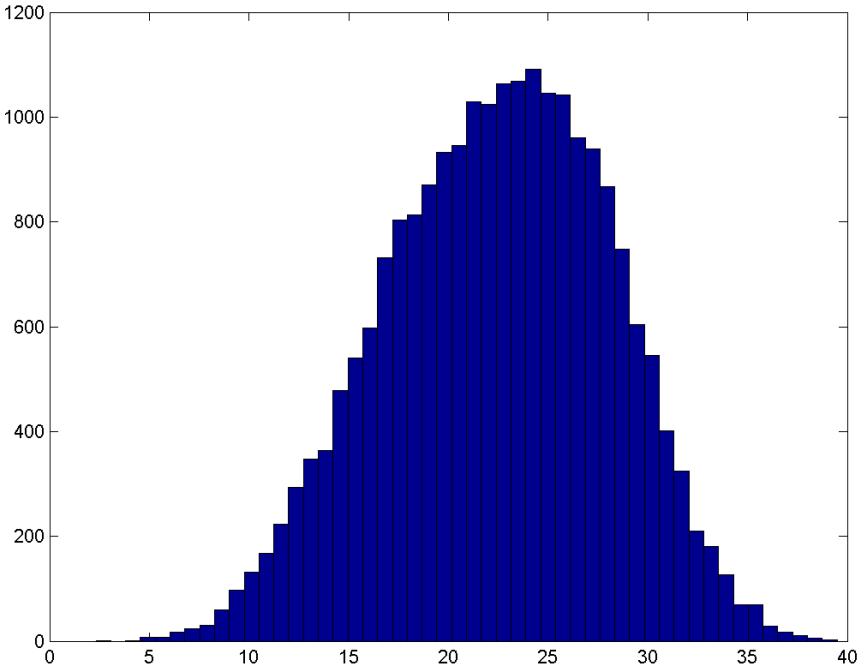

Figure 45: Localization accuracy: PBS-control Ch. 488 (s1)

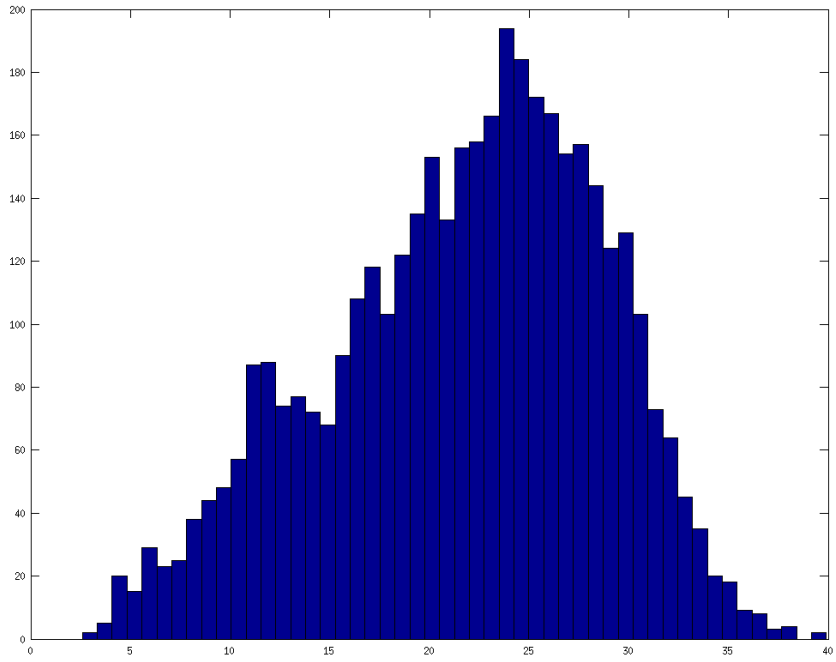

Figure 46: Localization accuracy: PBS-control Ch. 568 (s3)

IV.1.3 Occludin

Same as for Claudin2 and Claudin5, six test series were performed to analyze the distribution of Occludin in the membranes of cells treated with PD-fluids. For all test series, the Occludin proteins were marked with Alexa Flour488 fluorescent dye.

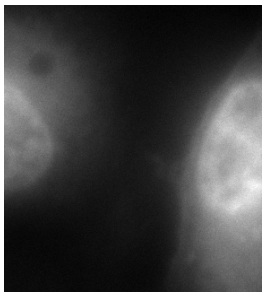

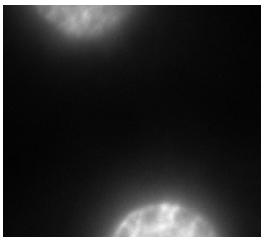

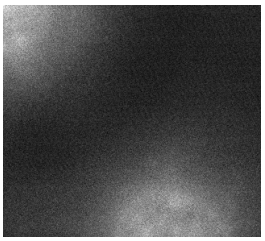

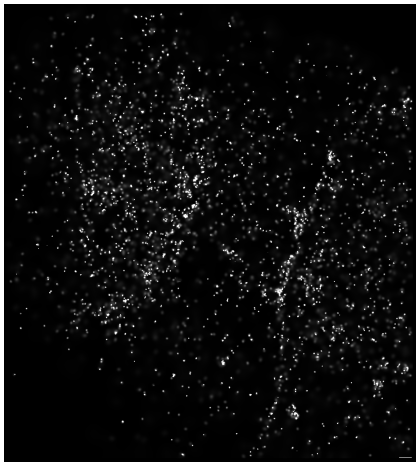

Figure 47: BicaVera (BPDF) Occludin: Ch. 488 (s2)

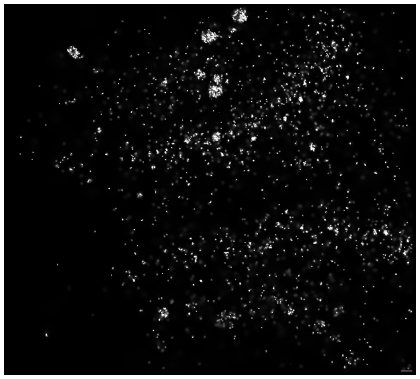

Figure 48: BicaVera + 8mmol AlaGlu Occludin: Ch. 488 (s2)

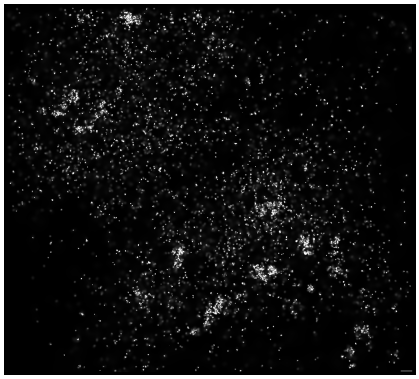

Figure 49: PBS-control Occludin: Ch. 488 (s2)

An overview over localization images of test series with different treatment solutions is given from Fig. 47 to Fig. 49. The label s2 refers to staining 2, meaning that for these test series, Occludin was stained in the 488nm channel and Claudin2 was stained in the 568nm channel. Wide-field overview images of the cell nuclei are displayed above the localization images.
An accumulation of signals around the cell nuclei and between cells indicates that Occludin signals were primarily located in the cell membranes. In these exemplary localization images, a clustering of signals, especially in the PBS-test series and BicaVera + alanyl-glutamine test series, could be observed. In all three examples, the position of the cells clearly corresponded to the signal distribution in the localization images.
Additional examples of localization images from Occludin test series are given from Fig. 50 to Fig. 52. The additional specification s3 relates to the test series with Occludin stained in the 488 nm channel and Claudin5 stained in the 568 nm channel, see also Chapter IV.1.2. Again, overview images of the cell nuclei are displayed above the localization images. Compared to the s2 series (Fig. 47 to Fig. 49), the cellular features in the localization images were less distinct. As the signals appeared to be more homogeneously distributed in the localization images, it was difficult to make an assumption about the relative position of signals to the cells. Additionally, signal clustering appeared to be much less frequent in all s3 test series as compared to the s2 test series.

To compare the signal numbers in different Occludin test series, an overview is given in Fig. 53.

Signal numbers for the different treatments followed a similar trend for both, the s2 and the s3 stained test series: the least amount of signals was detected in the test series treated with BicaVera + alanyl-glutamine. However, while for the s2 staining the highest number of signals was detected in the PBS-treated test series, the

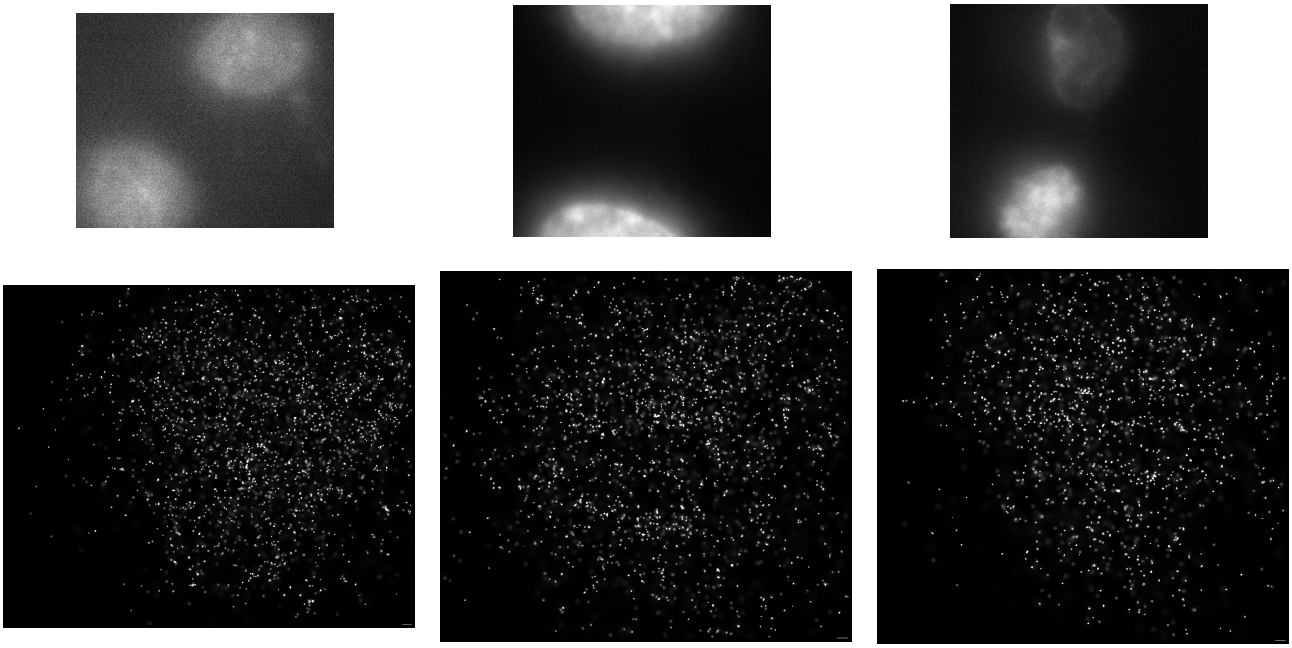

Figure 50: BicaVera (BPDF) Occludin: Ch. 488 (s3)

Figure 51: BicaVera + 8mmol AlaGln Occludin: Ch. 488 (s3)

Figure 52: PBS-control Occludin: Ch. 488 (s3)

signal numbers for the s3 PBS-control were substantially lower than for the s3 BicaVera test series. The BicaVera test series for both, the s2 and s3 staining, showed similar signal numbers. Thus, a big difference between signal numbers of the two control groups could be observed, with the number of signals being substantially lower for the s3 staining. Additionally, the signal numbers for the BicaVera + alanyl-glutamine treatment were slightly lower in the s3 staining as compared to the same treatment in the s2 staining.
To evaluate the structural differences in signal distribution between the test series, a distance analysis plot of all distances between signals for all Occludin test series was created (Fig. 54).

Differences in the distribution of distances between signals in the test series with s2 staining compared to the series with s3 staining could be observed (Fig. 54). Close to all distances in the 20 to 200 nm range appeared more frequently in the s2 test series. This was likely due to the signal numbers being generally higher for these test series. However, while the distance distribution for s2 series showed a slight peak at around 50 nm, the clustering of distances in the s3 staining test series were more pronounced with a distinct maximum at around 40 nm.
To better compare the characteristic distances, a distance analysis plot with a scaled y-axis according to the Norm3 method was created (Fig. 55).

The test series with the same treatment solutions and different stainings s2 or s3 did not show similar distance distributions for any of the treatment solutions, see Fig. 55. All Occludin test series with a Occludin-Claudin2 staining (s2) showed similar properties, while all Occludin-Claudin5 test series (s3) also followed similar trends. It is possible that cell preparation affected the measurements for the Occludin test series.

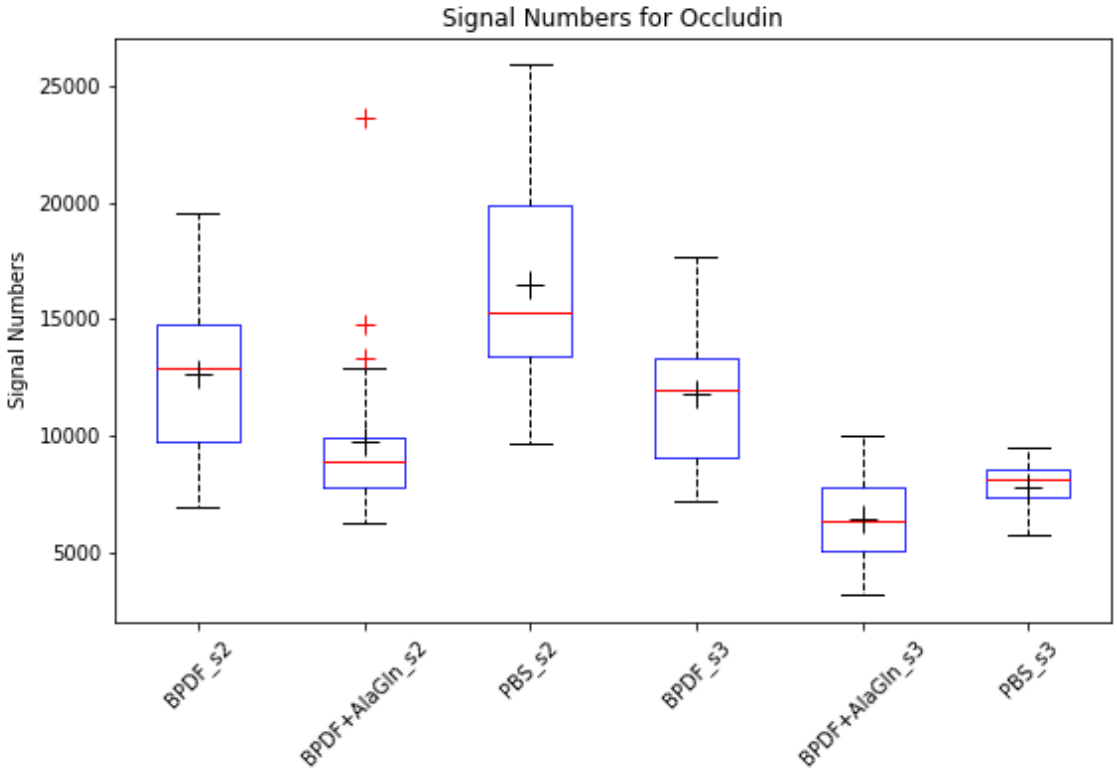

Figure 53: Number of Occludin signals: The y-axis gives the number of signals found in recordings of different test series. The black cross gives the mean, a red line relates to the median, the bock contains 50% of the recordings of a series. The names of the test series are displayed on the x-axis.

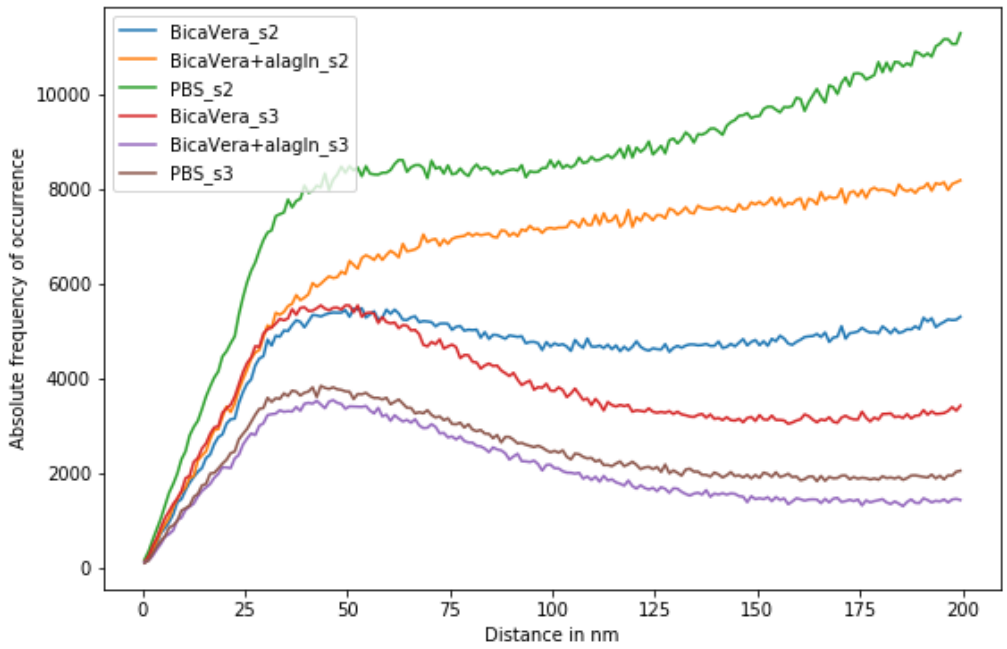

Figure 54: Distance analysis for Occludin test series: All distances; x-axis: Distance in nm; y-axis: Absolute frequency of occurrence

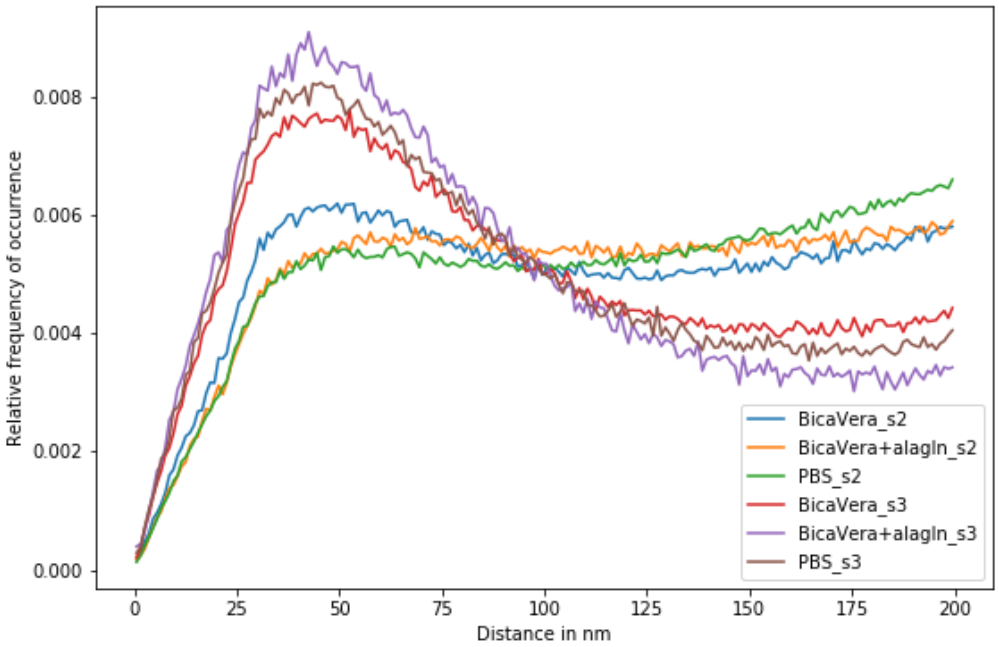

Figure 55: Distance analysis for Occludin test series: Norm 3; x-axis: Distance in nm; y-axis: Relative frequency of occurrence

Treatment	Slice No.	Staining	Channel	Target	Signal Numbers	Loc. Accuracy [nm]
CAPD	7	s1	568	Cldn2	45900 ± 4250	13 ± 5
CAPD	7	s1	488	Cldn5	9630 ± 240	33 ± 8
CAPD	8	s2	568	Cldn2	40680 ± 3590	13 ± 6
CAPD	8	s2	488	Ocl	9470 ± 410	32 ± 8
CAPD	9	s3	568	Cldn5	10580 ± 250	29 ± 11
CAPD	9	s3	488	Ocl	9160 ± 570	32 ± 8
CAPD + AlaGln	10	s1	568	Cldn2	21020 ± 2630	12 ± 4
CAPD + AlaGln	10	s1	488	Cldn5	440 ± 40	33 ± 8
CAPD + AlaGln	11	s2	568	Cldn2	16260 ± 1890	12 ± 4
CAPD + AlaGln	11	s2	488	Ocl	370 ± 30	29 ± 7
CAPD + AlaGln	12	s3	568	Cldn5	2980 ± 130	23 ± 9
CAPD + AlaGln	12	s3	488	Ocl	370 ± 20	27 ± 8
PBS	13	s1	568	Cldn2	112370 ± 10190	14 ± 5
PBS	13	s1	488	Cldn5	21780 ± 1200	31 ± 8
PBS	14	s2	568	Cldn2	69240 ± 4380	13 ± 6
PBS	14	s2	488	Ocl	16450 ± 780	32 ± 8
PBS	15	s3	568	Cldn5	7550 ± 290	30 ± 11
PBS	15	s3	488	Ocl	7800 ± 220	32 ± 8

Table 9: Overview over signal numbers and localization accuracies of the analyzed samples: Total signal numbers were calculated by Chromatinanalyse, the mean and standard deviation were calculated using Python. The listed uncertainties were calculated by $\Delta = \frac{\sigma}{\sqrt{N}}$ with N the number of recordings in a test series. Additionally, a python script was used to calculate the mean and standard deviation of the localization accuracies of the test series as given by startSPDM.

IV.2 CPDF (CAPD)

CAPD is a conventional peritoneal dialysis fluid (CPDF) by Fresenius Medical Care. A total of 6 slices with CAPD or CAPD + alanyl-glutamine treatment were analyzed, see Table 9.

IV.2.1 Claudin2

Exemplary localization images of recordings with CAPD and CAPD + alanyl-glutamine treatments as well as a localization image of the control group are shown from Fig. 56 to Fig. 58. All images were taken in Channel 568. As the s1 (Claudin2 and Claudin5) and the s3 (Claudin2 and Occludin) stained test series showed similar characteristics in the localization images, Fig. 56 to Fig. 58 were exemplary for all 6 Claudin2 test series treated with CAPD or CAPD + alanyl-glutamine as well as the control group (slice number 7,8,10,11,13,14).

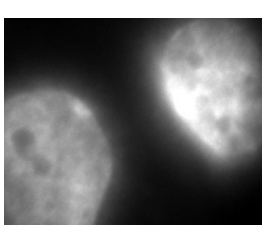

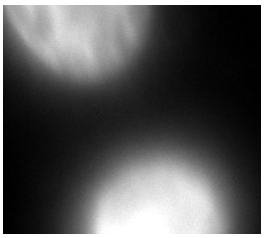

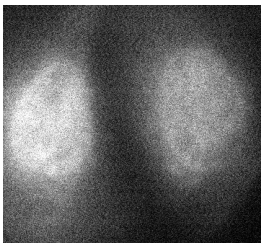

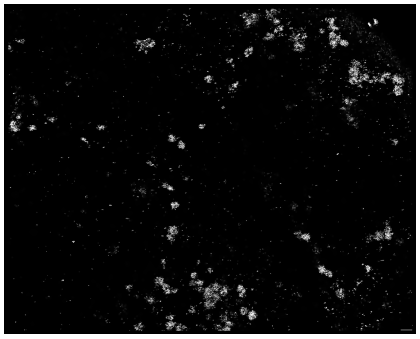

Figure 56: CAPD Claudin2 Ch. 568

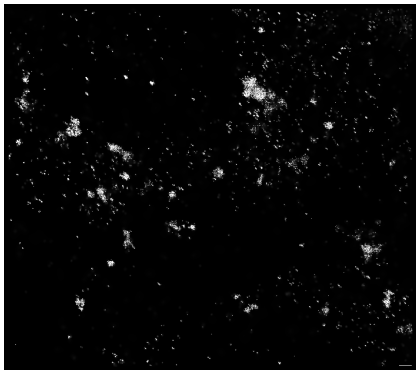

Figure 57: CAPD + 8mMol alanyl-glutamine Cldn2 Ch. 568

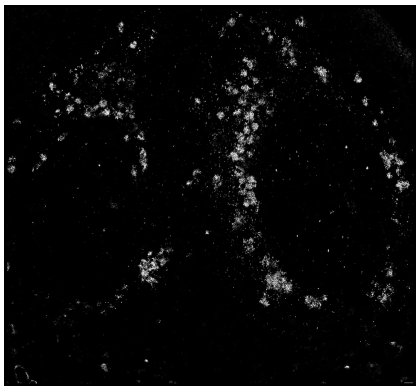

Figure 58: PBS-control Cldn2 Ch. 568

As for other test series, the Cldn2 signals for CAPD-treated samples were primarily located around the cell nuclei, which could be derived from comparing the localization images to the wide-field overview images displayed above. Signals appeared in cluster-like structures and seemed to be of similar quantity.
To further bring out the structural organization of signals, density images were created for every recording (Fig. 59 to Fig. 61).

The software Chromatinanalyse was used to calculate and compare the total number of signals of the test series (Fig. 62).
The highest signal numbers could be observed in the control groups. As discussed before, the control group signal numbers were different for the two stainings s1 and s2, which could possibly be attributed to cell preparation and staining. The CAPD + alanyl-glutamine test series showed the lowest signal numbers for all of the compared test series. For both, CAPD and CAPD + alanyl-glutamine treated test series, the differently stained test series showed very similar total signal numbers.

Distance analysis plots were created with Chromatinanalyse (Fig. 63 and Fig. 64). When calculating all distances, test series with the same treatment solution showed very similar characteristics, except for the two control groups. The difference between the control groups could likely be attributed to the difference in signal

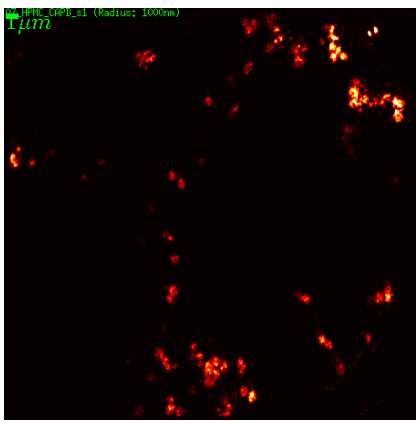

Figure 59: CAPD density image

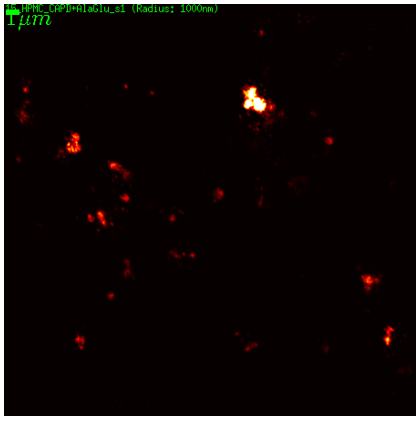

Figure 60: CAPD + 8mmol AlaGln density image

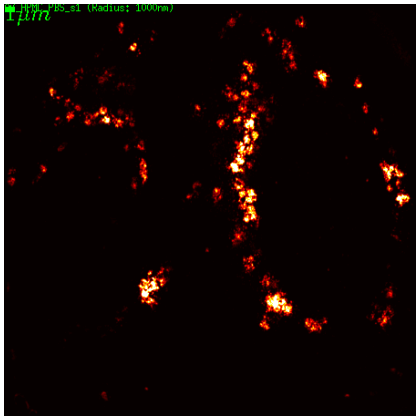

Figure 61: PBS-control density image

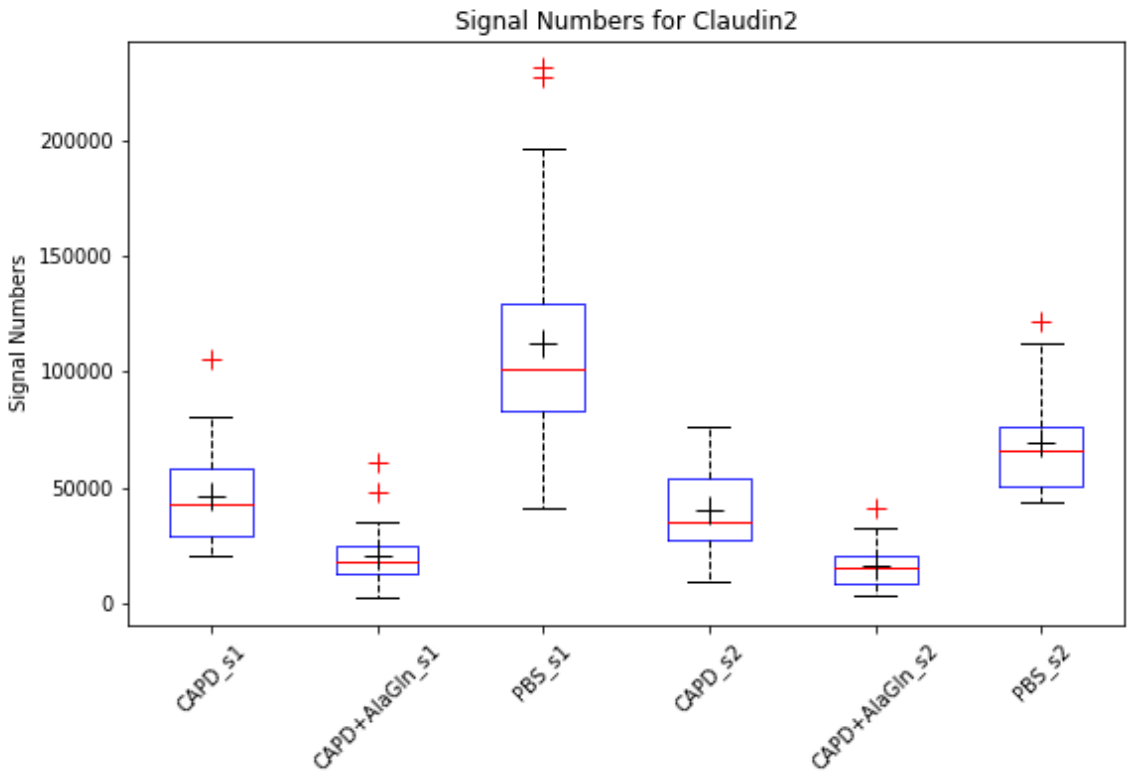

Figure 62: Claudin2 signal numbers for CAPD related test series:
Box: 50% of recordings, Black cross: mean; Red line: median; Dotted black line: Connection of highest and lowest value; Red crosses: Runaway values

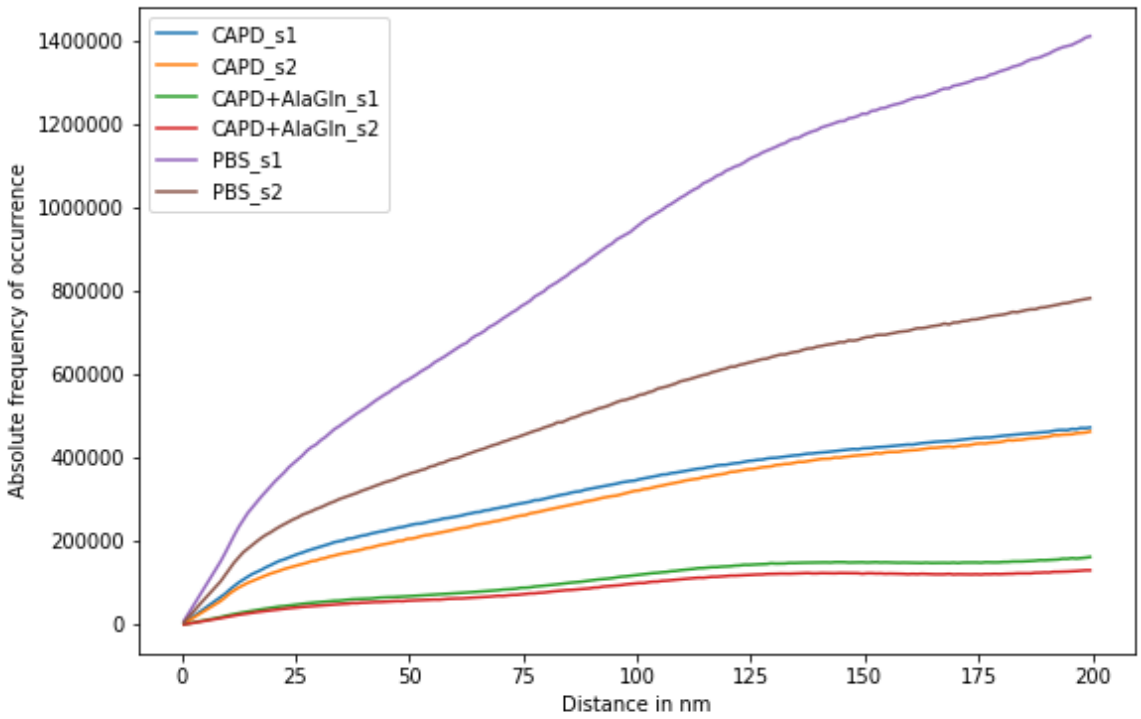

Figure 63: Claudin2 distance analysis: All distances
x-axis: Distance between signals in nm; y-axis: Absolute frequency of occurrence

numbers. All test series showed an almost linear relationship between distance and frequency of occurrence, with a bend at around 20 to 30 nm. Additionally, the CAPD + alanyl-glutamine test series expressed a second bend at around 130 nm.

As the test series with different treatment solutions had different signal numbers, a distance analysis plot with scaled y-axis was created to further compare the characteristic distances (Fig. 64). With the y-axis scaled according to the Norm 3 method, the distance distribution of all Claudin2 test series showed similar behavior. The bend at the 20 to 30 nm mark seemed to be similarly pronounced for all test series, but the bend at 120 nm was only noticeable for the CAPD + alanyl-glutamine treatment.

The localization accuracy for these test series was in the range of 5 to 15 nm.

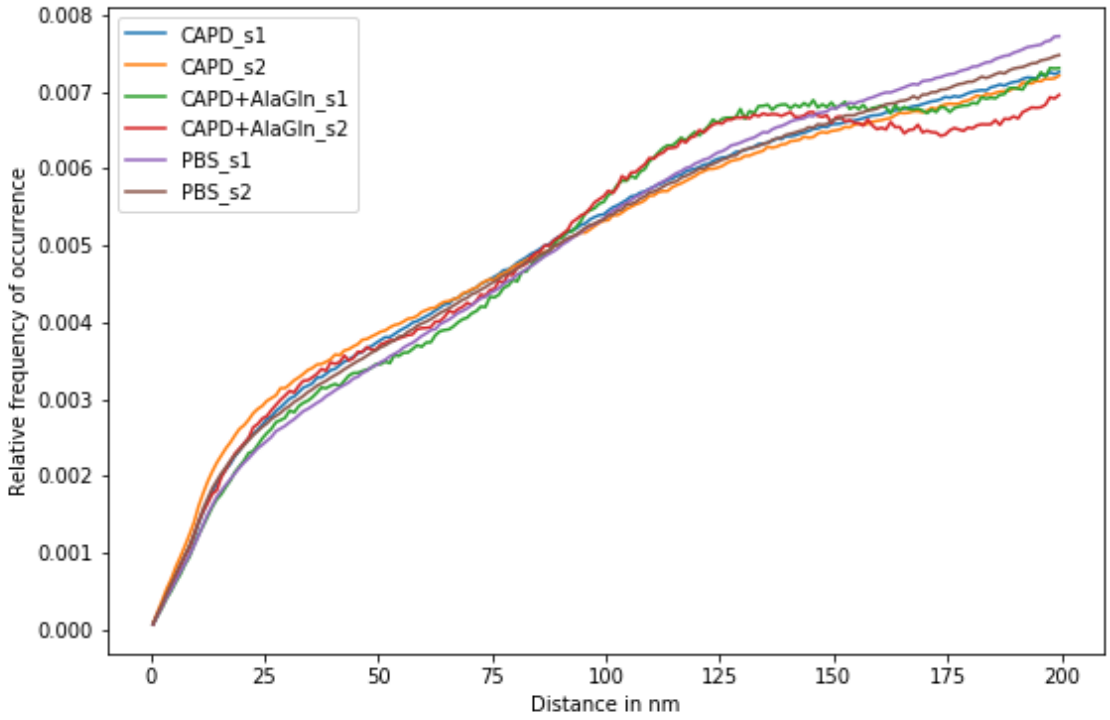

Figure 64: Claudin2 distance analysis: Norm 3
x-axis: Distance between signals in nm; y-axis: Relative frequency of occurrence

IV.2.2 Claudin5

Two different stainings were performed for Claudin5, using the two fluorescent dyes AlexaFluor488 and AlexaFluor568. Localization images of the first staining (Ch. 488) are shown from Fig. 65 to Fig. 67.

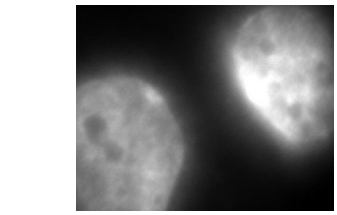

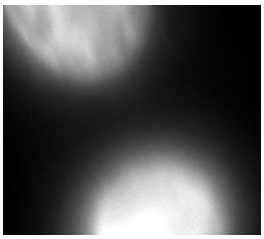

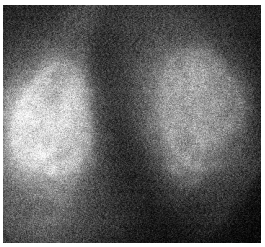

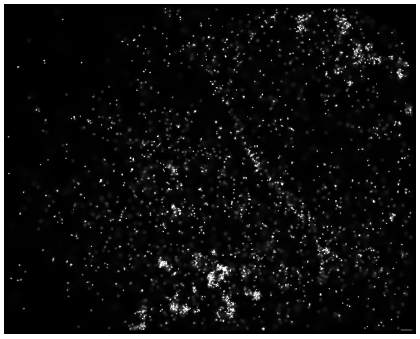

Figure 65: CAPD Claudin5 Ch. 488

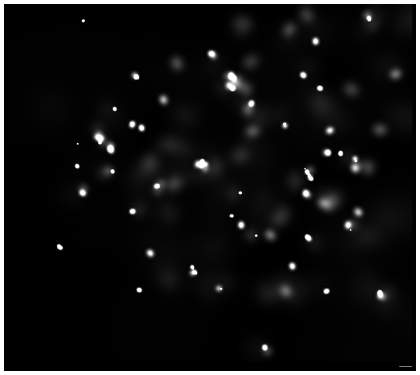

Figure 66: CAPD + 8mMol alanyl-glutamine Cldn5 Ch. 488

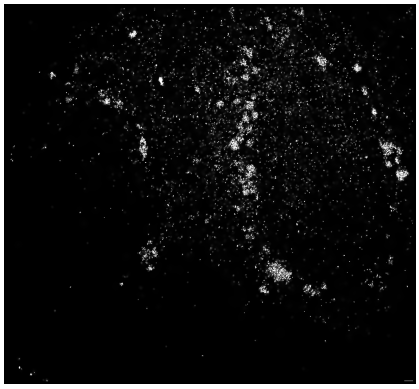

Figure 67: PBS-control Cldn5 Ch. 488

From these exemplary images it became obvious that signal numbers for the CAPD + alanyl-glutamine were much lower than for the other two test series with this staining. While the position of the cell nuclei could be seen in the localization images of the CAPD test series and the PBS control group, no cellular features could be identified in the localization image of the CAPD + alanyl-glutamine test series. Density images were created for all recordings (Fig. 68 to Fig. 70). Similarly as for the localization images, the positioning of the signals around the cell nuclei became very clear for the PBS test series. Features were less distinct in the CAPD treated samples and least distinct for the CAPD + alanyl-glutamine treatment.

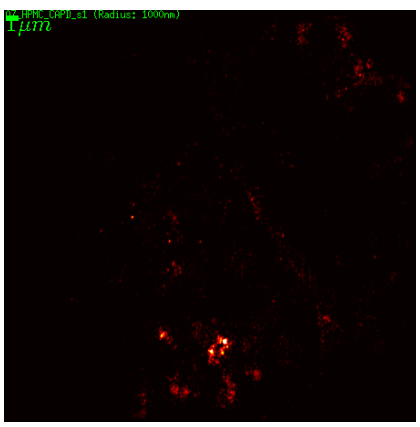

Figure 68: CAPD density image

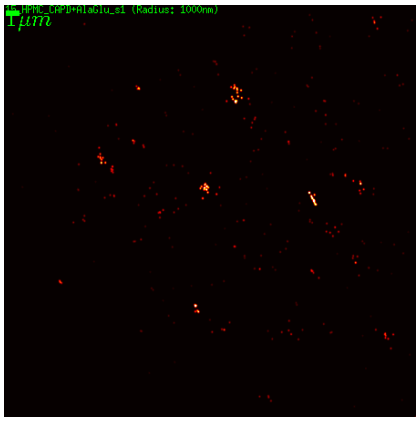

Figure 69: CAPD + 8mmol AlaGln density image

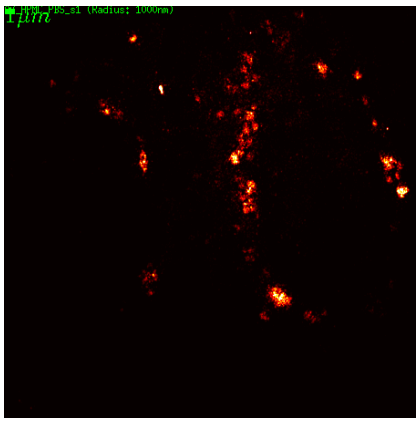

Figure 70: PBS-control density image

Exemplary localization images of the Claudin5 s3 staining (Ch. 568) are shown from Fig. 71 to Fig. 73.

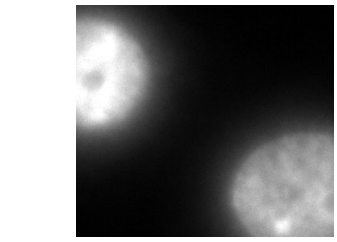

Figure 71: CAPD Claudin5 Ch. 568

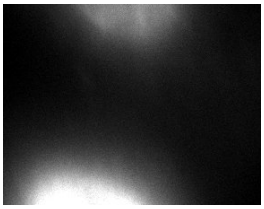

Figure 72: CAPD + 8mMol alanyl-glutamine Cldn5 Ch. 568

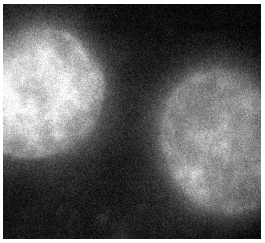

Figure 73: PBS-control Cldn5 Ch. 568

Comparing the localization images to the s1 staining, a difference in signal number and distribution could be proposed. Most obviously, signal numbers for the CAPD + alanyl-glutamine treatment seemed to be much higher for the s3 staining than for the s1 staining. Additionally, the signals appeared to be more homogeneously distributed and cellular features were less distinct in the s3 staining.
The same observations could be made when comparing the density images (Fig. 74 to Fig. 76) of the different stainings: because of the very homogeneous distribution of signals, the signal density for the CAPD and CAPD + alanyl-glutamine treatment in s3 staining was very similar for most of the image frame. As a result, the density images appeared dark except for very few points of higher density. For the PBS control, some structures could be seen in the density images for the s3 staining, but were less distinct than for the s1 staining.
To further quantify these differences, a signal number comparison plot was created (Fig. 77).

As expected from the localization images, CAPD + alanyl-glutamine signals in s1 staining were substantially fewer than for all other test series. In general, a similar trend as for Claudin2 signals could be observed: Signal numbers were higher for PBS test series and lowest for CAPD + alanyl-glutamine test series with CAPD signal numbers in between. The exception to this trend was the PBS test series in the s3 staining, as signal numbers

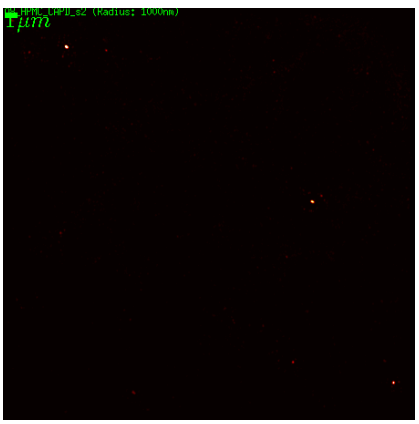

Figure 74: CAPD density image

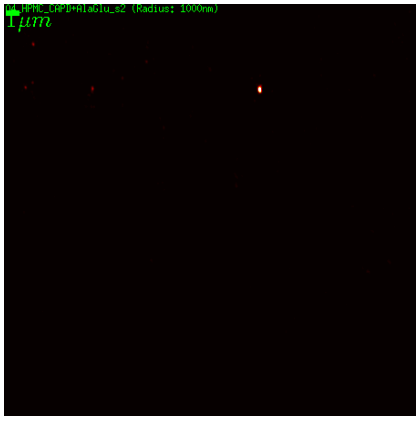

Figure 75: CAPD + 8mmol AlaGln density image

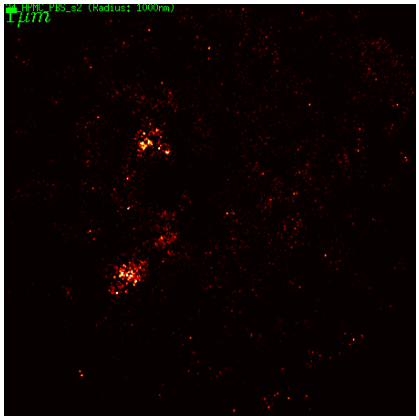

Figure 76: PBS-control density image

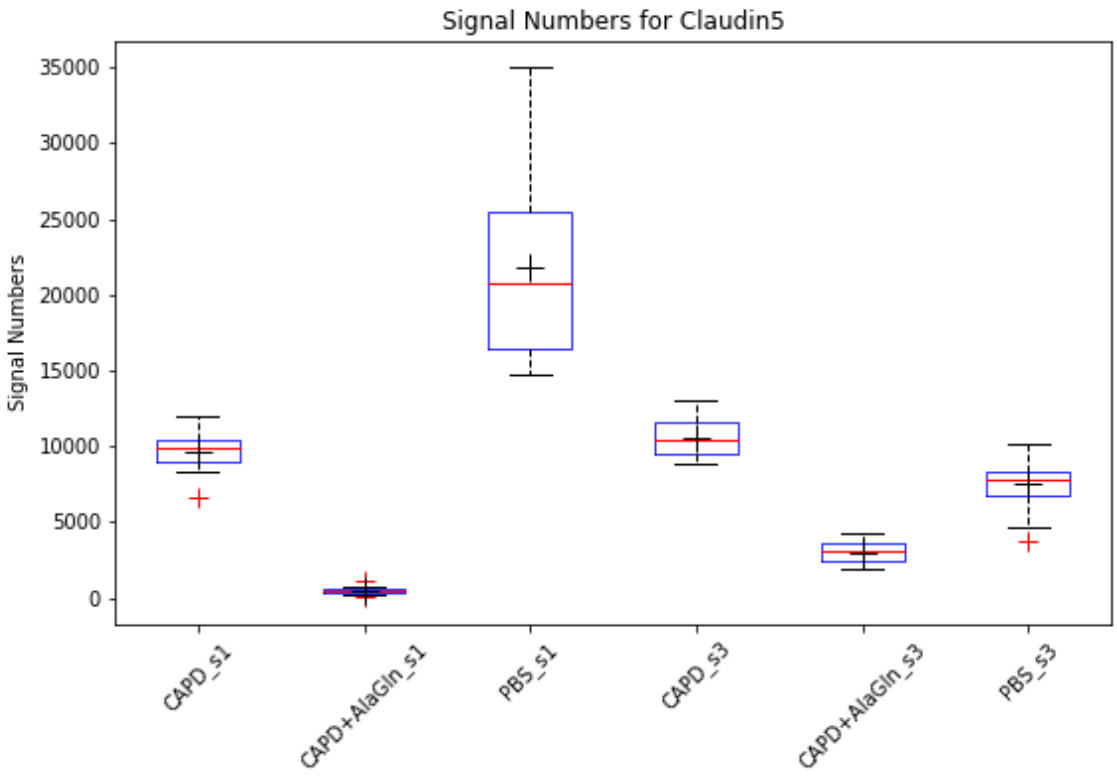

Figure 77: Signal numbers for Claudin5 in CAPD related test series:
Box: 50% of recordings, Black cross: mean; Red line: median; Dotted black line: Connection of highest and lowest value; Red crosses: Runaway values

for this test series were lower than the number of signals of the corresponding CAPD test series. As signal numbers of this test series also were substantially lower than the for the s1 PBS test series, it is possible that cell preparation affected the measurements. The two CAPD treated test series showed similar signal numbers, as expected. Another substantial difference between test series with the same treatment solution could be observed between the CAPD + alanyl-glutamine test series in s1 and s3 staining. Interestingly, fewer signals were detected in s1 for CAPD + alanyl-glutamine, whereas for PBS, signal numbers were lower for s3.

To further assess the differences in signal distribution, distance analysis plots were created (Fig. 78 and Fig. 79).

Distance distribution for the same treatment solutions but with different staining s1 or s3 were substantially different for all test series. As the "All distances" distance analysis plot (Fig. 78) does not scale the y-axis according to the signal numbers, differences for PBS and CAPD + alanyl-glutamine test series were expected. The CAPD test series however showed similar signal numbers but different distance distributions, indicating a difference in spatial organization of the targets. This corresponded well to the observed differences in the localization images of the test series with different stainings.

A scaled distance analysis plot (Fig. 79) was created to further analyze relative distance distributions of the test series. As signal numbers for the CAPD + alanyl-glutamine treatment in s1 were exceptionally low, the scaled distance analysis plot showed great fluctuations and it was difficult to deduce actual characteristic distances from the plot. For the other treatment solutions, the s3 staining showed a peak in relative frequency of occurrence for distances of about 30 nm that was much less pronounced in the s1 staining for both, CAPD and PBS test series. The CAPD and the PBS treated test series in the s3 staining showed an almost identical distance distribution after scaling of the y-axis.

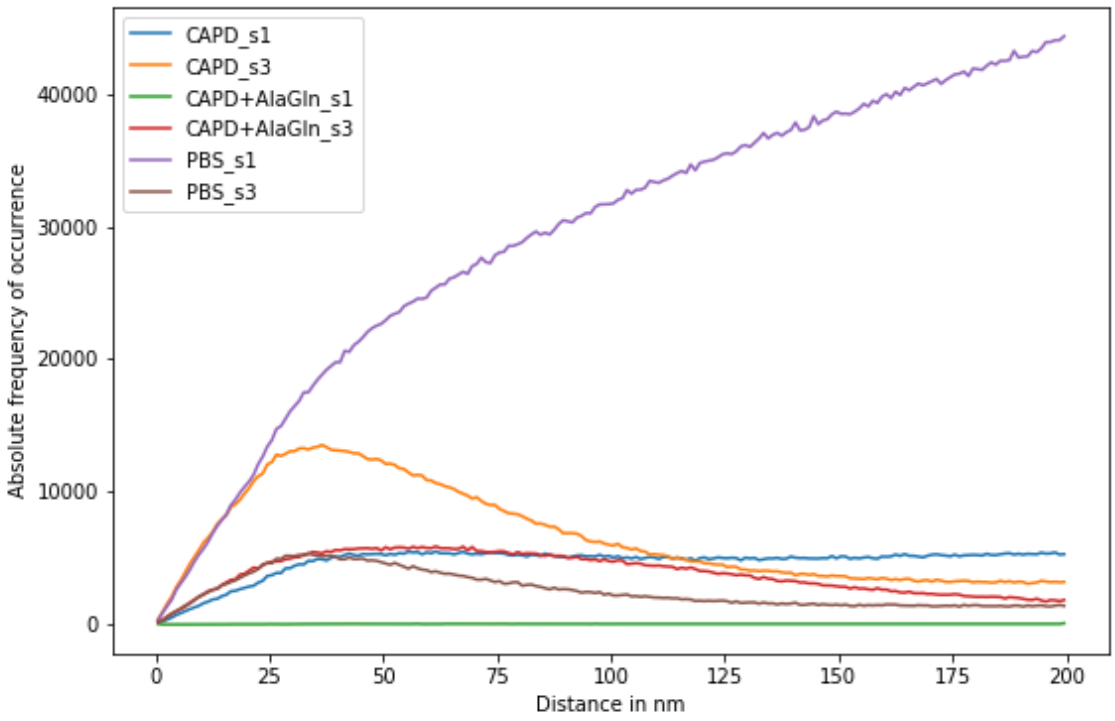

Figure 78: Distance analysis for Claudin5 in CAPD related test series: All distances; x-axis: Distance between signals in nm; y-axis: Absolute frequency of occurrence

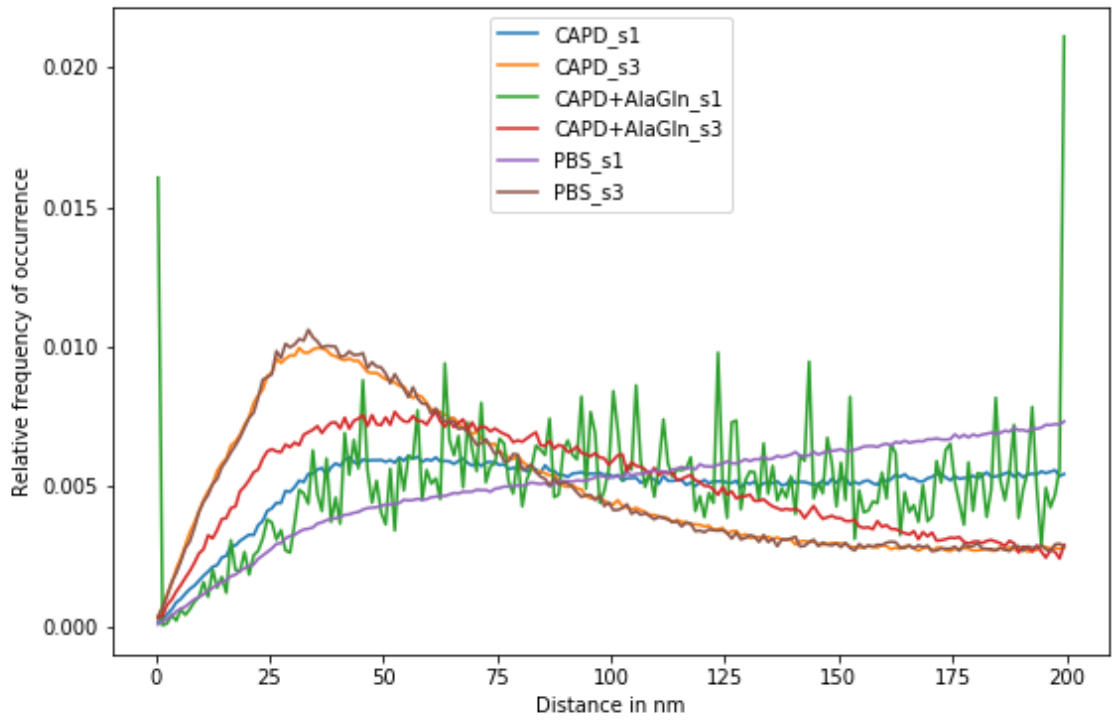

Figure 79: Distance analysis for Claudin5 in CAPD related test series: Norm 3; x-axis: Distance between signals in nm; y-axis: Relative frequency of occurrence

IV.2.3 Occludin

Six test series were performed to analyze the effect of CAPD and CAPD + alanyl-glutamine on the distribution of Occludin in human peritoneal mesothelial cells. The analyzed samples included slice number 8, 9, 11, 12, 14 and 15 from Table 6. An overview over localization images of the different test series is given from Fig. 80 to Fig. 82.

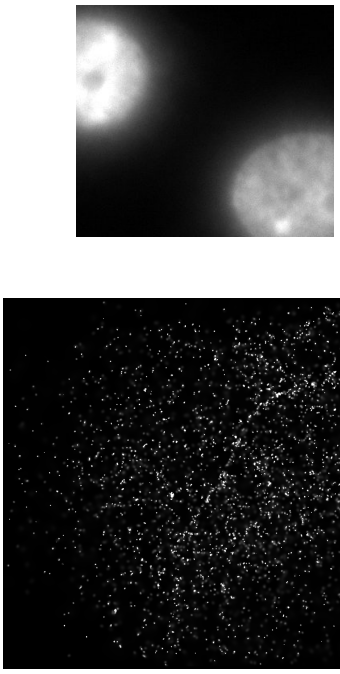

Figure 80: CAPD Occludin Ch. 488

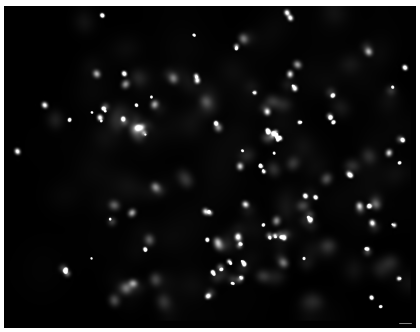

Figure 81: CAPD + 8mMol alanyl-glutamine Occludin Ch. 488

Figure 82: PBS-control Occludin Ch. 488

In all analyzed test series, Occludin was stained with AlexaFluor488 and localization images of test series with the same treatment solution but different staining s2 (Occludin - Claudin2) or s3 (Occludin - Claudin5) showed similar properties. From the exemplary localization images, it became obvious that less signals were detected for the CAPD + alanyl-glutamine test series than for the test series with different treatment solutions. For the CAPD and the PBS test series, signals appeared less structured than for the bicaVera s2 test series (see Chapter IV.1.3), although some cellular features could still be identified. For example in Fig. 80, a line that possibly represents the boundary of the cells could be seen.

Density images were created (Fig. 83 to Fig. 85) to further visualize the signal distribution in the images. Since the signals appeared to be less clustered for the analyzed samples than in other test series, it was difficult to identify cellular features in the density images.

A comparison of signal numbers for the analyzed test series is shown in Fig. 86. As expected from the localization images, signal numbers were substantially lower for the CAPD + alanyl-glutamine test series in both, the s2 and s3 staining. Both test series treated with CAPD showed similar signal numbers, but differences between the PBS s2 and s3 test series could be observed: signal numbers were lower in the s3 staining than in the s2 staining for PBS. Since both of these test series were in the control group and exposed to the same treatment during cell preparation, these changes were likely due to disruptive factors. Similarly as for the other analyzed proteins, a general trend of signal numbers being highest in the control group and lowest in the CAPD + alanyl-glutamine treated test series could be seen.

As signal numbers were much lower for the two test series treated with CAPD + alanyl-glutamine, the distance distributions were difficult to compare to the other treatments when displaying the absolute frequency

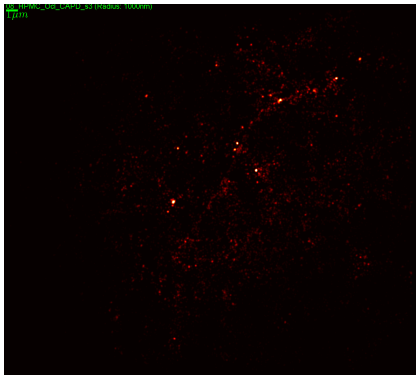

Figure 83: CAPD Occludin density image

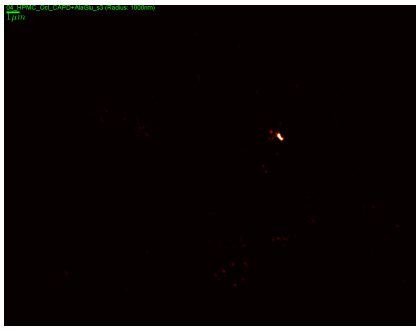

Figure 84: CAPD + 8mmol AlaGln Occludin density image

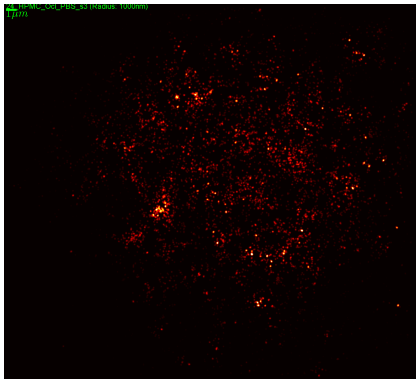

Figure 85: PBS-control Occludin density image

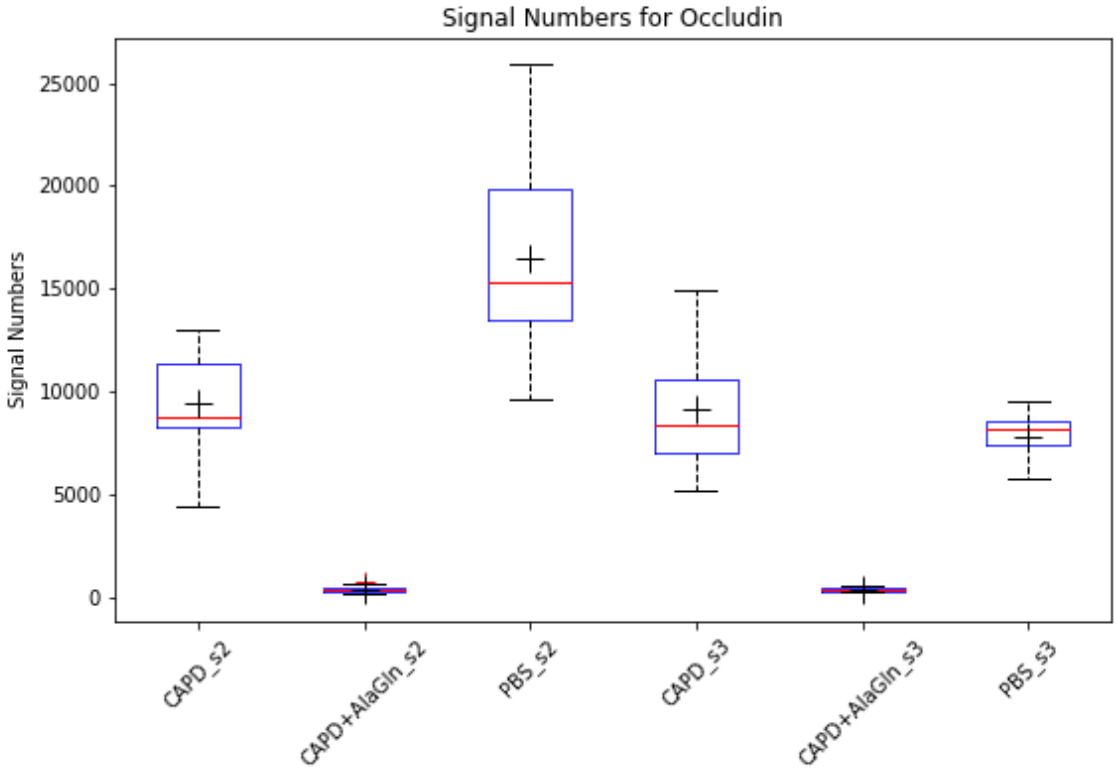

Figure 86: Signal numbers for Occludin in CAPD related test series:
Box: 50% of recordings, Black cross: mean; Red line: median; Dotted black line: Connection of highest and lowest value; Red crosses: Runaway values

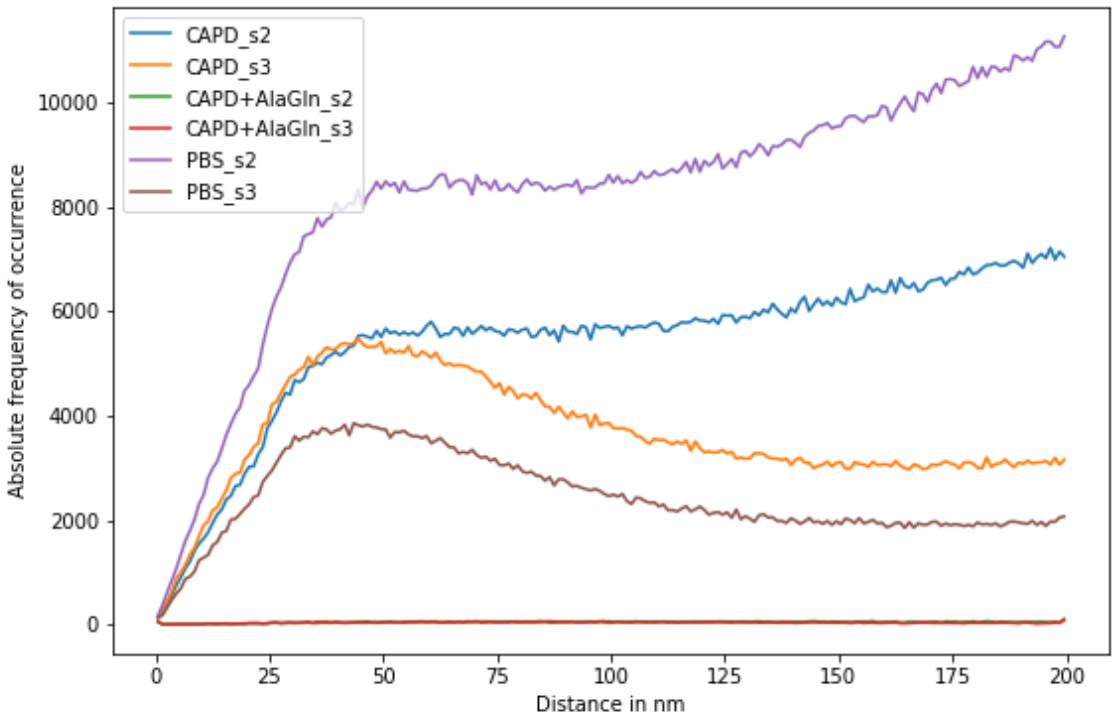

Figure 87: Distance analysis for Occludin in CAPD related test series: All distances; x-axis: Distance between signals in nm; y-axis: Absolute frequency of occurrence

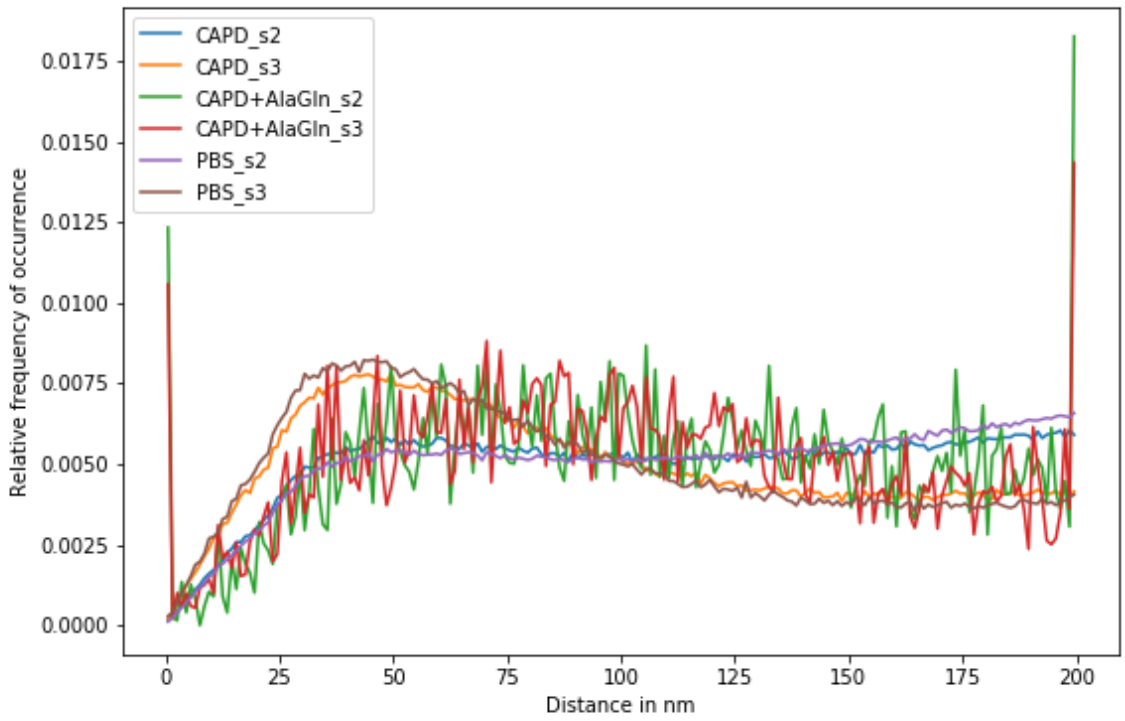

Figure 88: Distance analysis for Occludin in CAPD related test series: Norm 3; x-axis: Distance between signals in nm; y-axis: Relative frequency of occurrence

of occurrence of distances (Fig. 87). However, when comparing the distance distributions of CAPD and PBS treatments, it appeared that different treatment solutions in the same staining showed very similar properties. Scaling the y-axis according to the signal numbers (Norm 3 method, Fig. 88) supported this finding. Similarly as for the Claudin5 scaled distance analysis, signal numbers for the CAPD + alanyl-glutamine treatment were very low, thus the scaling resulted in great fluctuations.

A peak at around 40 nm could be observed in the distance analysis that was comparably distinct for CAPD and PBS test series in s3 staining, but less distinct in the CAPD and PBS test series in s2 staining.

Localization accuracies were in the range of 15 to 30 nm for all test series.

Slice No.	Staining	Channel	Target	Signal Numbers	Loc. Accuracy [nm]
18	s4	488	Claudin2	211 ± 3	28 ± 7
18	s4	568	Claudin5	3504 ± 238	22 ± 9
19	s5	488	Claudin2	437 ± 31	28 ± 7
19	s5	568	Occludin	5368 ± 190	22 ± 10
20	s6	488	Claudin5	313 ± 17	28 ± 7
20	s6	568	Occludin	3459 ± 155	23 ± 10

Table 10: Overview over test series treated with PBS+AlaGln

IV.3 PBS + Alanyl-glutamine

An additional set of samples was prepared to analyze the influence of PBS + alanyl-glutamine solution on human peritoneal mesothelial cells. The same protocol as described in Chapter III.1 was applied, but cells were prepared on a separate occasion from the other analyzed test series. A list of analyzed test series with signal numbers and localization accuracies is given in Table 10. All test series were analyzed with the program startSPDM and a threshold factor of 3. Exemplary localization images of all test series with this treatment are shown below (Fig. 89 to Fig. 94).

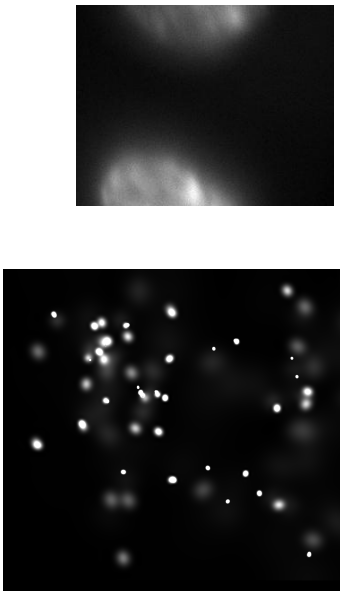

Figure 89: Claudin2 Ch. 488 s4

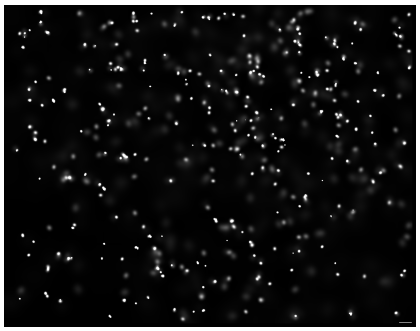

Figure 90: Claudin5 Ch. 568 s4

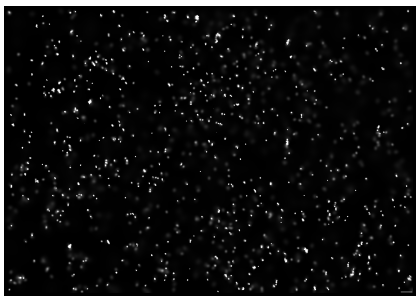

Figure 91: Occludin Ch. 568 s5

From the shown examples, it becomes clear that signal numbers for the 488 nm channel (AlexaFluor488) were substantially lower than signal numbers in the 568 nm channel. For both stainings of Claudin2 (s4 and s5), signal numbers were too low to identify cellular features or other structures. The 488 nm staining of Claudin5 (s6) showed similar properties. Significantly more signals were registered in the test series of Claudin5 with AlexaFluor568 staining (s5, Fig. 90), but structures were difficult to identify from the localization images.
Signal numbers and organization seemed to be more comparable between the two Occludin test series, possibly because both test series were stained with AlexaFluor568.

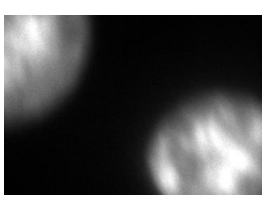

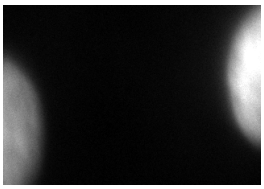

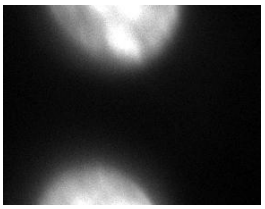

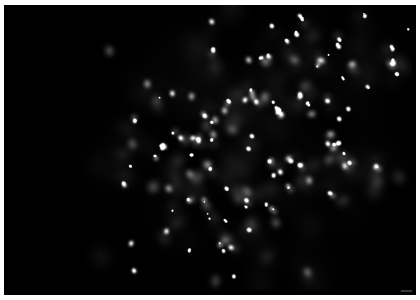

Figure 92: Claudin2 Ch. 488 s5

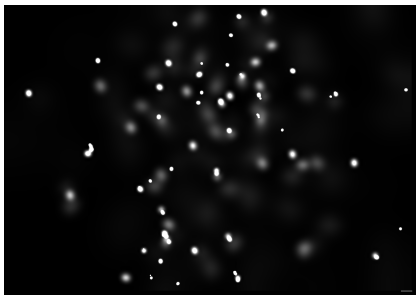

Figure 93: Claudin5 Ch. 488 s6

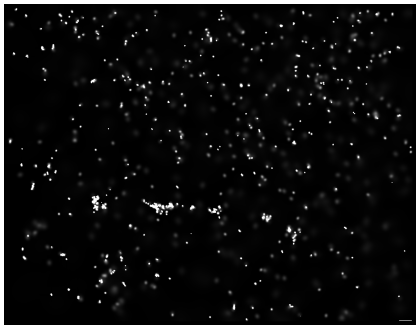

Figure 94: Occludin Ch. 568 s6

To further compare the signal numbers of the different test series, a box plot was created (Fig. 95). As already indicated by the localization pictures, all channel 488 test series showed significantly lower signal numbers. For Claudin5 (s5) and Occludin in both stainings, a sufficient amount of signals could be detected to allow further analysis of the signal distribution. Distance analysis plots were created (Fig. 96 and Fig. 97) to analyze characteristic distances of the test series.

For all test series, a peak in frequency of occurrence of signal distances between 30 nm and 40 nm could be registered. Distribution of distances was very similar for the analyzed test series, and differences in absolute frequency of occurrence were mainly due to different signal numbers. The Occludin targeting test series in the two different stainings showed differences in signal numbers with the s5 series having significantly more signals. After scaling of the y-axis (Fig. 97), distance distributions appeared almost identical for the different targets.

Because the cells were prepared on a different occasion than other test series and disruptive factors likely influenced the cell preparation process, especially in the 568 nm channel, these test series were not listed in earlier comparisons. However, other test series were prepared simultaneously and can provide further results for comparison in future studies. Additionally, these results provide an important insight into the effects of cell preparation on results such as signal numbers and distance distribution.

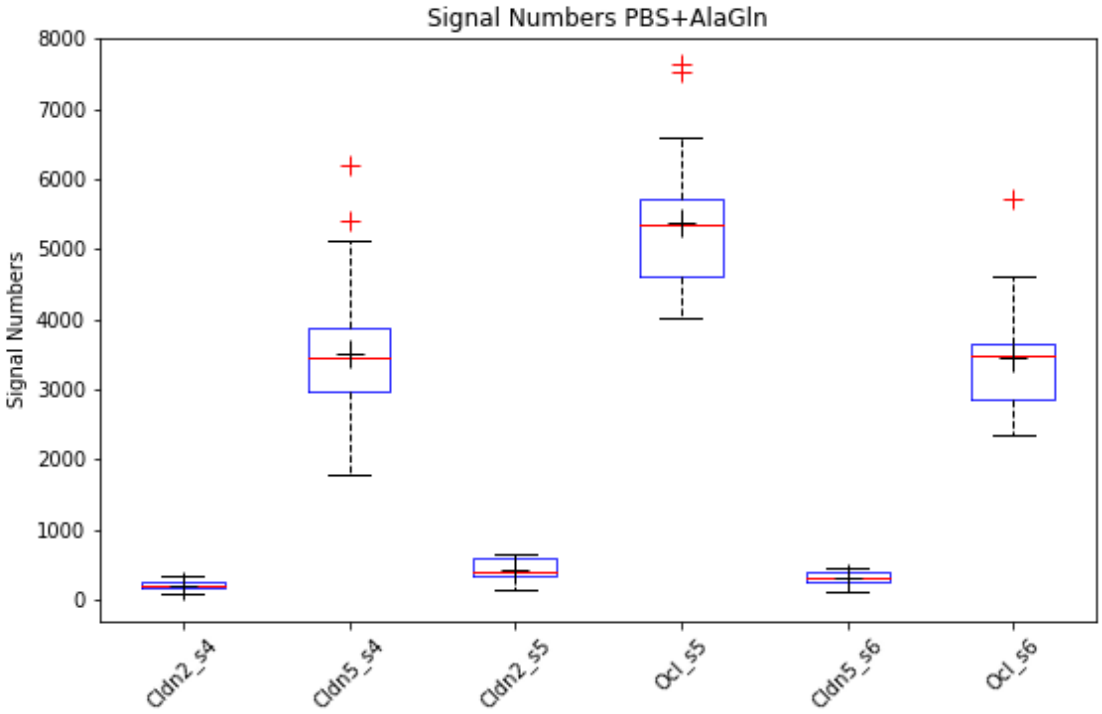

Figure 95: Signal numbers for all test series with PBS + AlaGln treatment: Blue Box: 50% of values, black dotted lines reach to 1.5 the quartile values. Median is represented by a red line and mean is represented by a black cross.

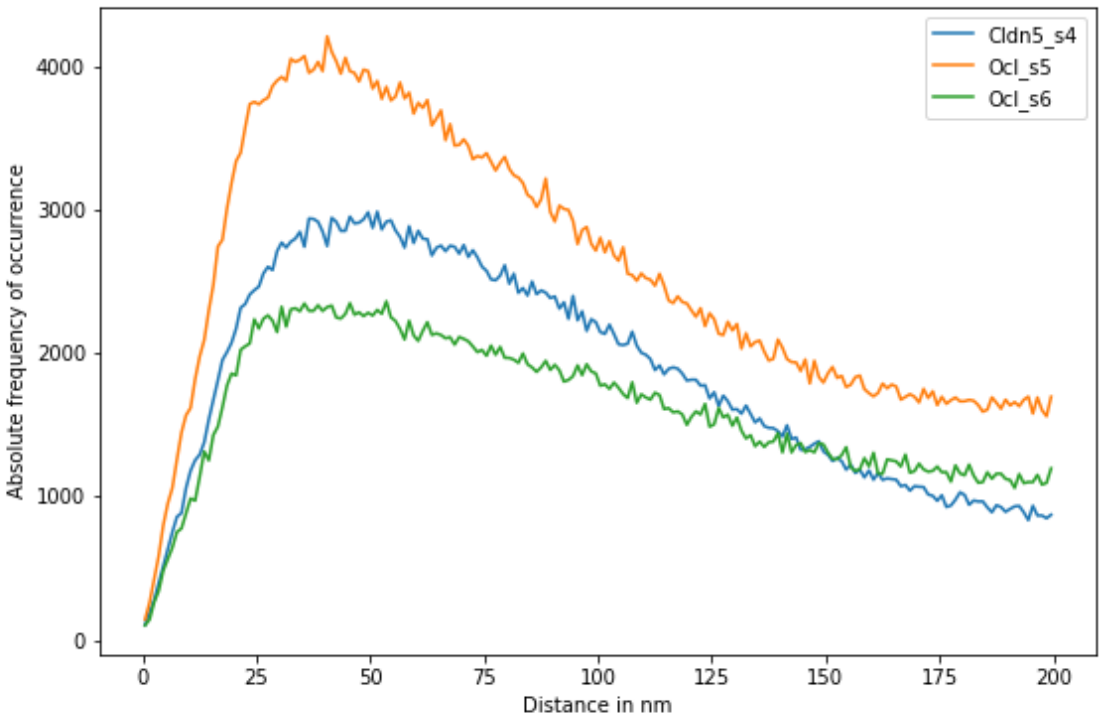

Figure 96: Distance analysis for PBS + AlaGln: All distances. X-axis: Distances between signals in nm; Y-axis: Absolute frequency of occurrence.

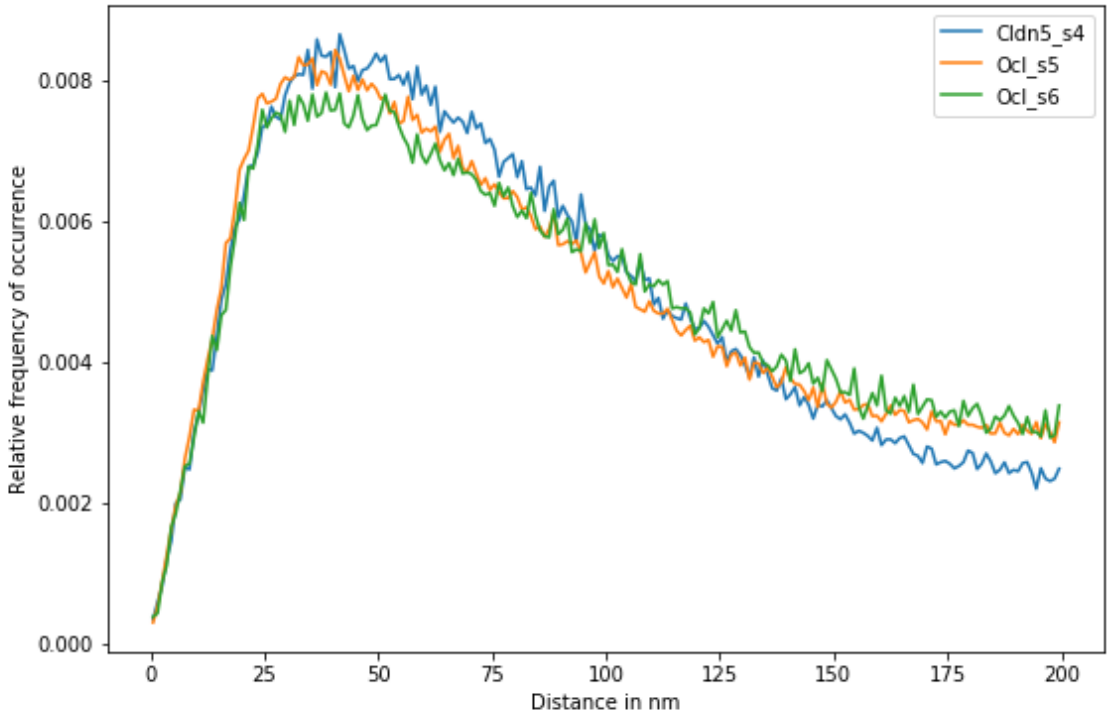

Figure 97: Distance analysis for PBS + AlaGln: Norm 3. X-axis: Distances between signals in nm; Y-axis: Relative frequency of occurrence.

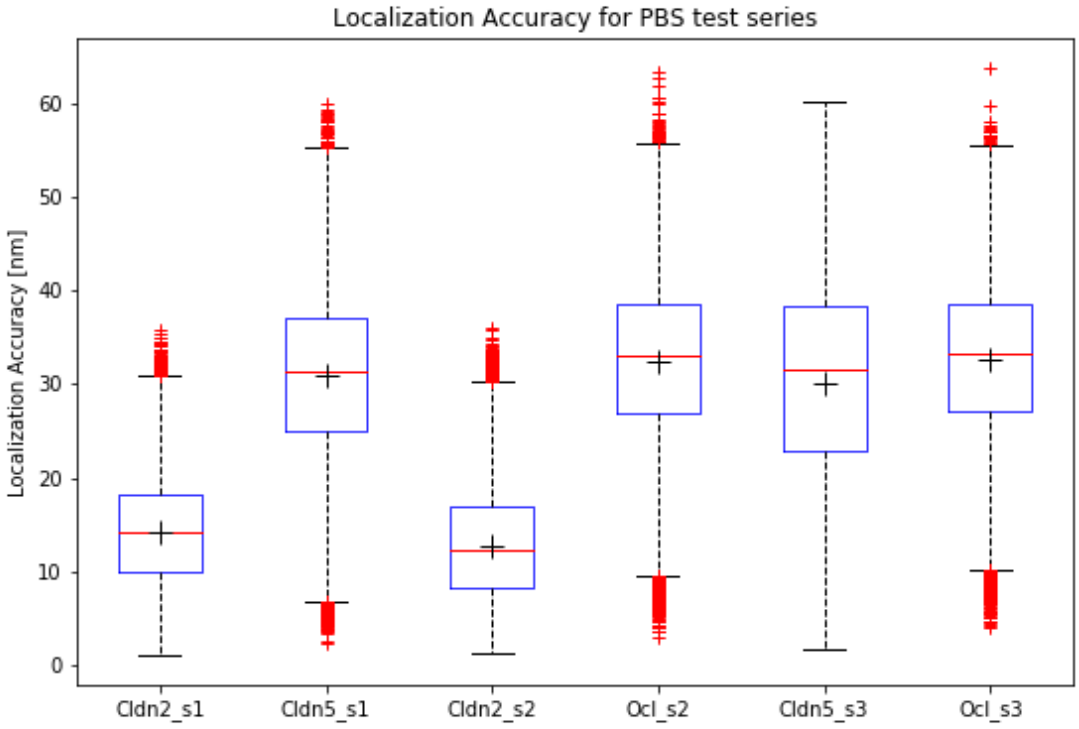

Figure 98: Boxplot of localization accuracies of PBS treated test series. Boxes reach from the lower to the upper end of quartile values of the data. The median is represented by a line. Names of test series left to right: Cldn2_s1, Cldn5_s1, Cldn2_s2, Ocl_s2, Cldn5_s3, Ocl_s3

V Discussion

A complete list of all test series with calculated signal numbers and localization accuracies is given in Table 11.

V.1 Localization Accuracy

The localization accuracy of a signal refers to the width of the fitted point spread function and gives information about the maximal resolution of a localization image. As described in Chapter II.2.3, background noise and the number of captured photons per signal influence the localization accuracy. From Table 11, it can be seen that test series with different treatment solutions but the same target proteins and fluorescent dyes had very similar localization accuracies. However, localization accuracies for Claudin2 test series were systematically lower than for Claudin5 or Occludin test series, regardless of the treatment solution. An overview over the localization accuracies in different PBS-treated test series is given in Fig. 98.

The differences in localization accuracy between Claudin2 and other targets can likely be attributed to the signal detection process: while Claudin5 and Occludin signals were detected using a threshold factor of 3, all Claudin2 test series were analyzed with a threshold factor of 5 in startSPDM. The higher threshold factor results in a more favorable signal-to-noise ratio for all detected signals and thus in a better localization accuracy. The reason why different targets were analyzed with different threshold factors was that qualitatively, the most detailed localization images were achieved with this setting.

For Claudin5, a polyclonal antibody (rabbit) and AlexaFluor488 was used for the s1 staining and a monoclonal antibody (mouse) with AlexaFluor568 for s3 staining. From Table 11 and Fig. 98, it can be seen that the different antibodies and fluorescent dyes resulted in similar localization accuracies.

Treatment	Slice No.	Staining	Channel	Target	Signal Numbers	Loc. Accuracy [nm]
BicaVera	1	s1	568	Cldn2	43790 ± 5020	14 ± 5
BicaVera	1	s1	488	Cldn5	9330 ± 1110	31 ± 8
BicaVera	2	s2	568	Cldn2	23980 ± 2850	15 ± 5
BicaVera	2	s2	488	Ocl	12630 ± 660	33 ± 8
BicaVera	3	s3	568	Cldn5	12320 ± 830	30 ± 10
BicaVera	3	s3	488	Ocl	11790 ± 660	33 ± 8
BicaVera + AlaGln	4	s1	568	Cldn2	64210 ± 6420	14 ± 6
BicaVera + AlaGln	4	s1	488	Cldn5	18900 ± 713	31 ± 8
BicaVera + AlaGln	5	s2	568	Cldn2	48950 ± 4910	13 ± 5
BicaVera + AlaGln	5	s2	488	Ocl	9760 ± 700	33 ± 8
BicaVera + AlaGln	6	s3	568	Cldn5	10930 ± 734	30 ± 10
BicaVera + AlaGln	6	s3	488	Ocl	6460 ± 340	33 ± 8
CAPD	7	s1	568	Cldn2	45900 ± 4250	13 ± 5
CAPD	7	s1	488	Cldn5	9630 ± 240	33 ± 8
CAPD	8	s2	568	Cldn2	40680 ± 3590	13 ± 6
CAPD	8	s2	488	Ocl	9470 ± 410	32 ± 8
CAPD	9	s3	568	Cldn5	10580 ± 250	29 ± 11
CAPD	9	s3	488	Ocl	9160 ± 570	32 ± 8
CAPD + AlaGln	10	s1	568	Cldn2	21020 ± 2630	12 ± 4
CAPD + AlaGln	10	s1	488	Cldn5	440 ± 40	33 ± 8
CAPD + AlaGln	11	s2	568	Cldn2	16260 ± 1890	12 ± 4
CAPD + AlaGln	11	s2	488	Ocl	370 ± 30	29 ± 7
CAPD + AlaGln	12	s3	568	Cldn5	2980 ± 130	23 ± 9
CAPD + AlaGln	12	s3	488	Ocl	370 ± 20	27 ± 8
PBS	13	s1	568	Cldn2	112370 ± 10190	14 ± 5
PBS	13	s1	488	Cldn5	21780 ± 1200	31 ± 8
PBS	14	s2	568	Cldn2	69240 ± 4380	13 ± 6
PBS	14	s2	488	Ocl	16450 ± 780	32 ± 8
PBS	15	s3	568	Cldn5	7550 ± 290	30 ± 11
PBS	15	s3	488	Ocl	7800 ± 220	32 ± 8
PBS	16	s4	568	Cldn5	4956 ± 249	24 ± 9
PBS	16	s4	488	Cldn2	50 ± 8	16 ± 3
PBS	17	s3	568	Ocl	6860 ± 555	22 ± 10
PBS	17	s3	488	Cldn2	62 ± 9	16 ± 3
PBS + AlaGln	18	s4	488	Cldn2	211 ± 3	28 ± 7
PBS + AlaGln	18	s4	568	Cldn5	3504 ± 238	22 ± 9
PBS + AlaGln	19	s5	488	Cldn2	437 ± 31	28 ± 7
PBS + AlaGln	19	s5	568	Ocl	5368 ± 190	22 ± 10
PBS + AlaGln	20	s6	488	Cldn5	313 ± 17	28 ± 7
PBS + AlaGln	20	s6	568 64	Ocl	3459 ± 155	23 ± 10

V.2 Signal Numbers

The mean values of signal numbers for all test series are listed in Table 11 with uncertainties ($\Delta = \frac{\sigma}{\sqrt{N}}$). In general, more signals were detected for Claudin2 targeting test series. As different threshold factors were used for signal detection of Claudin2 than for the other targets, it is difficult to directly compare the signal numbers of the different test series. However, since a higher threshold factor should result in a reduction of signals, it is reasonable to assume that the differences in signal numbers would be more severe if the test series were analyzed using the same threshold factor. As cell preparation was performed together for all samples, this indicates that Claudin2 was more abundant in the analyzed cells than Occludin and Claudin5. The reason for this might be the nature of the analyzed cells. Claudin5 is associated with tight junctions in tissue that is non-permeable, such as the blood-brain-barrier [42]. Claudin2 on the other hand is associated with leaky tissue and the forming of water pores as well as cation specific channels [43] [44] [45]. It is possible that Claudin2 in general is more expressed than Claudin5 and Occludin in human peritoneal mesothelial cells, thus resulting in the greater signal numbers.

Other reasons for the differences might be cell preparation and staining. In immunostaining, a primary antibody binds a specific target and a secondary antibody containing a fluorescent label specifically binds the primary antibody. Depending on the number and spatial orientation of targets, it is possible that fluorescent staining is bounded by the accessibility of targets. Additionally, the concentration of antibodies in the solution during cell preparation and other factors such as temperature can influence the quality of the staining.

For this work, the cells were treated with a particular treatment solution (PD-fluid), then blocked and labeled with the primary antibody. Afterwards, the secondary antibody was prepared in a solution containing a blocking buffer and used for all cells at the same time. The channel using polyclonal antibodies was prepared first (Rabbit, AlexaFluor488), and the channel using monoclonal antibodies (Mouse, AlexaFlour568) was prepared second. As the solution containing the secondary antibody was the same for all cells, differences in signal numbers can not be attributed to different concentrations of the secondary antibody and the fluorescent dye. Additionally, all Claudin2 stainings were performed with AlexaFlour568 and monoclonal antibodies and thus after the staining of the first (488) channel was already completed. As a result, the accessibility of targets did not favor the Claudin2 staining. However, it is possible that the binding of the primary antibody corresponding to Claudin2 was more successful than for the other targets, resulting in greater signal numbers for Claudin2.

An additional set of samples was prepared with switched channels for the same target proteins to further analyze the influence of the antibody staining on signal numbers, see Table 11. The same observations could not be made for this set of samples. In fact, Claudin2 signal counts were much lower than for other test series. The Claudin2 test series on slice number 16 (PBS, Cldn5-Cldn2) for example averaged only 50 signals per recording as compared to over 100.000 signals for other test series. However, other test series in the 568 channel (Claudin5 and Occludin) were comparable in signal numbers to earlier measurements. Additionally, other targets in the 488 channel in this set of samples (Claudin5 on slice 20) showed similarly little signal numbers. Thus, it seems likely that the binding of the secondary antibody in the 488 channel was inhibited by disruptive factors, as the antibody binding was performed together for all samples.

V.2.1 Effects of BPDF (BicaVera) on signal numbers

The effects of BPDF and BPDF + AlaGln on signal numbers depended on the target protein and on the staining of the test series.

- **Claudin2:** For Claudin2, signal numbers were reduced in samples treated with BPDF as compared to the PBS control group. Test series with BPDF + AlaGln treatment showed signal numbers that were in between the control group and BPDF test series. Although signal numbers for the same treatment but

different staining s1 or s2 did not match within uncertainties (Table 11), this trend could be observed for both stainings (s1: Cldn5(488)-Cldn2(568), s2: Ocl(488)-Cldn2(568)).

For test series with the same treatment solution, the exposure of the samples to the PD-fluids and the immunostaining of Claudin2 were performed together. Differences in cell preparation for these test series were the staining of the first target (Ch. 488), which was Claudin5 for s1 and Occludin for s2. As the staining with AlexaFluor488 was performed first, it is possible that the second channel staining (AlexaFluor568) was affected, for example because of reduced target accessibility. A higher signal number of Occludin compared to Claudin5 signals could indicate a reduced accessibility of Claudin2 targets in s2 and could provide an explanation for the differences in Claudin2 signal numbers. Claudin2 signal numbers were significantly higher for s1 than for s2 (BicaVera: 4σ, BicaVera + AlaGln: 3σ, PBS: 5σ; from Table 11). However, while Occludin(s2) signals were higher than Claudin5(s1) signals for the BicaVera treatment, the opposite was the case for BicaVera + AlaGln and PBS test series. The differences in Claudin2 signals and therefore likely not due to reduced target accessibility.

Other disruptive factors could have affected the measurements. Firstly, all samples were prepared at the same time (June 2018), but measured on different occasions. As the flourophores are light sensitive, a decrease of signals over time even in properly stored samples is possible. Secondly, small differences in the optical setup such as the laser focus on the sample can have great influence on the signal numbers. Even though the optical setup was not changed in general over the course of this work, some sporadic adjustments were necessary as other experiments were also conducted on the same microscope. A region of interest (ROI) for recording was individually selected at the start of each measurement, and size and position of the ROI can greatly influence the results such as signal numbers. Though an effort was made to keep position and size of the ROIs comparable between measurements, some differences between test series might be due to differences in ROIs.

As the trend of reduced signal numbers after treatment with BPDF could be seen in both stainings, it is possible that the difference in signal numbers correspond to morphological changes induced by PD-fluids. Among the observed changes to peritoneal tissue related to peritoneal dialysis, loss of ultrafiltration is one of the more prominent ones [4]. A study with patients that experienced permanent loss of ultrafiltration while on PD revealed a high diffusive mass transport coefficients for small solutes as well as an increased lymphatic flow [50]. Based on these findings, one might expect an increase in Claudin2 signals for PD-fluid treated cells, as Claudin2 has been associated with water pores and cation channels (see Chapter II.3.3). However, with mesothelial-mesenchymal transitions in peritoneal tissue likely being a key process in PD-related health issues [23], and the details of this process still remaining largely unclear, it is possible that reduction of Claudin2 is a part of the morphological changes in the peritoneal cells. In this context, the fact that the addition of alanyl-glutamine to BicaVera seemed to lead to a regeneration of Claudin2 signals is consistent with other studies that suggested a beneficial effect of alanyl-glutamine in PD-fluids for the peritoneal membrane [34].

- **Claudin5:** For Claudin5 in s1 staining, a similar trend as for both Claudin2 stainings could be observed: signal numbers were reduced after treatment with BPDF, and test series treated with BPDF + AlaGln showed signal numbers higher than BPDF test series but lower than the control group. If this trend in signal numbers relates to the number of proteins in the cells, this could indicate that Claudin5 is also affected by PD-treatments. Since Claudin5 has been associated with non-permeable tissue and an increase of diffusive mass coefficients is among the observed consequences of PD [50], a connection between Claudin5 expression and properties of the peritoneal membrane seems possible.

  However, the same trend could not be observed in s3 staining. In fact, an opposite development could be seen: signal numbers were highest for the BPDF test series and lowest for the PBS control with the BPDF + AlaGln test series in between. Claudin5 was marked with AlexaFluor488 in s1 and AlexaFluor568 in s3, but differences in fluorescent dyes can not fully explain the changes in signal number trends between

the two stainings. While signal numbers were significantly lower for PBS in s3 than in s1, a higher number of signals could be observed in the BPDF treated test series in s3 as compared to BPDF_s1. Thus, it is possible that other disruptive factors for example during binding of the primary antibody affected the number of signals.

- **Occludin:** The BPDF treated test series showed similar signal numbers for both Occludin test series, but differences between stainings s2 and s3 were more severe for BPDF + AlaGln and PBS, see Table 11. For both Claudin2 stainings and the s1 staining for Claudin5, an increase of signals in the BPDF + AlaGln test series as compared to the BPDF treatment could be observed. This trend could not be seen for Occludin, as BPDF + AlaGln treatments showed substantially less signals than the BPDF test series for both stainings. In s2 staining, the highest number of signals for Occludin could be detected in the control group. This is consistent with other test series targeting other proteins, where treatment of the cells with PD-fluids resulted in a reduction of signals. In s3 staining however, PBS signal numbers were lower than for the BPDF treated test series and thus also lower than for PBS_s2. Interestingly, a similar observation could be made for the Claudin5 targeting test series on the same sample. Since signal numbers also depend on the density of cells in the sample, it is possible that a reduced number of cells on the PBS treated Occludin-Claudin5 stained sample influenced the signal numbers. Regions for picture acquisition were selected based on the relative position of cells, among other factors. Though an effort was made to record similar objects on all different samples, it is possible that on slices with low density of cells, more objects with greater distance between cells were chosen for recording. This could have influenced the signal numbers.
  Occludin is classified as a thight junction associated marvel protein (TAMP). The role of Occludin in tight junctions was a subject of research for several studies in the past, some of which were able to show functioning tight junctions without Occludin [39]. It is therefore possible that while restoring some peritoneal membrane functionality [33], the addition of alanyl-glutamine might not be beneficial for Occludin expression in human peritoneal mesothelial cells. However, since the signal numbers for the control groups were not consistent, it is difficult to make assumptions about the effects of the cell treatments.

V.2.2 Effects of CPDF (CAPD) on signal numbers

The samples treated with CPDF were prepared simultaneously with the BPDF treated samples, but analyzed on a later occasion. Even though about six months passed between cell preparations and the measurements of CPDF samples for this work, signal numbers seemed to be comparable to BPDF test series, which were measured up to 3 months earlier.

- **Claudin2:** The CPDF treated test series showed similar signal numbers for Claudin2 in both, the s1 and s2 staining. Signal count averages for recordings were around 40000 to 45000 and thus substantially lower than for the PBS control group (for PBS s1: 112000 ± 10000; s2: 69000 ± 4000). As a similar trend could already be observed for BPDF treatment, a decrease in signal numbers after CPDF treatment was expected.
  Signal count averages for CPDF+AlaGln treatment were lower than both, CPDF treatment and the control group. This trend could be observed for both, the s1 and s2 staining for Claudin2. This observation did not meet the expectations based on earlier analysis of BPDF treatment. For BPDF, an increase in signal numbers after addition of AlaGln to the treatment solution could be observed. This corresponded well to other findings that alanyl-glutamine in PD-fluids mitigates peritoneal membrane damage and can lead to a regeneration of mesothelial cell properties [34] [33]. The PD-fluid CAPD is a conventional glucose based peritoneal dialysis fluid (CPDF) with lactate buffer (pH≈5,5), stored in single chamber bags [28]. As most PD-fluids are heat sterilized, a single-chamber storage results in high concentrations of glucose degradation products in the PD-fluid. A proposed mechanism to explain damages to the peritoneal membrane after

continuous peritoneal dialysis centers around the effects of acidic pH and glucose degradation products on mesothelial cells [31] [27]. If the addition of alanyl-glutamine to PD-fluids helps to mitigate these damages, the beneficial effects of AlaGln after addition to CPDF should be more severe than for BPDF. In this work, an opposite trend could be seen. Treatment of cells with CPDF and the addition of AlaGln led to results that were more different from the control group than for the cells treated with only CPDF.

- **Claudin5:** Similarly as for Claudin2, signal numbers were comparable for CPDF treatments in both stainings s1 and s3. However, PBS control group and CPDF+AlaGln treatments showed differences between s1 and s3. With an average of only 440 signals per recording, the CAPD+AlaGln_s1 test was exceptionally low in signal counts. Possible reasons for this could be problems during binding of the primary antibody to the Claudin5 targets. In general, a similar trend as for Claudin2 signals could be observed in the s1 staining: signal numbers were highest for the control group and lowest for the CAPD+AlaGln treatment.
  In the s3 staining, a decrease in signal numbers for the CAPD+AlaGln treatment as compared to the CAPD treatment could be observed, too. However, the control group signal numbers in this staining were lower than the for the CAPD test series. Counts for the PBS control group in s3 were substantially lower than s1. As already discussed above, this might be due to disruptive factors during cell preparation or differences in cell distribution on the slices.
  The trend that could be observed for both stainings for Claudin5 as well as for Claudin2 is a reduction of signals in CAPD+AlaGln treated test series as compared to the CAPD treatment. As discussed above, this was unexpected as a regeneration of peritoneal membrane properties could be associated with alanyl-glutamine in PD-fluids by other studies. Additionally, the fact that signal numbers for the CAPD+AlaGln_s1 were extremely low might be an indication that cell preparation or other disruptive factors influenced the measurements.

- **Occludin:** Signal numbers for Occludin were very similar to the Claudin5 s1 staining. The CAPD test series in s2 and s3 staining had similar signal numbers of on average 9000 to 9500 signals per recording. For the CAPD+AlaGln treatment, signal numbers were extremely low with around 370 signals per recording for both stainings. The PBS_s3 test series showed lower signal numbers than PBS_s2, as already discussed. As a result, the control group showed higher signal numbers than the CAPD treatment in s2 but lower signal numbers in s3.
  Again, the trend of a drastic reduction in signal numbers in CAPD+AlaGln treatments as compared to CAPD test series or the control group could be observed. For Occludin, both stainings were performed with AlexaFluor488. The same fluorescent dye was used for Claudin5 in s1, where a similar low number of signals was detected for CAPD+AlaGln. Since for Claudin5, a test series with another dye was performed that showed substantially more signals, it is very likely that cell preparation affected the signal numbers for these test series.

To summarize, a reduction of signals after treatment with CAPD as compared to the control groups could be observed for some targets and stainings. A further reduction of signals for test series treated with CAPD+AlaGln was observed for all targets. Signal numbers were extremely low for all CAPD+AlaGln test series stained with AlexaFluor488, possibly indicating problems during immunostaining.

V.2.3 PBS+AlaGln

An additional set of samples was prepared on a separate occasion (January 2019), and test series treated with PBS+AlaGln were tested to analyze the effect of alanyl-glutamine on human peritoneal mesothelial cells. However, since cell preparation was performed separately from other test series, it is difficult to directly compare the results. Additionally, all test series stained with AlexaFluor488 showed very low signal numbers (Table 11).

Target	Conjugate	Class	Clone	Supplier	Immunogen
Claudin2	Alexa Fluor568	Monoclonal	12H12	Thermofisher	26 aa-sequence on C-terminus
Claudin5	Alexa Flour568	Monoclonal	4C3C2	Invitrogen	On synthetic peptide derived from mouse Claudin5
Claudin5	Alexa Flour488	Polyclonal	Z43.JK	Invitrogen	On synthetic peptide derived from mouse Claudin5
Occludin	Alexa Flour488	Polyclonal		Invitrogen (Ref. 71-1500)	In the region of C-terminal 150 aa

Table 12: List of antibody immunogen locations

Other samples with PBS treatment prepared on the same occasion (slice no. 16 and 17) showed very similar properties for the 488 nm channel. Since all samples were incubated in the solution containing the secondary antibody with AlexaFlour488 simultaneously, it is possible that problems occurred during this step in cell preparation.

V.3 Distance Analysis

To gather additional information about the signal distribution in samples, distance analysis tools were used to calculate the frequency of occurrence of distances between targets in the range of 0 to 200 nm. As the resolution of SMLM is bounded by different limiting factors, it is important to consider the localization accuracy of test series when discussing specific distances in the range of few nanometers. Additionally, antibodies were used in immunostaining to label targets with a fluorescent dye, which later were recognized by the microscope and the signal detection algorithm. Antibody molecules themselves have lengths in the range of 10 nm. Depending on the target and the antibody, rotation of the fluorophore around the target is possible, which can affect the accuracy of a measurement.
Antibodies bind to a specific immunogen. For large protein targets such as Claudins or Occludin, the location of the immunogen in the amino acid sequence of the protein can be important for interpretation, as proteins can extent over distances far greater than the localization accuracy. The antibodies used for this work as well as specifications about their immunogen as given on the website of the supplier are listed in Table 12.

The Occludin and Claudin2 targeting antibodies bind to a sequence at the C-terminus of the proteins. For Claudin5 antibodies, no further specification of the location of the immunogen on the amino acid sequence could be found. Both, Claudin2 and Occludin are trans-membrane proteins with the C-terminus inside the cell.

V.3.1 Distance distribution after BPDF-treatment

- **Claudin2:** Absolute and relative frequency of occurrence of distances in the range of 0 to 200 nm were calculated for all Claudin2 test series. The same treatment solutions in different staining s1 or s2 showed very similar properties in relative distance distribution. Thus, differences in absolute frequency of occurrence can mostly be attributed to different signal numbers of the test series.
  Distance distributions for the control groups were similar to a straight line with smooth points of inflection for distances around 25 nm and 130 nm. As localization accuracies for all Claudin2 test series were in the range of 15 nm, it is reasonable to assume that characteristics in distance distribution for distances greater than 20 nm corresponded to the target distribution in the samples. Straight lines in distance analysis relate to a homogeneous or random distribution of samples, as discussed in Chapter III.4.3. After treatment with BicaVera, an increase in frequency of occurrence of distances around 25 nm could be observed. A change in distance distribution on this scale might be related to a change in tight junction functionality. As Claudin2 is involved in the forming of cation specific channels and water pores [44] [43],

a change in Claudin2 distribution in the cellular membrane might be related to differences in paracellular transport properties. Since increased lymphatic water flow and changes in diffusion coefficients for small solutes are among the observed changes to the peritoneal membrane induced by PD-fluids [50], a direct correlation to the distance distribution of the proteins is possible. However, further research would be necessary to validate a connection between tight junction properties and Claudin2 distribution.

- **Claudin5:** Similarly as for Claudin2, distance analysis plots displaying the absolute and the relative frequency of occurrence of distances between signals ranging from 0 to 200 nm were created. Other than for Claudin2, the samples with the same treatment solutions in different staining s1 or s3 did not show similar distance distributions, even after scaling of the y-axis.
  The test series in s1 showed similar properties as the Claudin2 test series after scaling: the distance distribution of the PBS control group was close to a straight line, while BPDF and BPDF+AlaGln treated test series showed a peak in distances at around 40 nm. Localization accuracy was around 30 nm for the Claudin5 test series in both stainings. If the changes in Claudin5 distance distribution corresponded to changes in tight junction functionality, the fact that the addition of AlaGln to BPDF resulted in a distance distribution resembling the control group is consistent with other studies [33]. However, distance distributions of Claudin5 in s3 staining did not match this trend. In fact, the most pronounced peak in frequency of occurrence for distances around 40 nm of all Claudin5 test series could be observed in the PBS control group in s3. When comparing the distance distributions to the signal numbers, a connection between low signal numbers and a peak of distances of around 40 nm seems apparent. The height of the peak in distance distribution after scaling seems to directly correlate to the signal numbers. However, BPDF_s1 and PBS_s3 treatment were comparable in signal numbers, but showed different distance distributions.

- **Occludin:** Relative and absolute frequency of occurrence for Occludin signals have been analyzed in the range of 0 to 200 nm. Distance distributions were different in different stainings s2 or s3 for the same treatment solutions even after scaling of the y-axis according to the Norm 3 method. In fact, all test series in s2 and all test series in s3 seemed to resemble each other. In s2, a similar trend as for Claudin2 or Claudin5 in s1 staining could be observed, but less distinct: BPDF+AlaGln treatment distance distribution resembled the control group and a peak in relative frequency of occurrence of distances around 40 nm could be observed for the BPDF treatment. However, a much more pronounced peak for similar distances could be observed in all s3 test series. As for Claudin5 in s3, a connection between signal numbers and height of said peak after scaling seemed likely. But even though signal numbers for both BPDF test series were similar (12630 ± 660 for s2 and 11790 ± 660 for s3), distance distributions showed a different behavior, with the BPDF_s3 test series having a more pronounced peak in relative frequency of occurrence of distances at around 40 nm. This characteristic distance is therefore not only a result of the signal numbers.

To summarize, matching trends could be observed in both Claudin2 stainings and in s1 for Claudin5 and s2 for Occludin. PBS control groups seemed to resemble homogeneous target distributions and the treated samples showed an increase in relative frequency of occurrence for distances of around 25 nm for Claudin2 and around 40 nm for Claudin5 and Occludin. However, the same trend could not be seen in the Claudin5 s3 and the Occludin s3 test series. An increase in frequency of occurrence for similar distances ($\approx$40nm) could be observed, but height of the peak in distance distribution seemed to be related to signal numbers of the test series.
The fact that peaks in relative frequency of occurrence seemed to correlate to signal numbers of the test series suggests that the observed characteristic distances were partly a result of cell preparation or image acquisition. Another indicator for this is that the peak in distance distribution was at lower distances for Claudin2 test series, which fits the difference in localization accuracy of the different test series. However, some test series showed similar signal numbers but differences in distance distribution. Additionally, the BPDF+AlaGln treatment

for Claudin2 showed very similar distance distributions as the PBS control group in both stainings despite having different signal numbers. As a result, it is likely that treatment with PD-fluids affected the spatial organization of the targets, and it is possible that these differences corresponded to changes in paracellular membrane properties. But further research would be necessary to validate a connection between characteristic distances and tight junction functionality, as it is possible that the results of this work were also affected by disruptive factors.

V.3.2 Distance distribution after CPDF-treatment

The same distance analysis tools that were discussed for the BPDF treatment were used to analyze the spatial distribution of Claudin2, Claudin5 and Occludin after treatment with CPDF (CAPD) and CPDF+AlaGln.

- **Claudin2:** Distance distributions for absolute frequency of occurrence were very similar between test series treated with the same treatment solution. From the comparison of relative frequency of occurrence, it became clear that CAPD treated test series showed similar characteristics in distance distribution as the PBS control group. For comparison, if the observed changes in distance distribution after treatment with BPDF (BicaVera) corresponded to changes in membrane protein structure and tight junction functionality, this was unexpected. As CAPD is a conventional peritoneal dialysis fluid (CPDF) and BicaVera is a biocompatible peritoneal dialysis fluid (BPDF), changes to the peritoneal cells should be more severe after CPDF treatment than after BPDF treatment.
  A small peak in relative frequency of occurrence of distances around 120 nm to 140 nm could be seen for the CAPD+AlaGln treatment. As discussed before, it was expected that CAPD+AlaGln treatment would show similar characteristics as the control group. Thus, it was unexpected that the test series with this treatment showed the greatest differences from the control group, as already observed for the signal numbers. However, it is possible that the scaling of the y-axis for the relative frequency of occurrence amplified small features of the absolute distance distribution, as the CAPD+AlaGln test series also had the lowest number of signals.
  The characteristic distance of about 25 nm from the BPDF treated test series could not be observed for Claudin2 in any sample treated with CAPD or CAPD+AlaGln. As signal numbers were comparably high for Claudin2 in the CAPD and CAPD+AlaGln treated test series, this further supports the hypothesis that said characteristic distance is connected to low signal numbers.

- **Claudin5:** Differences between test series with the same treatment solution in different staining s1 or s3 could be observed for Claudin5. The CAPD_s3 test series showed an almost identical distance distribution as the PBS_s3 control group after scaling. As discussed before, this included a peak in relative frequency of occurrence for distances of about 40 nm. This peak was less noticeable in the CAPD_s1 test series and even less pronounced in the PBS control group in s1. The CAPD+AlaGln treatment in s1 showed exceptionally low signal numbers, thus scaling of the distance distribution resulted in a highly fluctuating curve. As differences in signal numbers were very severe for this test series compared to the other analyzed test series, it is difficult to make assumptions about characteristic distances in the sample. Additionally, the extremely low signal numbers already indicated that the test series was affected by disruptive factors during cell preparation or image acquisition. Signal numbers for CAPD+AlaGln_s3 were sufficiently high to compare the frequency of occurrence of distances to the other test series. Interestingly, a peak in relative frequency of occurrence could be found for distances of about 50 nm. Thus, the peak in distance distribution was shifted to longer distances and also less pronounced compared to the CAPD_s3 and PBS_s3 treatment. In other test series, a connection between low signal numbers and height of a similar peak in distance distributions could be found. Of the analyzed test series in s3 staining, CAPD+AlaGln had the lowest number of signals, but the peak in distance distribution was less pronounced.
  Another phenomenon that could already be observed for other targets and treatments is that the distance

distributions of samples with different treatment solution but the same staining were more similar than the distributions of the test series with the same treatment. As the staining should ideally not affect the target proteins in the sample, this observation was unexpected.

- **Occludin:** For Occludin, both test series with CAPD+AlaGln treatment showed extremely low signal numbers. As a result, absolute distance distributions of the samples were hard to compare to the other test series, and scaling for relative distance distribution resulted in high noise levels. It is therefore difficult to make an assumption about characteristic distances in the samples and how they relate to test series treated with different treatment solutions. The CAPD test series did not show similar distance distributions. Instead, relative frequency of occurrence of distances were almost identical between CAPD_s2 and PBS_s2, while CAPD_s3 resembled PBS_s3. As already observed for other treatments, the difference between s2 and s3 stainings was a more pronounced peak in relative frequency of occurrence of distances around 40 nm in s3.

V.4 Conclusion

Quantitative analysis of the localization data was able to reveal a number of differences between samples treated with PD-fluids and the control groups. However, many of these findings were not consistent over different stainings of the same targets and treatment solutions.
For Claudin2, a consistent trend could be seen in all test series treated with BPDF (BicaVera) and BPDF + AlaGln. Treatment with the PD-fluid resulted in a decrease in signal numbers as compared to the control group, and test series treated with BPDF+AlaGln showed a regeneration of signal numbers. This corresponded well to studies that linked the addition of alanyl-glutamine to PD-fluids with the regeneration of peritoneal membrane functionality [34] [33] [28]. Treatment with CPDF (CAPD) also led to a reduction of Claudin2 signals. However, instead of an increase in signal numbers, a further reduction of signals was observed in cells treated with CPDF + AlaGln. If a reduction of Claudin2 signal numbers is related to morphological changes in the peritoneal cells that lead to a loss of peritoneal membrane function, this would imply that the addition of alanyl-glutamine to CPDF induces further damage to the peritoneal cells. This is not consistent with other studies.
Additional differences in Claudin2 signal distribution could be found using distance analysis tools. After scaling the frequency of occurrence of distances between signals according to the signal numbers, a peak in distance distribution at around 25 nm could be observed in BPDF-treated test series. Again, BPDF + AlaGln treated samples showed properties similar to the control group. The changes in distance distribution could not be observed after treatment with CPDF. It is possible that changes in spatial organization of Claudin2 are directly related to a change in tight junction functionality and peritoneal membrane properties. However, it was unexpected that the same trend could not be seen after CPDF treatment.
Results for Claudin5 test series differed depending on the staining of the samples. In the slices where Claudin5 (AlexaFluor488) was labeled together with Claudin2 (AlexaFluor568), similar trends as discussed for Claudin2 could be observed for signal numbers and distance distribution of Claudin5. However, in samples with Occludin (AlexaFluor488) and Claudin5 (AlexaFluor568) staining, an opposite trend could be observed: signal numbers were highest for the BPDF treatment and lowest for the PBS control group, and a peak in relative frequency of occurrence of distances ($\approx$40 nm) was most pronounced in the control group. Similar observations were made for CPDF and CPDF + AlaGln treatment, but as already seen for Claudin2, the CPDF + AlaGln treated test series showed greatly reduced signal numbers.
Additionally, distance analysis of test series with the same treatment solution did not correspond to each other. Instead, distance distributions of different treatment solutions but with the same staining seemed to resemble each other. Since test series with the same target proteins and treatment solutions should theoretically show similar properties in signal numbers and distance distribution, this finding indicates that the results for Claudin5 were influenced by cell preparation.

Similar conclusions can be drawn from the results of the Occludin targeting test series. Samples with the same treatment solutions yielded different results in signal numbers and distance distribution, especially for the control group. A difference of Occludin test series compared to other targets is that signal numbers were lower for BPDF + AlaGln than for BPDF treatment, and exceptionally low for CPDF + AlaGln treatment. However, as all test series with CPDF + AlaGln treatment stained with AlexaFluor488 showed extremely low signal numbers, it is very likely that problems occurred during cell preparation.
Similarly as for Claudin5, distance distributions of test series with the same staining seemed to resemble each other more than distance distribution of samples with the same treatment solutions. Additionally, for the BPDF treated test series, a connection between signal numbers and distance distribution could be seen. Low signal numbers seemed to result in an increase in relative frequency of occurrence of distances around 40 nm. However, the same relationship could not be seen for the CPDF or CPDF + AlaGln treated test series.
To conclude, promising results that could lead to further insight regarding the mechanism underlying peritoneal membrane damage after continuous peritoneal dialysis were obtained using super-resolution localization microscopy. Differences in signal numbers and distance distribution of Claudin2, Claudin5 and Occludin could help to explain changes in peritoneal cells after exposure to PD-fluids. However, since the results were not consistent over all analyzed test series, further studies to examine the influence of the cell preparation process on the localization data are necessary to validate the findings of this work.

References

[1] Ernst Karl Abbe. „Contributions to the theory of the microscope and of microscopic perception“. In: *Archiv für mikroskopische Anatomie* (1873). ISSN: 01767364. DOI: 10.1007/BF02956173.

[2] WHO. *WHO model formulary 2008*. 2009, p. 453. ISBN: 978 92 4 154765 9. DOI: 10.1021/ac101568h.

[3] José A. Jiménez-Heffernan et al. „Immunohistochemical characterization of fibroblast subpopulations in normal peritoneal tissue and in peritoneal dialysis-induced fibrosis“. In: *Virchows Archiv* (2004). ISSN: 09456317. DOI: 10.1007/s00428-003-0963-3.

[4] A. Slingeneyer, B. Canaud, and C. Mion. „Permanent Loss of Ultrafiltration Capacity of the Peritoneum in Long-Term Peritoneal Dialysis: An Epidemiological Study“. In: *Nephron* (2008). ISSN: 1660-8151. DOI: 10.1159/000182927.

[5] María Yáñez-Mó et al. „Peritoneal Dialysis and Epithelial-to-Mesenchymal Transition of Mesothelial Cells“. In: *New England Journal of Medicine* (2003). ISSN: 0028-4793. DOI: 10.1056/NEJMoa020809.

[6] Lord Rayleigh. „On the Theory of Optical Images, with Special Reference to the Microscope“. In: *Journal of the Royal Microscopical Society* (1903). ISSN: 03683974. DOI: 10.1111/j.1365-2818.1903.tb04831.x.

[7] T.W.J. Gadella. *Fret and Flim Techniques*. 2009. ISBN: 9780080549583. DOI: 10.1016/S0075-7535(08)00012-0.

[8] David Baddeley et al. „4D super-resolution microscopy with conventional fluorophores and single wavelength excitation in optically thick cells and tissues“. In: *PLoS ONE* (2011). ISSN: 19326203. DOI: 10.1371/journal.pone.0020645.

[9] David Baddeley et al. „Light-Induced Dark States of Organic Fluochromes Enable 30 nm Resolution Imaging in Standard Media“. In: *Biophysical Journal* (2009). ISSN: 00063495. DOI: 10.1016/j.bpj.2008.11.002.

[10] Michael J. Rust, Mark Bates, and Xiaowei Zhuang. „Sub-diffraction-limit imaging by stochastic optical reconstruction microscopy (STORM)“. In: *Nature Methods* (2006). ISSN: 15487091. DOI: 10.1038/nmeth929. arXiv: nmeth929 [:10.1038].

[11] Samuel T. Hess, Thanu P.K. Girirajan, and Michael D. Mason. „Ultra-high resolution imaging by fluorescence photoactivation localization microscopy“. In: *Biophysical Journal* (2006). ISSN: 00063495. DOI: 10.1529/biophysj.106.091116.

[12] Matthias Krufczik. „Reaktionen der Genomarchitektur auf ionisierende Strahlung: Quantitative Analyse mittels neuer Konzepte zur hochauflösenden Lokalisationsmikroskopie“. PhD thesis. Heidelberg University, 2017.

[13] Russell E. Thompson, Daniel R. Larson, and Watt W. Webb. „Precise nanometer localization analysis for individual fluorescent probes“. In: *Biophysical Journal* (2002). ISSN: 00063495. DOI: 10.1016/S0006-3495(02)75618-X. arXiv: NIHMS150003.

[14] D.M. Billings. *Lippincott's content review for NCLEX-RN®*. 2011. ISBN: 9781451162455.

[15] Haralampos V. Harissis et al. „A new simplified one port laparoscopic technique of peritoneal dialysis catheter placement with intra-abdominal fixation“. In: *American Journal of Surgery* (2006). ISSN: 00029610. DOI: 10.1016/j.amjsurg.2006.01.033.

[16] Katherine Balkerma et al. *Lippincott's review for medical-surgical nursing certification*. 2012. ISBN: 9788578110796. DOI: 10.1017/CBO9781107415324.004. arXiv: arXiv:1011.1669v3.

[17] Zbylut J. Twardowski. *Textbook of Peritoneal Dialysis*. Third. 2013, pp. 133–151. DOI: 10.1007/978-94-017-3225-3.

[18] G. Abraham et al. „Continuous ambulatory peritoneal dialysis“. In: *Journal of Association of Physicians of India* (1996). ISSN: 00045772.

[19] Kenneth Lim, Ragnar Palsson, and Andrew Siedlecki. *Dialysis Initiation During the Hospital Stay*. 2016. DOI: 10.1016/j.ehmc.2016.05.008.

[20] Peter J Margetts et al. „Antiangiogenic and antifibrotic gene therapy in a chronic infusion model of peritoneal dialysis in rats.“ In: *Journal of the American Society of Nephrology : JASN* (2002). ISSN: 1046-6673.

[21] Philip Kam Tao Li et al. „Peritoneal dialysis-related infections recommendations: 2010 update“. In: *Peritoneal Dialysis International* (2010). ISSN: 08968608. DOI: 10.3747/pdi.2010.00049.

[22] Raymond T. Krediet and Dirk G. Struijk. *Peritoneal changes in patients on long-term peritoneal dialysis*. 2013. DOI: 10.1038/nrneph.2013.99.

[23] Qin Zhou et al. *Preventing peritoneal membrane fibrosis in peritoneal dialysis patients*. 2016. DOI: 10.1016/j.kint.2016.03.040.

[24] Joanne M. Bargman. „Advances in Peritoneal Dialysis: A Review“. In: *Seminars in Dialysis* (2012). ISSN: 08940959. DOI: 10.1111/j.1525-139X.2012.01124.x.

[25] Jose A. Diaz-Buxo, Dixie Ann Sawin, and Rainer Himmele. „PD solutions: New and old“. In: *Dialysis and Transplantation* (2011). ISSN: 00902934. DOI: 10.1002/dat.20601.

[26] John D Williams et al. „Morphologic Changes in the Peritoneal Membrane of Patients with Renal Disease“. In: *Journal of the American Society of Nephrology* (2002).

[27] Jeffrey Perl, Sharon J. Nessim, and Joanne M. Bargman. *The biocompatibility of neutral pH, low-GDP peritoneal dialysis solutions: Benefit at bench, bedside, or both*. 2011. DOI: 10.1038/ki.2010.515.

[28] Claus Peter Schmitt and Christoph Aufricht. *Is there such a thing as biocompatible peritoneal dialysis fluid?* 2017. DOI: 10.1007/s00467-016-3461-y.

[29] John D. Williams et al. „The Euro-Balance Trial: The effect of a new biocompatible peritoneal dialysis fluid (balance) on the peritoneal membrane“. In: *Kidney International* (2004). ISSN: 00852538. DOI: 10.1111/j.1523-1755.2004.00747.x.

[30] Claus Peter Schmitt et al. „Effects of pH-neutral, bicarbonate-buffered dialysis fluid on peritoneal transport kinetics in children“. In: *Kidney International* (2002). ISSN: 00852538. DOI: 10.1046/j.1523-1755.2002.00255.x.

[31] Yeoungjee Cho et al. *Biocompatible dialysis fluids for peritoneal dialysis*. 2014. DOI: 10.1002/14651858.CD007554.pub2.

[32] Mario Bonomini et al. „Effect of an l-carnitine-containing peritoneal dialysate on insulin sensitivity in patients treated with CAPD: A 4-Month, prospective, multicenter randomized trial“. In: *American Journal of Kidney Diseases* (2013). ISSN: 02726386. DOI: 10.1053/j.ajkd.2013.04.007.

[33] Klaus Kratochwill et al. „Alanyl-glutamine dipeptide restores the cytoprotective stress proteome of mesothelial cells exposed to peritoneal dialysis fluids“. In: *Nephrology Dialysis Transplantation* (2012). ISSN: 14602385. DOI: 10.1093/ndt/gfr459.

[34] Evelina Ferrantelli et al. „The dipeptide alanyl-glutamine ameliorates peritoneal fibrosis and attenuates IL-17 dependent pathways during peritoneal dialysis“. In: *Kidney International* (2016). ISSN: 15231755. DOI: 10.1016/j.kint.2015.12.005.

[35] James M. Anderson and Christina M. Van Itallie. *Physiology and function of the tight junction*. 2009.

[36] H. Wolburg, A. Lippoldt, and K. Ebnet. „Tight junctions in the blood-brain barrier“. In: *Handbook of Neurochemistry and Molecular Neurobiology: Neural Membranes and Transport*. 2007. ISBN: 9780387303468. DOI: 10.1007/978-0-387-30380-2_1.

[37] Wei Ye Liu et al. *Tight junction in blood-brain barrier: An overview of structure, regulation, and regulator substances*. 2012. DOI: 10.1111/j.1755-5949.2012.00340.x.

[38] Gemma J. Feldman, James M. Mullin, and Michael P. Ryan. *Occludin: Structure, function and regulation*. 2005. DOI: 10.1016/j.addr.2005.01.009.

[39] Mitinori Saitou et al. „Occludin-deficient embryonic stem cells can differentiate into polarized epithelial cells bearing tight junctions". In: *Journal of Cell Biology* (1998). ISSN: 00219525. DOI: 10.1083/jcb.141.2.397.

[40] Mikio Furuse et al. „Claudin-1 and -2: Novel integral membrane proteins localizing at tight junctions with no sequence similarity to occludin". In: *Journal of Cell Biology* (1998). ISSN: 00219525. DOI: 10.1083/jcb.141.7.1539.

[41] M. Heiskala, P. A. Peterson, and Y. Yang. *The roles of claudin superfamily proteins in paracellular transport*. 2001. DOI: 10.1034/j.1600-0854.2001.020203.x.

[42] Haixia Jiao et al. „Specific role of tight junction proteins claudin-5, occludin, and ZO-1 of the blood-brain barrier in a focal cerebral ischemic insult". In: *Journal of Molecular Neuroscience* (2011). ISSN: 08958696. DOI: 10.1007/s12031-011-9496-4.

[43] Rita Rosenthal et al. „Claudin-2, a component of the tight junction, forms a paracellular water channel". In: *Journal of Cell Science* (2010). ISSN: 0021-9533. DOI: 10.1242/jcs.060665.

[44] S. Amasheh. „Claudin-2 expression induces cation-selective channels in tight junctions of epithelial cells". In: *Journal of Cell Science* (2002). ISSN: 00219533. DOI: 10.1242/jcs.00165.

[45] Shigeaki Muto et al. „Claudin2 deficient mice are defective in the leaky and cation selective paracellular permeability properties of renal proximal tubules". In: *Proceedings of the National Academy of Sciences* (2010). ISSN: 0027-8424. DOI: 10.1073/pnas.0912901107.

[46] Sabrina Roßberger. „Kombination von Strukturierter Beleuchtung und Lokalisationsmikroskopie in einem neuen Setup mit Anwendungen an retinale Strukturen". PhD thesis. 2014, pp. 1–131.

[47] Sabrina Rossberger et al. „Combination of structured illumination and single molecule localization microscopy in one setup". In: *Journal of Optics (United Kingdom)* (2013). ISSN: 20408978. DOI: 10.1088/2040-8978/15/9/094003.

[48] Frederik Grüll et al. „Accelerating image analysis for localization microscopy with FPGAs". In: *Proceedings - 21st International Conference on Field Programmable Logic and Applications, FPL 2011*. 2011. ISBN: 9780769545295. DOI: 10.1109/FPL.2011.11.

[49] Manfred Kirchgessner. „FPGA-Based Hardware Acceleration of Localization Microscopy". PhD thesis. 2011.

[50] Olof Heimbürger et al. „Peritoneal transport in CAPD patients with permanent loss of ultrafiltration capacity". In: *Kidney International* 38.3 (1990), pp. 495–506. ISSN: 00852538. DOI: 10.1038/ki.1990.231.

Acknowledgments

I would like to thank Prof. Michael Hausmann for supervising this thesis.
Furthermore, I thank Jin-Ho Lee for his support and the time he dedicated to helping me finish this project.
Additional thanks go to Hanna Jenei, Eszter Levai, Maria Bartosova and the Nephrology Laboratory of the Center for Pediatric and Adolescent Medicine for providing the samples, Margund Bach for supervising the microscope and Malte Buchholz, Arne Kersting, Jasper Metzbaur and Jadga Hügle for proof reading.

Erklärung

Ich versichere, dass ich diese Arbeit selbstständig verfasst und keine anderen als die angegebenen Quellen und Hilfsmittel benutzt habe.

Heidelberg, den 3. April 2019,